CHAPTER

12

APERTURE ANTENNAS

12.1 INTRODUCTION

Aperture antennas are most common at microwave frequencies. There are many different geometrical configurations of an aperture antenna with some of the most popular shown in Figure 1.4. They may take the form of a waveguide or a horn whose aperture may be square, rectangular, circular, elliptical, or any other configuration. Aperture antennas are very practical for space applications, because they can be flush-mounted on the surface of the spacecraft or aircraft. Their opening can be covered with a dielectric material to protect them from environmental conditions. This type of mounting does not disturb the aerodynamic profile of the craft, which in high-speed applications is critical.

In this chapter, the mathematical tools will be developed to analyze the radiation characteristics of aperture antennas. The concepts will be demonstrated by examples and illustrations. Because they are the most practical, emphasis will be given to the rectangular and circular configurations. Due to mathematical complexities, the observations will be restricted to the far-field region. The edge effects, due to the finite size of the ground plane to which the aperture is mounted, can be taken into account by using diffraction methods such as the Geometrical Theory of Diffraction, better known as GTD. This is discussed briefly and only qualitatively in Section 12.10.

The radiation characteristics of wire antennas can be determined once the current distribution on the wire is known. For many configurations, however, the current distribution is not known exactly and only physical intuition or experimental measurements can provide a reasonable approximation to it. This is even more evident in aperture antennas (slits, slots, waveguides, horns, reflectors, lenses). It is therefore expedient to have alternate methods to compute the radiation characteristics of antennas. Emphasis will be placed on techniques that for their solution rely primarily not on the current distribution but on reasonable approximations of the fields on or in the vicinity of the antenna structure. One such technique is the *Field Equivalence Principle*.

12.2 FIELD EQUIVALENCE PRINCIPLE: HUYGENS' PRINCIPLE

The *field equivalence* is a principle by which actual sources, such as an antenna and transmitter, are replaced by equivalent sources. The fictitious sources are said to be

equivalent within a region because *they produce the same fields within that region.* The formulations of scattering and diffraction problems by the equivalence principle are more suggestive to approximations.

The field equivalence was introduced in 1936 by S. A. Schelkunoff [1], [2], and it is a more rigorous formulation of Huygens' principle [3] which states that "*each point on a primary wavefront can be considered to be a new source of a secondary spherical wave and that a secondary wavefront can be constructed as the envelope of these secondary spherical waves* [4]." The equivalence principle is based on the *uniqueness theorem* which states that "*a field in a lossy region is uniquely specified by the sources within the region plus the tangential components of the electric field over the boundary, or the tangential components of the magnetic field over the boundary, or the former over part of the boundary and the latter over the rest of the boundary* [2], [5]." The field in a lossless medium is considered to be the limit, as the losses go to zero, of the corresponding field in a lossy medium. Thus if the tangential electric and magnetic fields are completely known over a closed surface, the fields in the source-free region can be determined.

By the equivalence principle, the fields outside an imaginary closed surface are obtained by placing over the closed surface suitable electric- and magnetic-current densities which satisfy the boundary conditions. The current densities are selected so that the fields inside the closed surface are zero and outside they are equal to the radiation produced by the actual sources. Thus the technique can be used to obtain the fields radiated outside a closed surface by sources enclosed within it. The formulation is exact but requires integration over the closed surface. The degree of accuracy depends on the knowledge of the tangential components of the fields over the closed surface.

In most applications, the closed surface is selected so that most of it coincides with the conducting parts of the physical structure. This is preferred because the vanishing of the tangential electric field components over the conducting parts of the surface reduces the physical limits of integration.

The equivalence principle is developed by considering an actual radiating source, which electrically is represented by current densities $\mathbf{J}_1$ and $\mathbf{M}_1$, as shown in Figure 12.1(a). The source radiates fields $\mathbf{E}_1$ and $\mathbf{H}_1$ everywhere. However, it is desired to develop a method that will yield the fields outside a closed surface. To accomplish this, a closed surface S is chosen, shown dashed in Figure 12.1(a), which encloses the current densities $\mathbf{J}_1$ and $\mathbf{M}_1$. The volume within S is denoted by V_1 and outside S by V_2. *The primary task will be to replace the original problem, shown in Figure 12.1(a),*

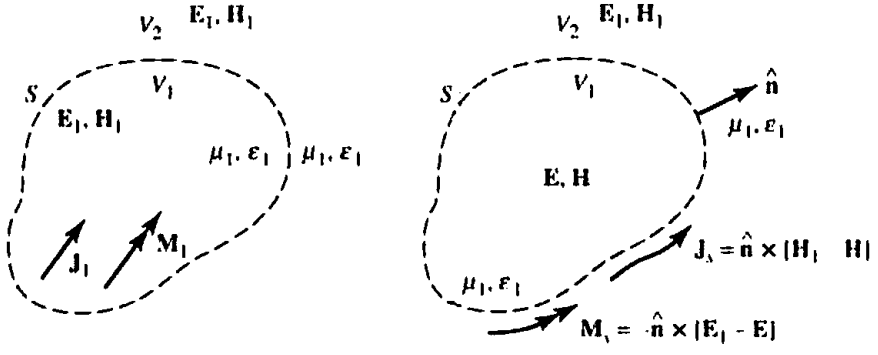

(a) Actual problem (b) Equivalent problem

Figure 12.1 Actual and equivalent problem models.

by an equivalent one which yields the same fields $\mathbf{E}_1$ *and* $\mathbf{H}_1$ *outside* S *(within* V_2*).* The formulation of the problem can be aided eminently if the closed surface is judiciously chosen so that fields over most, if not the entire surface, are known *a priori.*

An equivalent problem of Figure 12.1(a) is shown in Figure 12.1(b). The original sources $\mathbf{J}_1$ and $\mathbf{M}_1$ are removed, and we assume that there exist fields $\mathbf{E}$ and $\mathbf{H}$ inside S and fields $\mathbf{E}_1$ and $\mathbf{H}_1$ outside of S. For these fields to exist within and outside S, they must satisfy the boundary conditions on the tangential electric and magnetic field components. Thus on the imaginary surface S there must exist the *equivalent sources*

$$\mathbf{J}_s = \hat{\mathbf{n}} \times [\mathbf{H}_1 - \mathbf{H}] \tag{12-1}$$

$$\mathbf{M}_s = -\hat{\mathbf{n}} \times [\mathbf{E}_1 - \mathbf{E}] \tag{12-2}$$

and they radiate into an *unbounded space* (same medium everywhere). *The current densities of (12-1) and (12-2) are said to be equivalent only within* V_2*, because they produce the original fields* $(\mathbf{E}_1, \mathbf{H}_1)$ *only outside* S*. Fields* $\mathbf{E}$, $\mathbf{H}$, *different from the originals* $(\mathbf{E}_1, \mathbf{H}_1)$, *result within* V_1. Since the currents of (12-1) and (12-2) radiate in an unbounded space, the fields can be determined using (3-27)–(3-30a) and the geometry of Figure 12.2(a). In Figure 12.2(a), R is the distance from any point on the surface S, where $\mathbf{J}_s$ and $\mathbf{M}_s$ exist, to the observation point.

So far, the tangential components of *both* $\mathbf{E}$ and $\mathbf{H}$ have been used in setting up the equivalent problem. From electromagnetic uniqueness concepts, it is known that the tangential components of only $\mathbf{E}$ or $\mathbf{H}$ are needed to determine the fields. It will be demonstrated that equivalent problems can be found which require only the magnetic current densities (tangential $\mathbf{E}$) or only electric current densities (tangential $\mathbf{H}$). This requires modifications to the equivalent problem of Figure 12.1(b).

Since the fields $\mathbf{E}$, $\mathbf{H}$ within S can be anything (this is not the region of interest), it can be assumed that they are zero. In that case the equivalent problem of Figure 12.1(b) reduces to that of Figure 12.3(a) with the equivalent current densities being equal to

$$\mathbf{J}_s = \hat{\mathbf{n}} \times (\mathbf{H}_1 - \mathbf{H})|_{\mathbf{H}=0} = \hat{\mathbf{n}} \times \mathbf{H}_1 \tag{12-3}$$

$$\mathbf{M}_s = -\hat{\mathbf{n}} \times (\mathbf{E}_1 - \mathbf{E})|_{\mathbf{E}=0} = -\hat{\mathbf{n}} \times \mathbf{E}_1 \tag{12-4}$$

This form of the field equivalence principle is known as *Love's Equivalence Principle* [2], [6]. Since the current densities of (12-3) and (12-4) radiate in an unbounded medium (same μ, ϵ everywhere), they can be used in conjunction with (3-27)–(3-30a) to find the fields everywhere.

Love's Equivalence Principle of Figure 12.3(a) produces a null field within the imaginary surface S. Since the value of the $\mathbf{E} = \mathbf{H} = 0$ within S cannot be disturbed if the properties of the medium within it are changed, let us assume that it is replaced by a perfect electric conductor ($\sigma = \infty$). The introduction of the perfect conductor will have an effect on the equivalent source $\mathbf{J}_s$, and it will prohibit the use of (3-27)–(3-30a) since the current densities no longer radiate into an unbounded medium. Imagine that the geometrical configuration of the electric conductor is identical to the profile of the imaginary surface S, over which $\mathbf{J}_s$ and $\mathbf{M}_s$ exist. As the electric conductor takes its place, as shown in Figure 12.3(b), the electric current density $\mathbf{J}_s$, which is tangent to the surface S, is short-circuited by the electric conductor. Thus the equivalent problem of Figure 12.3(a) reduces to that of Figure 12.3(b). There exists only a magnetic current density $\mathbf{M}_s$ over S, and it radiates in the presence of the electric conductor producing outside S the original fields $\mathbf{E}_1$, $\mathbf{H}_1$. Within S the fields are zero but, as before, this is not a region of interest. The difficulty in trying

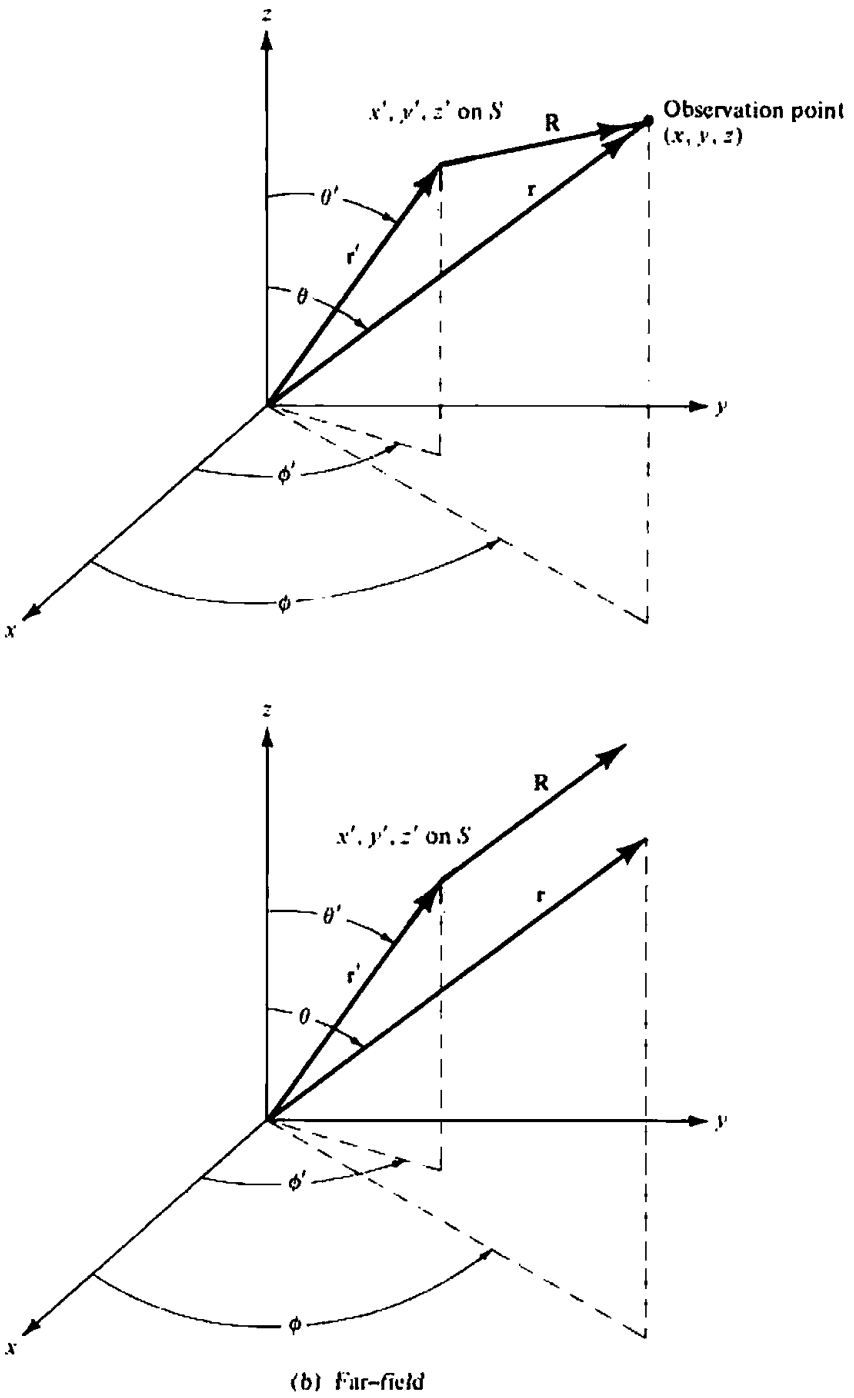

(b) Far-field

Figure 12.2 Coordinate system for aperture antenna analysis.

to use the equivalent problem of Figure 12.3(b) is that (3-27)–(3-30a) cannot be used, because the current densities do not radiate into an unbounded medium. The problem of a magnetic current density radiating in the presence of an electric conducting surface must be solved. So it seems that the equivalent problem is just as difficult as the original problem itself.

Before some special simple geometries are considered and some suggestions are made for approximating complex geometries, let us introduce another equivalent problem. Referring to Figure 12.3(a), let us assume that instead of placing a perfect electric conductor within S we introduce a perfect magnetic conductor which will short out the magnetic current density and reduce the equivalent problem to that

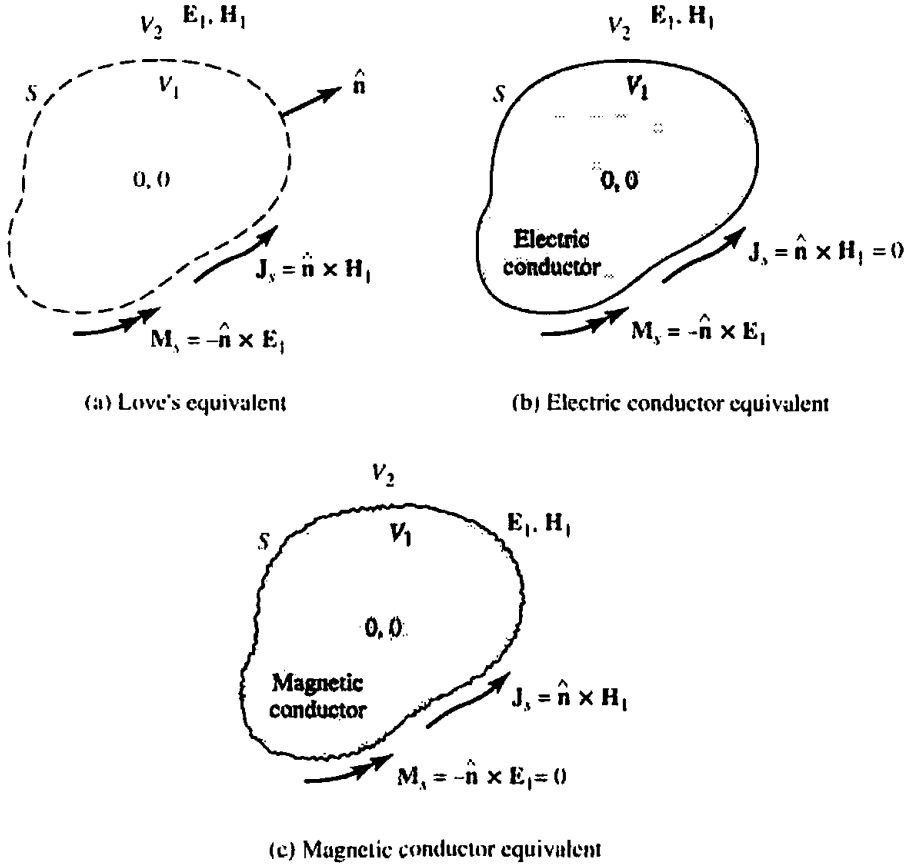

Figure 12.3 Equivalence principle models.

shown in Figure 12.3(c). As was with the equivalent problem of Figure 12.3(b), (3-27)–(3-30a) cannot be used with Figure 12.3(c) and the problem is just as difficult as that of Figure 12.3(b) or the original of Figure 12.1(a).

To begin to see the utility of the field equivalence principle, especially that of Figure 12.3(b), let us assume that the surface of the electric conductor is flat and extends to infinity as shown in Figure 12.4(a). For this geometry, the problem is to determine how a magnetic source radiates in the presence of a flat electric conductor. From image theory, this problem reduces to that of Figure 12.4(b) where an imaginary magnetic source is introduced on the side of the conductor and takes its place (remove conductor). Since the imaginary source is in the same direction as the equivalent source, the equivalent problem of Figure 12.4(b) reduces to that of Figure 12.4(c). The magnetic current density is doubled, it radiates in an unbounded medium, and (3-27)–(3-30a) can be used. The equivalent problem of Figure 12.4(c) yields the correct **E**, **H** fields to the right side of the interface. If the surface of the obstacle is not flat and infinite, but its curvature is large compared to the wavelength, a good approximation is the equivalent problem of Figure 12.3(c).

SUMMARY

In the analysis of electromagnetic problems, many times it is easier to form equivalent problems that yield the same solution within a region of interest. This is the case for scattering, diffraction, and aperture antenna problems. In this chapter, the main interest is in aperture antennas. The concepts will be demonstrated with examples.

The steps that must be used to form an equivalent and solve an aperture problem are as follows:

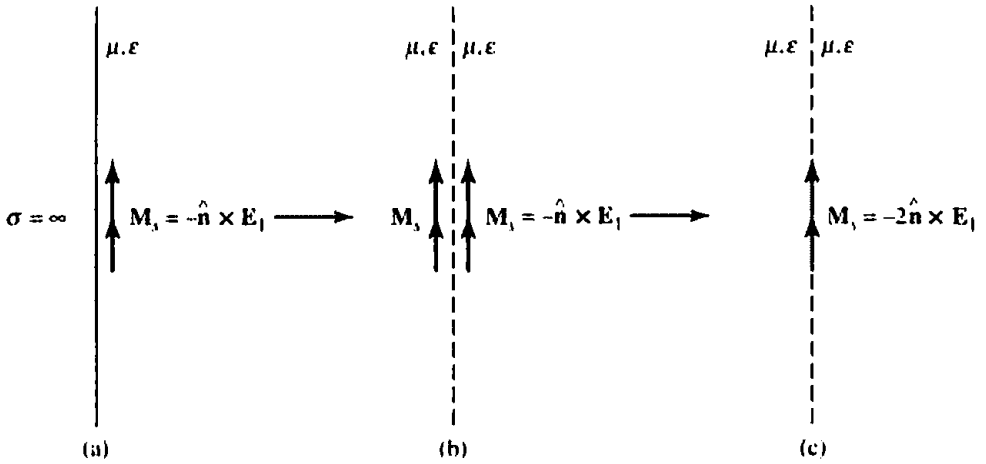

Figure 12.4 Equivalent models for magnetic source radiation near a perfect electric conductor.

1. Select an imaginary surface that encloses the actual sources (the aperture). The surface must be judiciously chosen so that the tangential components of the electric and/or the magnetic field are known, exactly or approximately, over its entire span. In many cases this surface is a flat plane extending to infinity.
2. Over the imaginary surface form equivalent current densities $\mathbf{J}_s$, $\mathbf{M}_s$ which take one of the following forms:
   a. $\mathbf{J}_s$ and $\mathbf{M}_s$ over S assuming that the **E**- and **H**-fields within S are not zero.
   b. or $\mathbf{J}_s$ and $\mathbf{M}_s$ over S assuming that the **E**- and **H**-fields within S are zero (Love's theorem)
   c. or $\mathbf{M}_s$ over S ($\mathbf{J}_s = 0$) assuming that within S the medium is a perfect electric conductor
   d. or $\mathbf{J}_s$ over S ($\mathbf{M}_s = 0$) assuming that within S the medium is a perfect magnetic conductor
3. Solve the equivalent problem. For forms (a) and (b), (3-27)–(3-30a) can be used. For form (c), the problem of a magnetic current source next to a perfect electric conductor must be solved [(3-27)–(3-30a) cannot be used directly, because the current density does not radiate into an unbounded medium]. If the electric conductor is an infinite flat plane the problem can be solved exactly by image theory. For form (d), the problem of an electric current source next to a perfect magnetic conductor must be solved. Again (3-27)–(3-30a) cannot be used directly. If the magnetic conductor is an infinite flat plane, the problem can be solved exactly by image theory.

To demonstrate the usefulness and application of the field equivalence theorem to aperture antenna theory, an example is considered.

Example 12.1

A waveguide aperture is mounted on an infinite ground plane, as shown in Figure 12.5(a). Assuming that the tangential components of the electric field over the aperture are known, and are given by $\mathbf{E}_a$, find an equivalent problem that will yield the same fields **E**, **H** radiated by the aperture to the right side of the interface.

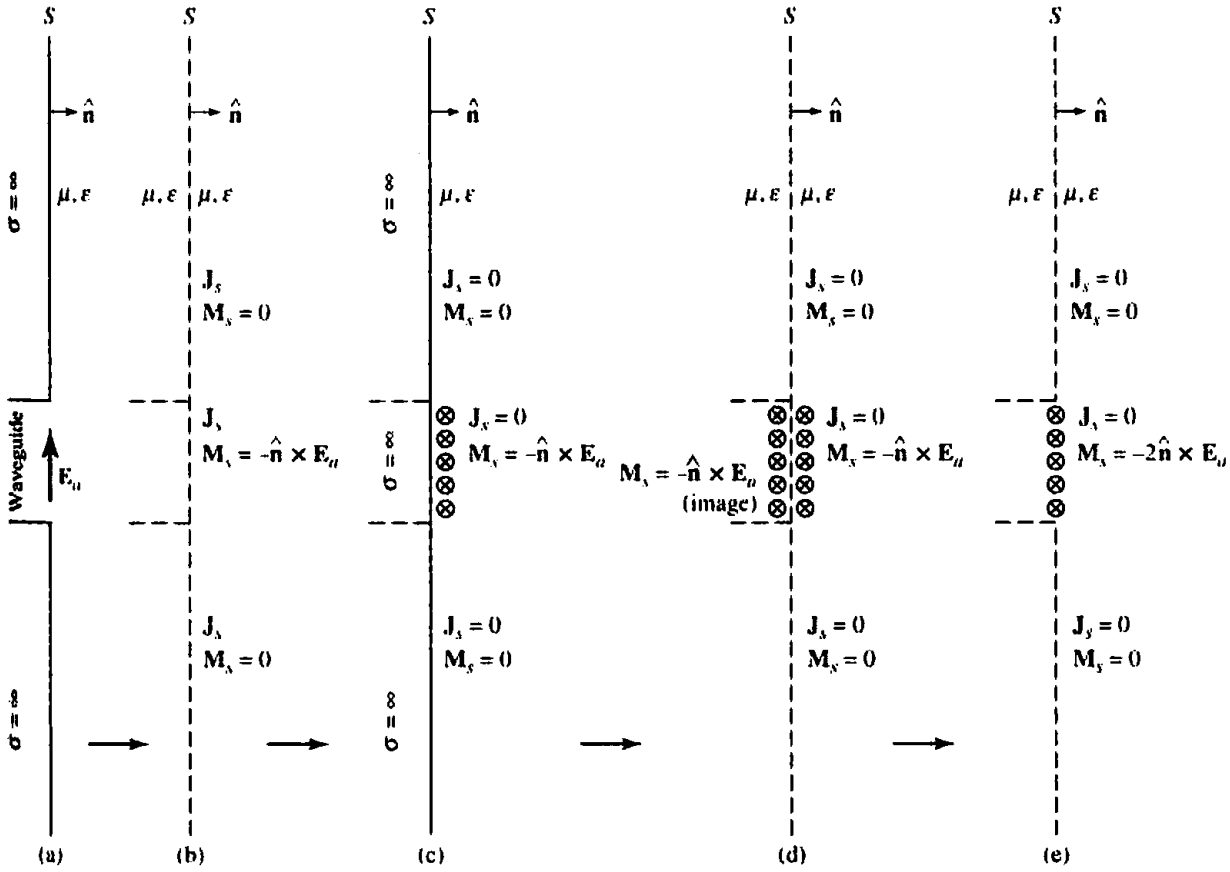

Figure 12.5 Equivalent models for waveguide aperture mounted on an infinite flat electric ground plane.

SOLUTION

First an imaginary closed surface is chosen. For this problem it is appropriate to select a flat plane extending from minus infinity to plus infinity, as shown in Figure 12.5(b). Over the infinite plane, the equivalent current densities $\mathbf{J}_s$ and $\mathbf{M}_s$ are formed. Since the tangential components of $\mathbf{E}$ do not exist outside the aperture, because of vanishing boundary conditions, the magnetic current density $\mathbf{M}_s$ is only nonzero over the aperture. The electric current density $\mathbf{J}_s$ is nonzero everywhere and is yet unknown. Now let us assume that an imaginary flat electric conductor approaches the surface S, and it shorts out the current density $\mathbf{J}_s$ everywhere. $\mathbf{M}_s$ exists only over the space occupied originally by the aperture, and it radiates in the presence of the conductor [see Figure 12.5(c)]. By image theory, the conductor can be removed and replaced by an imaginary (equivalent) source $\mathbf{M}_s$ as shown in Figure 12.5(d), which is analogous to Figure 12.4(b). Finally, the equivalent problem of Figure 12.5(d) reduces to that of Figure 12.5(e), which is analogous to that of Figure 12.4(c). The original problem has been reduced to a very simple equivalent and (3-27)–(3-30a) can be utilized for its solution.

In this chapter the theory will be developed to compute the fields radiated by an aperture, like that shown in Figure 12.5(a), making use of its equivalent of Figure 12.5(e). For other problems, their equivalent forms will not necessarily be the same as that shown in Figure 12.5(e).

12.3 RADIATION EQUATIONS

In Chapter 3 and in the previous section it was stated that the fields radiated by sources $\mathbf{J}_s$ and $\mathbf{M}_s$ in an unbounded medium can be computed by using (3-27)–(3-30a) where the integration must be performed over the entire surface occupied by $\mathbf{J}_s$ and $\mathbf{M}_s$. These equations yield valid solutions for all observation points [2], [7]. For most problems, the main difficulty is the inability to perform the integrations in (3-27) and (3-28). However for far-field observations, the complexity of the formulation can be reduced.

As was shown in Section 4.4.1, for far-field observations R can most commonly be approximated by

$$R \simeq r - r' \cos\psi \qquad \text{for phase variations} \tag{12-5a}$$

$$R \simeq r \qquad \text{for amplitude variations} \tag{12-5b}$$

where ψ is the angle between the vectors $\mathbf{r}$ and $\mathbf{r}'$, as shown in Figure 12.2(b). The primed coordinates (x', y', z', or r', θ', ϕ') indicate the space occupied by the sources $\mathbf{J}_s$ and $\mathbf{M}_s$, over which integration must be performed. The unprimed coordinates (x, y, z or r, θ, ϕ) represent the observation point. Geometrically the approximation of (12-5a) assumes that the vectors $\mathbf{R}$ and $\mathbf{r}$ are parallel, as shown in Figure 12.2(b).

Using (12-5a) and (12-5b), (3-27) and (3-28) can be written as

$$\mathbf{A} = \frac{\mu}{4\pi}\iint_S \mathbf{J}_s \frac{e^{-jkR}}{R}\,ds' \simeq \frac{\mu e^{-jkr}}{4\pi r}\mathbf{N} \tag{12-6}$$

$$\mathbf{N} = \iint_S \mathbf{J}_s e^{jkr'\cos\psi}\,ds' \tag{12-6a}$$

$$\mathbf{F} = \frac{\epsilon}{4\pi}\iint_S \mathbf{M}_s \frac{e^{-jkR}}{R}\,ds' \simeq \frac{\epsilon e^{-jkr}}{4\pi r}\mathbf{L} \tag{12-7}$$

$$\mathbf{L} = \iint_S \mathbf{M}_s e^{jkr'\cos\psi}\,ds' \tag{12-7a}$$

In Section 3.6 it was shown that in the far-field only the θ and ϕ components of the **E**- and **H**-fields are dominant. Although the radial components are not necessarily zero, they are negligible compared to the θ and ϕ components. Using (3-58a)–(3-59b), the $\mathbf{E}_A$ of (3-29) and $\mathbf{H}_F$ of (3-30) can be written as

$$(E_A)_\theta \simeq -j\omega A_\theta \tag{12-8a}$$

$$(E_A)_\phi \simeq -j\omega A_\phi \tag{12-8b}$$

$$(H_F)_\theta \simeq -j\omega F_\theta \tag{12-8c}$$

$$(H_F)_\phi \simeq -j\omega F_\phi \tag{12-8d}$$

and the $\mathbf{E}_F$ of (3-29) and $\mathbf{H}_A$ of (3-30), with the aid of (12-8a)–(12-8d), as

$$(E_F)_\theta \simeq +\eta(H_F)_\phi = -j\omega\eta F_\phi \tag{12-9a}$$

$$(E_F)_\phi \simeq -\eta(H_F)_\theta = +j\omega\eta F_\theta \tag{12-9b}$$

$$(H_A)_\theta \simeq -\frac{(E_A)_\phi}{\eta} = +j\omega\frac{A_\phi}{\eta} \tag{12-9c}$$

$$(H_A)_\phi \simeq +\frac{(E_A)_\theta}{\eta} = -j\omega\frac{A_\theta}{\eta} \tag{12-9d}$$

Combining (12-8a)–(12-8d) with (12-9a)–(12-9d), and making use of (12-6)–(12-7a) the total **E**- and **H**-fields can be written as

$$E_r \simeq 0 \tag{12-10a}$$

$$E_\theta \simeq -\frac{jke^{-jkr}}{4\pi r}(L_\phi + \eta N_\theta) \tag{12-10b}$$

$$E_\phi \simeq +\frac{jke^{-jkr}}{4\pi r}(L_\theta - \eta N_\phi) \tag{12-10c}$$

$$H_r \simeq 0 \tag{12-10d}$$

$$H_\theta \simeq \frac{jke^{-jkr}}{4\pi r}\left(N_\phi - \frac{L_\theta}{\eta}\right) \tag{12-10e}$$

$$H_\phi \simeq -\frac{jke^{-jkr}}{4\pi r}\left(N_\theta + \frac{L_\phi}{\eta}\right) \tag{12-10f}$$

The N_θ, N_ϕ, L_θ, and L_ϕ can be obtained from (12-6a) and (12-7a). That is,

$$\mathbf{N} = \iint_S \mathbf{J}_s e^{+jkr'\cos\psi}\,ds' = \iint_S (\hat{\mathbf{a}}_x J_x + \hat{\mathbf{a}}_y J_y + \hat{\mathbf{a}}_z J_z)e^{+jkr'\cos\psi}\,ds' \tag{12-11a}$$

$$\mathbf{L} = \iint_S \mathbf{M}_s e^{+jkr'\cos\psi}\,ds' = \iint_S (\hat{\mathbf{a}}_x M_x + \hat{\mathbf{a}}_y M_y + \hat{\mathbf{a}}_z M_z)e^{+jkr'\cos\psi}\,ds' \tag{12-11b}$$

Using the rectangular-to-spherical component transformation, obtained by taking the inverse (in this case also the transpose) of (4-5), (12-11a) and (12-11b) reduce for the θ and ϕ components to

$$N_\theta = \iint_S [J_x\cos\theta\cos\phi + J_y\cos\theta\sin\phi - J_z\sin\theta]e^{+jkr'\cos\psi}\,ds' \tag{12-12a}$$

$$N_\phi = \iint_S [-J_x\sin\phi + J_y\cos\phi]e^{+jkr'\cos\psi}\,ds' \tag{12-12b}$$

$$L_\theta = \iint_S [M_x\cos\theta\cos\phi + M_y\cos\theta\sin\phi - M_z\sin\theta]e^{+jkr'\cos\psi}\,ds' \tag{12-12c}$$

$$L_\phi = \iint_S [-M_x\sin\phi + M_y\cos\phi]e^{+jkr'\cos\psi}\,ds' \tag{12-12d}$$

SUMMARY

To summarize the results, the procedure that must be followed to solve a problem using the radiation integrals will be outlined. Figures 12.2(a) and 12.2(b) are used to indicate the geometry.

1. Select a closed surface over which the total electric and magnetic fields $\mathbf{E}_a$ and $\mathbf{H}_a$ are known.
2. Form the equivalent current densities $\mathbf{J}_s$ and $\mathbf{M}_s$ over S using (12-3) and (12-4) with $\mathbf{H}_1 = \mathbf{H}_a$ and $\mathbf{E}_1 = \mathbf{E}_a$.
3. Determine the $\mathbf{A}$ and $\mathbf{F}$ potentials using (12-6)–(12-7a) where the integration is over the closed surface S.
4. Determine the radiated $\mathbf{E}$- and $\mathbf{H}$-fields using (3-29) and (3-30).

The above steps are valid for all regions (near-field and far-field) outside the surface S. If, however, the observation point is in the far-field, steps 3 and 4 can be replaced by 3′ and 4′. That is,

3′. Determine N_θ, N_ϕ, L_θ and L_ϕ using (12-12a)–(12-12d).

4′. Determine the radiated $\mathbf{E}$- and $\mathbf{H}$-fields using (12-10a)–(12-10f).

Some of the steps outlined above can be reduced by a judicious choice of the equivalent model. In the remaining sections of this chapter, the techniques will be applied and demonstrated with examples of rectangular and circular apertures.

12.4 DIRECTIVITY

The directivity of an aperture can be found in a manner similar to that of other antennas. The primary task is to formulate the radiation intensity $U(\theta, \phi)$, using the far-zone electric and magnetic field components, as given by (2-12a) or

$$U(\theta, \phi) = \frac{1}{2}\text{Re}[(\hat{\mathbf{a}}_\theta E_\theta + \hat{\mathbf{a}}_\phi E_\phi) \times (\hat{\mathbf{a}}_\theta H_\theta + \hat{\mathbf{a}}_\phi H_\phi)^*] = \frac{1}{2\eta}(|E_\theta^0|^2 + |E_\phi^0|^2) \tag{12-13}$$

which in normalized form reduces to

$$\boxed{U_n(\theta, \phi) = (|E_\theta^0(\theta, \phi)|^2 + |E_\phi^0(\theta, \phi)|^2) = B_0 F(\theta, \phi)} \tag{12-13a}$$

The directive properties can then be found using (2-19)–(2-22).

Because the radiation intensity $U(\theta, \phi)$ for each aperture antenna will be of a different form, a general equation for the directivity cannot be formed. However, a general FORTRAN computer program, designated as DIRECTIVITY, has been written to compute the directivity of any antenna, including an aperture, once the radiation intensity is specified. The program is based on the formulations of (12-13a), (2-19)–(2-20), and (2-22), and it is shown at the end of Chapter 2. In the main program, it requires the lower and upper limits on θ and ϕ. The radiation intensity for the antenna in question must be specified in the subroutine $U(\theta, \phi, F)$ of the program.

Expressions for the directivity of some simple aperture antennas, rectangular and circular, will be derived in later sections of this chapter.

12.5 RECTANGULAR APERTURES

In practice, the rectangular aperture is probably the most common microwave antenna. Because of its configuration, the rectangular coordinate system is the most convenient system to express the fields at the aperture and to perform the integration. Shown in Figure 12.6 are the three most common and convenient coordinate positions used for the solution of an aperture antenna. In Figure 12.6(a) the aperture lies on the y-z plane,

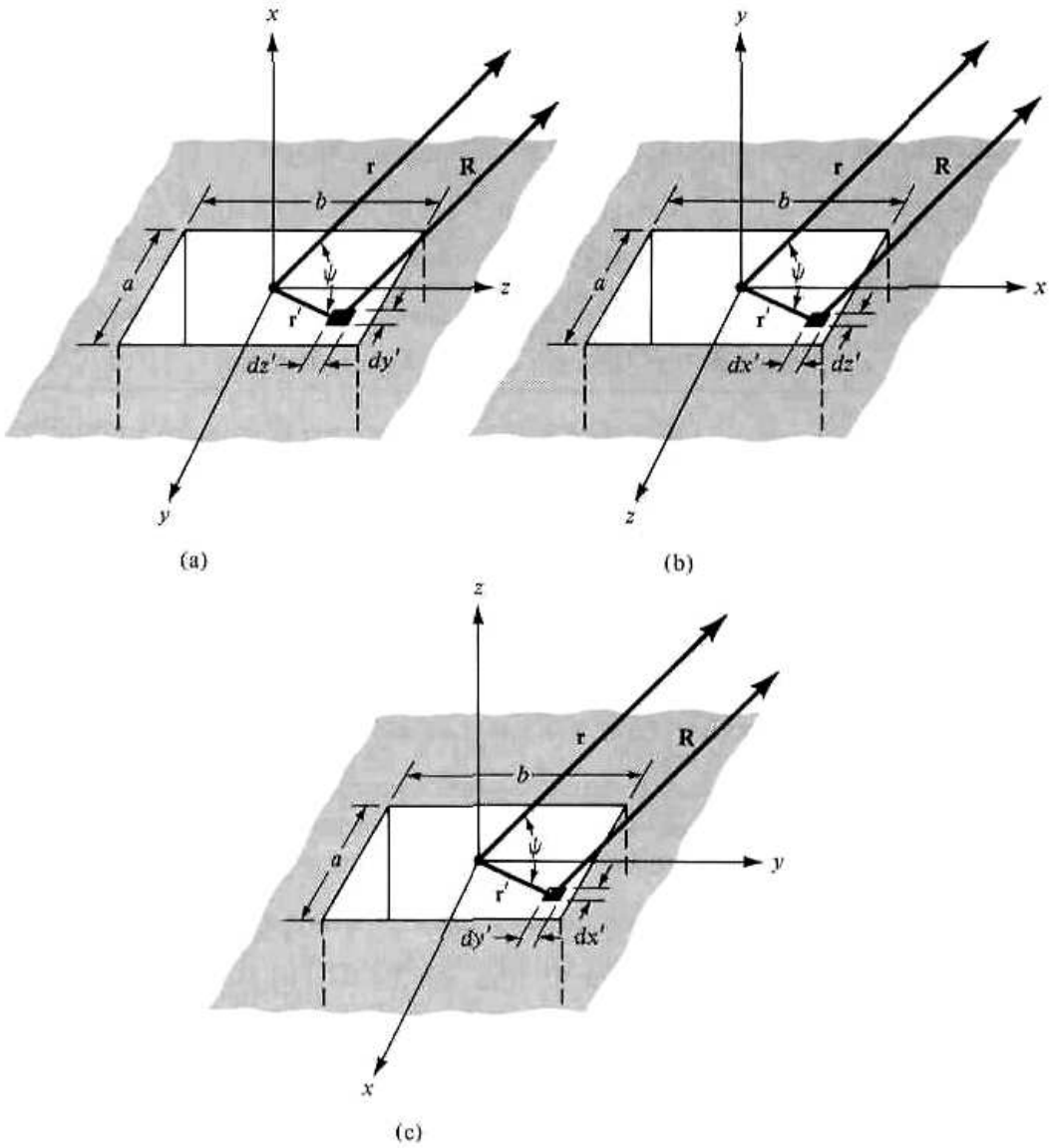

Figure 12.6 Rectangular aperture positions for antenna system analysis.

in Figure 12.6(b) on the x-z plane, and in Figure 12.6(c) on the x-y plane. For a given field distribution, the analytical forms for the fields for each of the arrangements are not the same. However the computed values will be the same, since the physical problem is identical in all cases.

For each of the geometries shown in Figure 12.6, the only difference in the analysis is in the formulation of

1. the components of the equivalent current densities (J_x, J_y, J_z, M_x, M_y, M_z)
2. the difference in paths from the source to the observation point ($r' \cos \psi$)
3. the differential area ds'

In general, the nonzero components of $\mathbf{J}_s$ and $\mathbf{M}_s$ are

$$J_y, J_z, M_y, M_z \qquad \text{[Figure 12.6(a)]} \qquad (12\text{-}14a)$$

$$J_x, J_z, M_x, M_z \qquad \text{[Figure 12.6(b)]} \qquad (12\text{-}14b)$$

$$J_x, J_y, M_x, M_y \qquad \text{[Figure 12.6(c)]} \qquad (12\text{-}14c)$$

The differential paths take the form of

$$r'\cos\psi = \mathbf{r}'\cdot\hat{\mathbf{a}}_r = (\hat{\mathbf{a}}_y y' + \hat{\mathbf{a}}_z z')\cdot(\hat{\mathbf{a}}_x \sin\theta\cos\phi + \hat{\mathbf{a}}_y \sin\theta\sin\phi + \hat{\mathbf{a}}_z\cos\theta)$$
$$= y'\sin\theta\sin\phi + z'\cos\theta \qquad \text{[Figure 12.6(a)]} \qquad (12\text{-}15a)$$

$$r'\cos\psi = \mathbf{r}'\cdot\hat{\mathbf{a}}_r = (\hat{\mathbf{a}}_x x' + \hat{\mathbf{a}}_z z')\cdot(\hat{\mathbf{a}}_x \sin\theta\cos\phi + \hat{\mathbf{a}}_y \sin\theta\sin\phi + \hat{\mathbf{a}}_z\cos\theta)$$
$$= x'\sin\theta\cos\phi + z'\cos\theta \qquad \text{[Figure 12.6(b)]} \qquad (12\text{-}15b)$$

$$r'\cos\psi = \mathbf{r}'\cdot\hat{\mathbf{a}}_r = (\hat{\mathbf{a}}_x x' + \hat{\mathbf{a}}_y y')\cdot(\hat{\mathbf{a}}_x \sin\theta\cos\phi + \hat{\mathbf{a}}_y \sin\theta\sin\phi + \hat{\mathbf{a}}_z\cos\theta)$$
$$= x'\sin\theta\cos\phi + y'\sin\theta\sin\phi \qquad \text{[Figure 12.6(c)]} \qquad (12\text{-}15c)$$

and the differential areas are represented by

$$ds' = dy'\,dz' \qquad \text{[Figure 12.6(a)]} \qquad (12\text{-}16a)$$
$$ds' = dx'\,dz' \qquad \text{[Figure 12.6(b)]} \qquad (12\text{-}16b)$$
$$ds' = dx'\,dy' \qquad \text{[Figure 12.6(c)]} \qquad (12\text{-}16c)$$

12.5.1 Uniform Distribution on an Infinite Ground Plane

The first aperture examined is a rectangular aperture mounted on an infinite ground plane, as shown in Figure 12.7. To reduce the mathematical complexities, initially the field over the opening is assumed to be constant and given by

$$\mathbf{E}_a = \hat{\mathbf{a}}_y E_0 \qquad -a/2 \le x' \le a/2, \quad -b/2 \le y' \le b/2 \qquad (12\text{-}17)$$

where E_0 is a constant. The task is to find the fields radiated by it, the pattern beamwidths, the side lobe levels of the pattern, and the directivity. To accomplish these, the equivalent will be formed first.

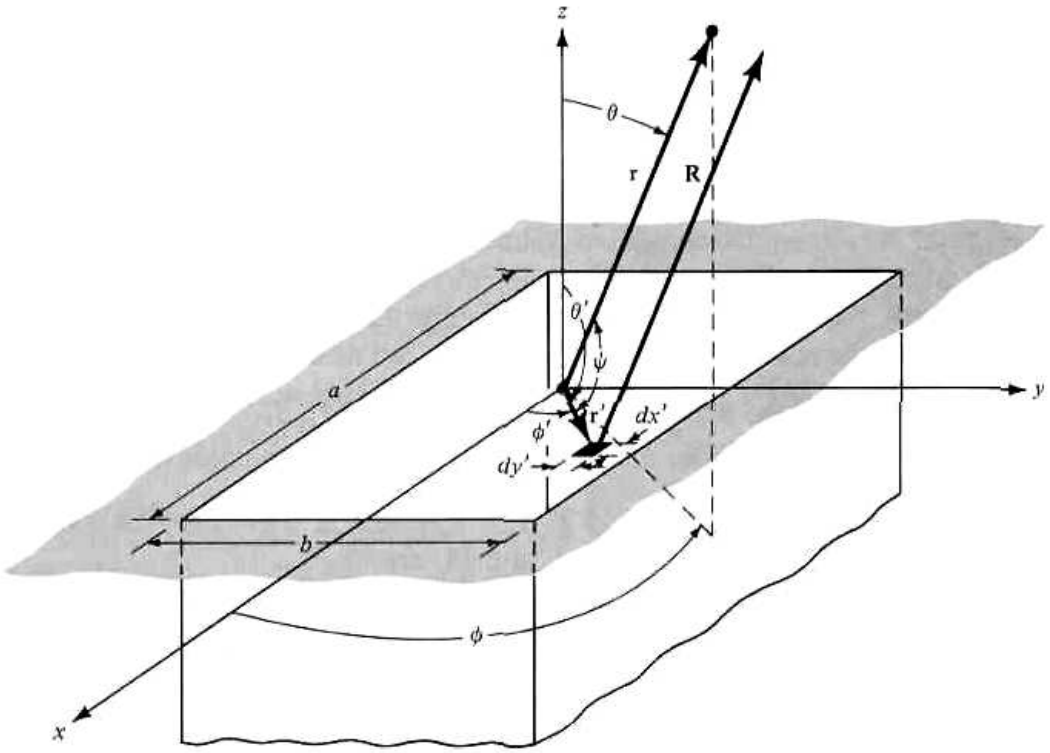

Figure 12.7 Rectangular aperture on an infinite electric ground plane.

A. Equivalent

To form the equivalent, a closed surface is chosen which extends from $-\infty$ to $+\infty$ on the x-y plane. Since the physical problem of Figure 12.7 is identical to that of Figure 12.5(a), its equivalents are those of Figures 12.5(a)–(e). Using the equivalent of Figure 12.5(e)

$$\mathbf{M}_s = \begin{cases} -2\hat{\mathbf{n}} \times \mathbf{E}_a = -2\hat{\mathbf{a}}_z \times \hat{\mathbf{a}}_y E_0 = +\hat{\mathbf{a}}_x 2E_0 & -a/2 \le x' \le a/2 \\ 0 & -b/2 \le y' \le b/2 \\ & \text{elsewhere} \end{cases} \qquad (12\text{-}18)$$

$$\mathbf{J}_s = 0 \qquad \text{everywhere}$$

B. Radiation Fields: Element and Space Factors

The far-zone fields radiated by the aperture of Figure 12.7 can be found by using (12-10a)–(12-10f), (12-12a)–(12–12d), (12-14c), (12-15c), (12-16c), and (12-18). Thus,

$$N_\theta = N_\phi = 0 \qquad (12\text{-}19)$$

$$L_\theta = \int_{-b/2}^{+b/2} \int_{-a/2}^{+a/2} [M_x \cos\theta \cos\phi]\, e^{jk(x'\sin\theta\cos\phi + y'\sin\theta\sin\phi)}\, dx'\, dy'$$

$$\boxed{L_\theta = \cos\theta\cos\phi \left[\int_{-b/2}^{+b/2} \int_{-a/2}^{+a/2} M_x e^{jk(x'\sin\theta\cos\phi + y'\sin\theta\sin\phi)}\, dx'\, dy' \right]} \qquad (12\text{-}19a)$$

In (12-19a), the integral within the brackets represents the *space factor* for a two-dimensional distribution. It is analogous to the space factor of (4-58a) for a line source (one-dimensional distribution). For the L_θ component of the vector potential $\mathbf{F}$, the *element factor* is equal to the product of the factor outside the brackets in (12-19a) and the factor outside the brackets in (12-10c). The total field is equal to the product of the element and space factors, as defined by (4-59), and expressed in (12-10b) and (12-10c).

Using the integral

$$\int_{-c/2}^{+c/2} e^{j\alpha z}\, dz = c \left[\frac{\sin\left(\frac{\alpha}{2} c\right)}{\frac{\alpha}{2} c} \right] \qquad (12\text{-}20)$$

(12-19a) reduces to

$$L_\theta = 2abE_0 \left[\cos\theta\cos\phi \left(\frac{\sin X}{X}\right)\left(\frac{\sin Y}{Y}\right) \right] \qquad (12\text{-}21)$$

where

$$X = \frac{ka}{2} \sin\theta\cos\phi \qquad (12\text{-}21a)$$

$$Y = \frac{kb}{2} \sin\theta\sin\phi \qquad (12\text{-}21b)$$

Similarly it can be shown that

$$L_\phi = -2abE_0 \left[\sin\phi \left(\frac{\sin X}{X}\right)\left(\frac{\sin Y}{Y}\right) \right] \qquad (12\text{-}22)$$

Substituting (12-19), (12-21), and (12-22) into (12-10a)–(12-10f), the fields radiated by the aperture can be written as

$$E_r = 0 \tag{12-23a}$$

$$E_\theta = j\frac{abkE_0e^{-jkr}}{2\pi r}\left[\sin\phi\left(\frac{\sin X}{X}\right)\left(\frac{\sin Y}{Y}\right)\right] \tag{12-23b}$$

$$E_\phi = j\frac{abkE_0e^{-jkr}}{2\pi r}\left[\cos\theta\cos\phi\left(\frac{\sin X}{X}\right)\left(\frac{\sin Y}{Y}\right)\right] \tag{12-23c}$$

$$H_r = 0 \tag{12-23d}$$

$$H_\theta = -\frac{E_\phi}{\eta} \tag{12-23e}$$

$$H_\phi = +\frac{E_\theta}{\eta} \tag{12-23f}$$

Equations (12-23a)–(12-23f) represent the three-dimensional distributions of the far-zone fields radiated by the aperture. Experimentally only two-dimensional plots can be measured. To reconstruct experimentally a three-dimensional plot, a series of two-dimensional plots must be made. In many applications, however, only a pair of two-dimensional plots are usually sufficient. These are the principal E- and H-plane patterns whose definition was stated in Section 2.2.2 and illustrated in Figure 2.3.

For the problem in Figure 12.7, the E-plane pattern is on the y-z plane ($\phi = \pi/2$) and the H-plane is on the x-z plane ($\phi = 0$). Thus

E-Plane ($\phi = \pi/2$)

$$E_r = E_\phi = 0 \tag{12-24a}$$

$$E_\theta = j\frac{abkE_0e^{-jkr}}{2\pi r}\left[\frac{\sin\left(\frac{kb}{2}\sin\theta\right)}{\frac{kb}{2}\sin\theta}\right] \tag{12-24b}$$

H-Plane ($\phi = 0$)

$$E_r = E_\theta = 0 \tag{12-25a}$$

$$E_\phi = j\frac{abkE_0e^{-jkr}}{2\pi r}\left\{\cos\theta\left[\frac{\sin\left(\frac{ka}{2}\sin\theta\right)}{\frac{ka}{2}\sin\theta}\right]\right\} \tag{12-25b}$$

To demonstrate the techniques, three-dimensional patterns have been plotted in Figures 12.8 and 12.9. The dimensions of the aperture are indicated in each figure. Multiple lobes appear, because the dimensions of the aperture are greater than one wavelength. The number of lobes increases as the dimensions increase. For the aperture whose dimensions are $a = 3\lambda$ and $b = 2\lambda$ (Figure 12.8), there are a total of five lobes in the principal H-plane and three lobes in the principal E-plane. The pattern in the H-plane is only a function of the dimension a whereas that in the E-plane is only influenced by b. In the E-plane, the side lobe formed on each side of the major lobe is a result of $\lambda < b \leq 2\lambda$. In the H-plane, the first minor lobe on each side of the major lobe is formed when $\lambda < a \leq 2\lambda$ and the second side lobe when $2\lambda < a$

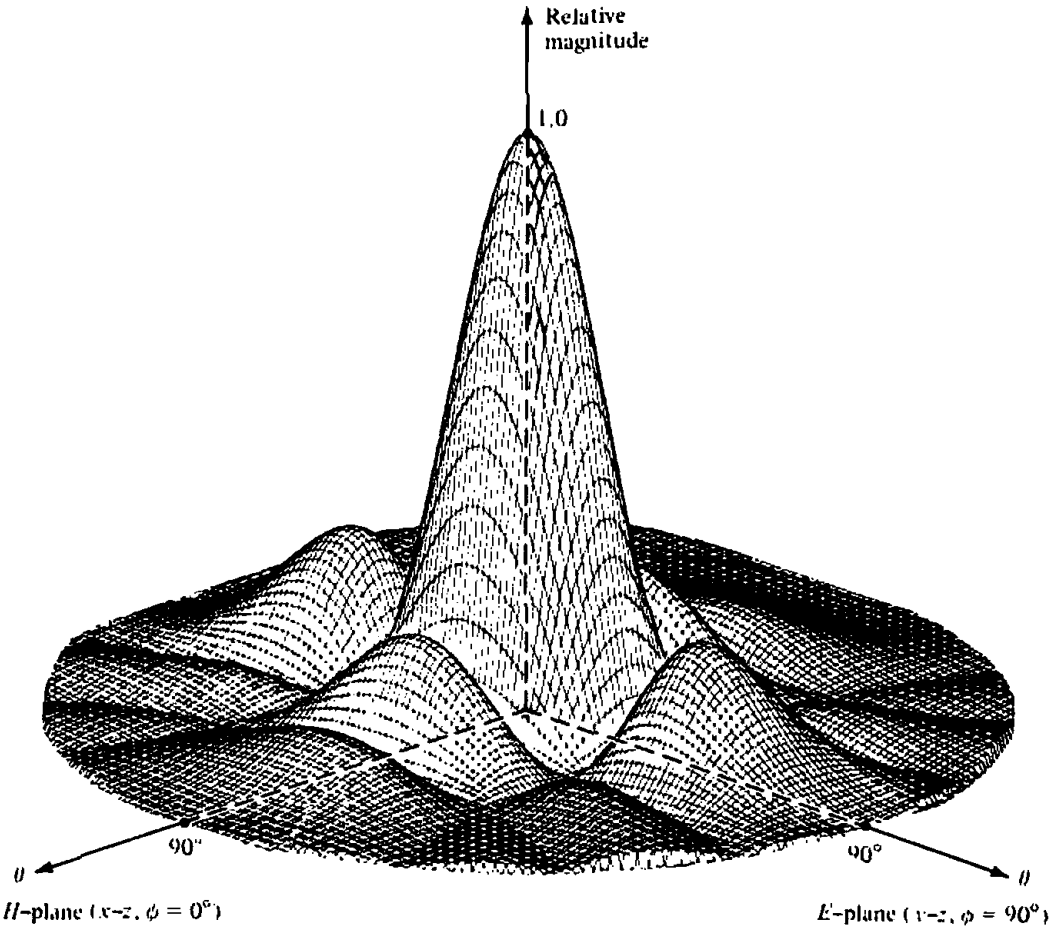

Figure 12.8 Three-dimensional field pattern of a constant field rectangular aperture mounted on an infinite ground plane ($a = 3\lambda$, $b = 2\lambda$).

$\leq 3\lambda$. Additional lobes are formed when one or both of the aperture dimensions increase. This is illustrated in Figure 12.9 for an aperture with $a = b = 3\lambda$.

The two-dimensional principal plane patterns for the aperture with $a = 3\lambda$, $b = 2\lambda$ are shown in Figure 12.10. For this and for all other size apertures mounted on an infinite ground plane, the H-plane patterns along the ground plane vanish. This is dictated by the boundary conditions. The E-plane patterns, in general, do not have to vanish along the ground plane, unless the dimension of the aperture in that plane (in this case b) is a multiple of a wavelength.

The patterns computed above assumed that the aperture was mounted on an infinite ground plane. In practice, infinite ground planes are not realizable, but they can be approximated by large structures. Edge effects, on the patterns of apertures mounted on finite size ground planes, can be accounted for by diffraction techniques. They will be introduced and illustrated in Section 12.9. Computed results, which include diffractions, agree extremely well with measurements [8]–[10].

C. Beamwidths

For the E-plane pattern given by (12-24b), the maximum radiation is directed along the z-axis ($\theta = 0$). The nulls (zeroes) occur when

$$\frac{kb}{2} \sin \theta|_{\theta = \theta_n} = n\pi, \qquad n = 1, 2, 3, \ldots \tag{12-26}$$

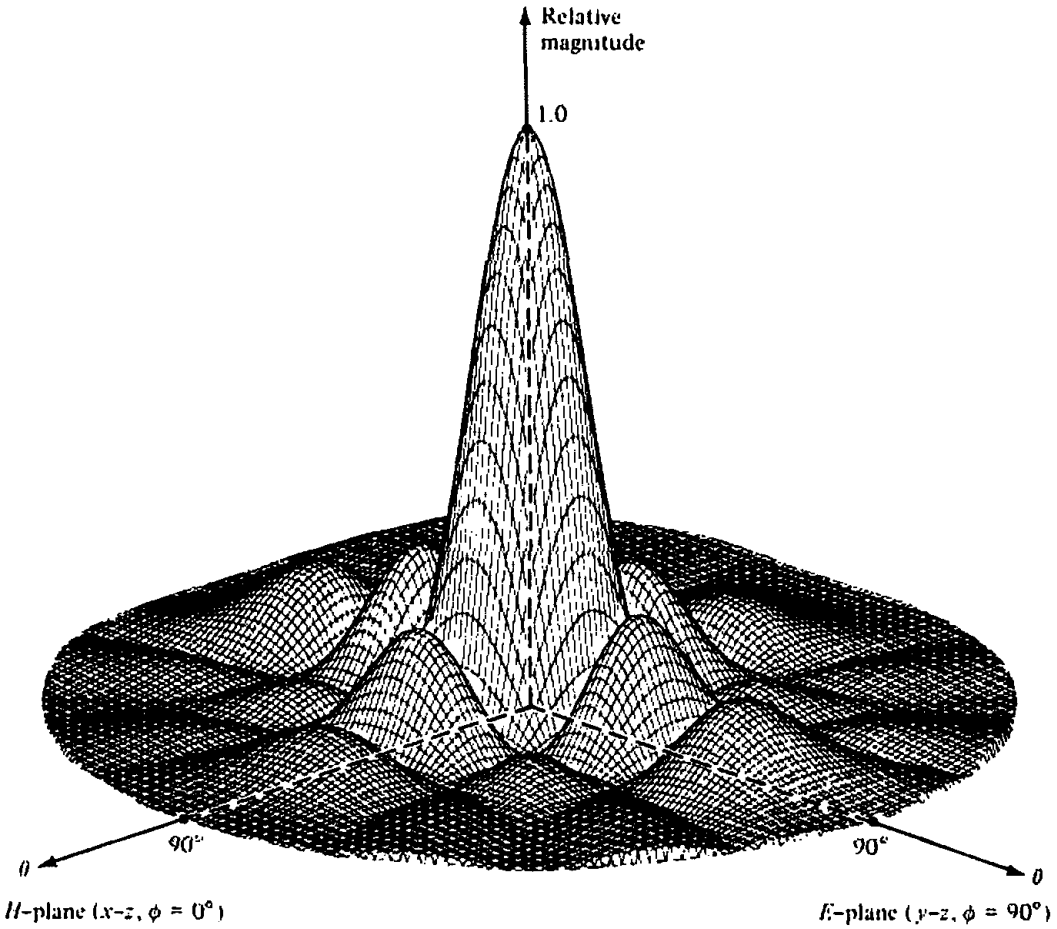

Figure 12.9 Three-dimensional field pattern of a constant field square aperture mounted on an infinite ground plane ($a = b = 3\lambda$).

or at the angles of

$$\theta_n = \sin^{-1}\left(\frac{2n\pi}{kb}\right) = \sin^{-1}\left(\frac{n\lambda}{b}\right) \text{ rad}$$
$$= 57.3 \sin^{-1}\left(\frac{n\lambda}{b}\right) \text{ degrees}, \quad n = 1, 2, 3, \ldots \tag{12-26a}$$

If $b \gg n\lambda$, (12-26a) reduces approximately to

$$\theta_n \approx \frac{n\lambda}{b} \text{ rad} = 57.3\left(\frac{n\lambda}{b}\right) \text{ degrees}, \quad n = 1, 2, 3, \ldots \tag{12-26b}$$

The total *beamwidth between nulls* is given by

$$\Theta_n = 2\theta_n = 2 \sin^{-1}\left(\frac{n\lambda}{b}\right) \text{ rad}$$
$$= 114.6 \sin^{-1}\left(\frac{n\lambda}{b}\right) \text{ degrees}, \quad n = 1, 2, 3, \ldots \tag{12-27}$$

or approximately (for large apertures, $b \gg n\lambda$) by

$$\Theta_n \approx \frac{2n\lambda}{b} \text{ rad} = 114.6\left(\frac{n\lambda}{b}\right) \text{ degrees}, \quad n = 1, 2, 3, \ldots \tag{12-27a}$$

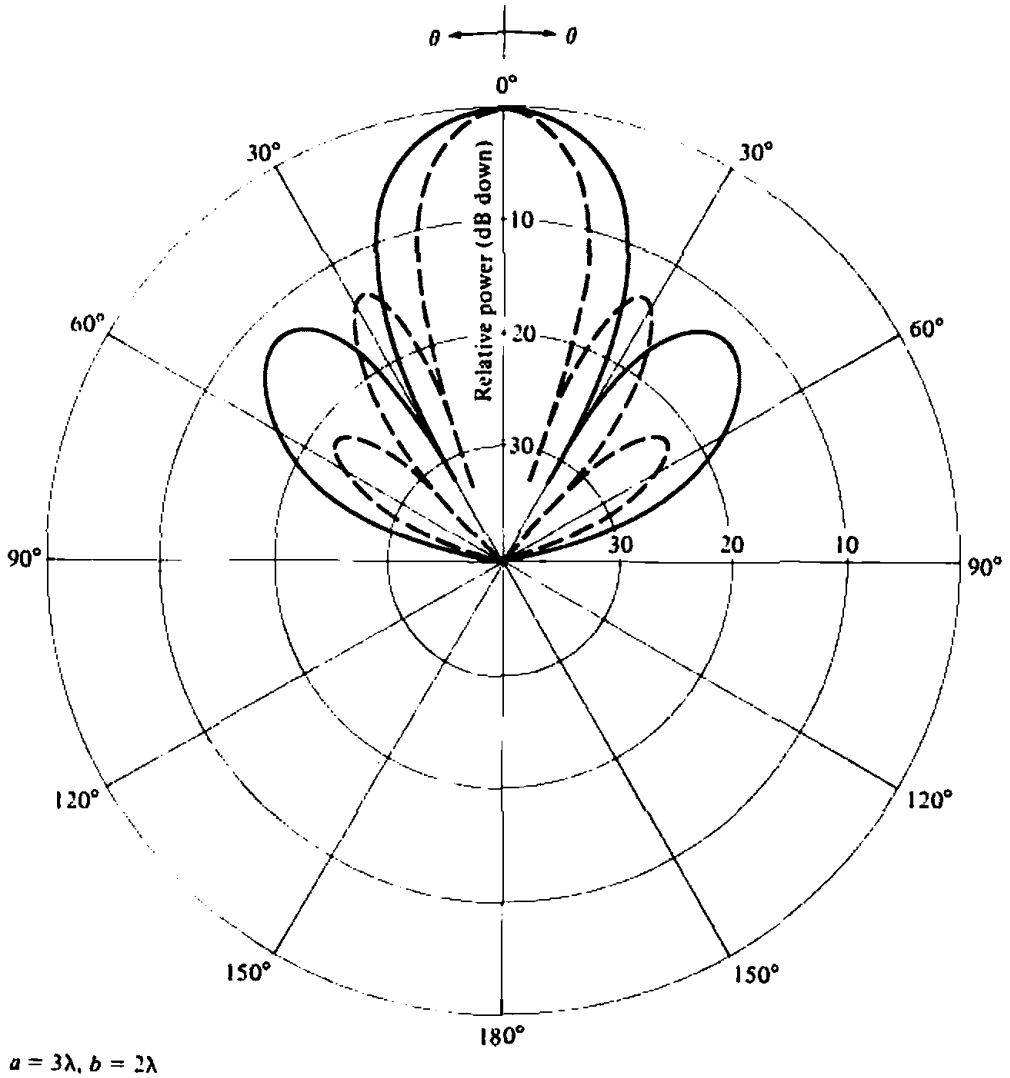

Figure 12.10 *E*- and *H*-plane amplitude patterns for uniform distribution aperture mounted on an infinite ground plane ($a = 3\lambda$, $b = 2\lambda$).

The *first null beamwidth* (FNBW) is obtained by letting $n = 1$.

The half-power point occurs when (see Appendix I)

$$\frac{kb}{2} \sin \theta\big|_{\theta=\theta_h} = 1.391 \tag{12-28}$$

or at an angle of

$$\begin{aligned} \theta_h &= \sin^{-1}\left(\frac{2.782}{kb}\right) = \sin^{-1}\left(\frac{0.443\lambda}{b}\right) \text{ rad} \\ &= 57.3 \sin^{-1}\left(\frac{0.443\lambda}{b}\right) \text{ degrees} \end{aligned} \tag{12-28a}$$

If $b \gg 0.443\lambda$, (12-28a) reduces approximately to

$$\theta_h \simeq \left(0.443 \frac{\lambda}{b}\right) \text{ rad} = 25.38 \left(\frac{\lambda}{b}\right) \text{ degrees} \tag{12-28b}$$

Thus the total *half-power beamwidth* (HPBW) is given by

$$\boxed{\Theta_h = 2\theta_h = 2\sin^{-1}\left(\frac{0.443\lambda}{b}\right)\text{ rad} = 114.6\sin^{-1}\left(\frac{0.443\lambda}{b}\right)\text{ degrees}} \tag{12-29}$$

or approximately (when $b \gg 0.443\lambda$) by

$$\boxed{\Theta_h \simeq \left(0.886\frac{\lambda}{b}\right)\text{ rad} = 50.8\left(\frac{\lambda}{b}\right)\text{ degrees}} \tag{12-29a}$$

The maximum of the first side lobe occurs when (see Appendix I)

$$\frac{kb}{2}\sin\theta\Big|_{\theta=\theta_s} = 4.494 \tag{12-30}$$

or at an angle of

$$\theta_s = \sin^{-1}\left(\frac{8.988}{kb}\right) = \sin^{-1}\left(\frac{1.43\lambda}{b}\right)\text{ rad} = 57.3\sin^{-1}\left(\frac{1.43\lambda}{b}\right)\text{ degrees} \tag{12-30a}$$

If $b \gg 1.43\lambda$, (12-30a) reduces to

$$\theta_s \simeq 1.43\left(\frac{\lambda}{b}\right)\text{ rad} = 81.9\left(\frac{\lambda}{b}\right)\text{ degrees} \tag{12-30b}$$

The total beamwidth between first side lobes (FSLBW) is given by

$$\boxed{\Theta_s = 2\theta_s = 2\sin^{-1}\left(\frac{1.43\lambda}{b}\right)\text{ rad} = 114.6\sin^{-1}\left(\frac{1.43\lambda}{b}\right)\text{ degrees}} \tag{12-30c}$$

or approximately (when $b \gg 1.43\lambda$) by

$$\boxed{\Theta_s \simeq 2.86\left(\frac{\lambda}{b}\right)\text{ rad} = 163.8\left(\frac{\lambda}{b}\right)\text{ degrees}} \tag{12-30d}$$

D. Side Lobe Level

The maximum of (12-24b) at the first side lobe is given by (see Appendix I)

$$\boxed{|E_\theta(\theta = \theta_s)| = \left|\frac{\sin(4.494)}{4.494}\right| = 0.217 = -13.26\text{ dB}} \tag{12-31}$$

which is 13.26 dB down from the maximum of the main lobe.

An approximate value of the maximum of the first side lobe can be obtained by assuming that the maximum of (12-24b) occurs when its numerator is maximum. That is, when

$$\frac{kb}{2}\sin\theta\Big|_{\theta=\theta_s} \simeq \frac{3\pi}{2} \tag{12-32}$$

Thus,

$$\boxed{|E_\theta(\theta = \theta_s)| \simeq \frac{1}{3\pi/2} = 0.212 = -13.47 \text{ dB}} \tag{12-33}$$

These values are very close to the exact ones given by (12-31).

A similar procedure can be followed to find the nulls, 3-dB points, beamwidth between nulls and 3-dB points, angle where the maximum of first side lobe occurs, and its magnitude at that point for the H-plane pattern of (12-25b). A comparison between the E- and H-plane patterns of (12-24b) and (12-25b) shows that they are similar in form except for the additional cos θ term that appears in (12-25b). An examination of the terms in (12-25b) reveals that the cos θ term is a much slower varying function than the $\sin(ka \sin \theta/2)/(ka \sin \theta/2)$ term, especially when a is large.

As a first approximation, (12-26)–(12-33), with b replaced by a, can also be used for the H-plane. More accurate expressions can be obtained by also including the cos θ term. In regions well removed from the major lobe, the inclusion of the cos θ term becomes more essential for accurate results.

E. Directivity

The directivity for the aperture can be found using (12-23a)–(12-23c), (12-13)–(12-13a), and (2-19)–(2-22). The analytical details using this procedure, especially the integration to compute the radiated power (P_{rad}), are more cumbersome.

Because the aperture is mounted on an infinite ground plane, an alternate and much simpler method can be used to compute the radiated power. The average power density is first formed using the fields at the aperture, and it is then integrated over the physical bounds of the opening. The integration is confined to the physical bounds of the opening. Using Figure 12.7 and assuming that the magnetic field at the aperture is given by

$$\mathbf{H}_a = -\hat{\mathbf{a}}_x \frac{E_0}{\eta} \tag{12-34}$$

where η is the intrinsic impedance, the radiated power reduces to

$$P_{\text{rad}} = \oint_S \mathbf{W}_{\text{av}} \cdot d\mathbf{s} = \frac{|E_0|^2}{2\eta} \iint_{S_a} ds = ab \frac{|E_0|^2}{2\eta} \tag{12-35}$$

The maximum radiation intensity ($U_{\max}$), using the fields of (12-23a)–(12-23b), occurs toward $\theta = 0°$ and it is equal to

$$U_{\max} = \left(\frac{ab}{\lambda}\right)^2 \frac{|E_0|^2}{2\eta} \tag{12-36}$$

Thus the directivity is equal to

$$\boxed{D_0 = \frac{4\pi U_{\max}}{P_{\text{rad}}} = \frac{4\pi}{\lambda^2} ab = \frac{4\pi}{\lambda^2} A_p = \frac{4\pi}{\lambda^2} A_{\text{em}}} \tag{12-37}$$

where

A_p = physical area of the aperture

A_{em} = maximum effective area of the aperture

Using the definition of (2-110), it is shown that *the physical and maximum effective areas of a constant distribution aperture are equal.*

The beamwidths, side lobe levels, and directivity of this and other apertures are summarized in Table 12.1.

Example 12.2

A rectangular aperture with a constant field distribution, with $a = 3\lambda$ and $b = 2\lambda$, is mounted on an infinite ground plane. Compute the

(a) FNBW in the E-plane
(b) HPBW in the E-plane
(c) FSLBW in the E-plane
(d) FSLMM in the E-plane
(e) directivity using (12-37)
(f) directivity using the DIRECTIVITY computer program at the end of Chapter 2, the fields of (12-23a)–(12-23f), and the formulation of Section 12.4

SOLUTION

(a) Using (12-27)

$$\Theta_1 = 114.6 \sin^{-1}(\tfrac{1}{2}) = 114.6(0.524) = 60°$$

(b) Using (12-29)

$$\Theta_h = 114.6 \sin^{-1}\left(\frac{0.443}{2}\right) = 114.6(0.223) = 25.6°$$

(c) Using (12-30c)

$$\Theta_s = 2\theta_s = 114.6 \sin^{-1}\left(\frac{1.43}{2}\right) = 114.6(0.796) = 91.3°$$

(d) Using (12-31)

$$|E_\theta|_{\theta=\theta_1} = 0.217 \simeq -13.26 \text{ dB}$$

(e) Using (12-37)

$$D_0 = 4\pi(3)(2) = 75.4 = 18.77 \text{ dB}$$

(f) Using the computer program at the end of Chapter 2

$$D_0 \simeq 80.4 \simeq 19.05 \text{ dB}$$

The difference in directivity values using (12-37) and the computer program is not attributed to the accuracy of the numerical method. The main contributor is the aperture tangential magnetic field of (12-34), which was assumed to be related to the aperture tangential electric field by the intrinsic impedance. Although this is a good assumption for large size apertures, it is not exact. Therefore the directivity value computed using the computer program should be considered to be the more accurate.

12.5.2 Uniform Distribution in Space

The second aperture examined is that of Figure 12.7 when it is *not* mounted on an infinite ground plane. The field distribution is given by

$$\left.\begin{aligned} \mathbf{E}_a &= \hat{\mathbf{a}}_y E_0 \\ \mathbf{H}_a &= -\hat{\mathbf{a}}_x \frac{E_0}{\eta} \end{aligned}\right\} \qquad \begin{aligned} -a/2 \le x' \le a/2 \\ -b/2 \le y' \le b/2 \end{aligned} \tag{12-38}$$

where E_0 is a constant. The geometry of the opening for this problem is identical to the previous one. However the equivalents and radiated fields are different, because this time the aperture is not mounted on an infinite ground plane.

A. Equivalent

To form the equivalent, a closed surface is chosen which again extends from $-\infty$ to $+\infty$ on the x-y plane. Over the entire surface $\mathbf{J}_s$ and $\mathbf{M}_s$ are formed. The difficulty encountered in this problem is that both $\mathbf{J}_s$ and $\mathbf{M}_s$ are not zero outside the opening, and expressions for them are not known there. The replacement of the semi-infinite medium to the left of the boundary (negative z) by an imaginary electric or magnetic conductor only eliminates one or the other current densities ($\mathbf{J}_s$ or $\mathbf{M}_s$) but not both. Thus, even though an exact equivalent for this problem exists in principle, it cannot be used practically because the fields outside the opening are not known *a priori*. We are therefore forced to adopt an approximate equivalent.

The usual and most accurate relaxation is to assume that both $\mathbf{E}_a$ and $\mathbf{H}_a$ (and in turn $\mathbf{M}_s$ and $\mathbf{J}_s$) exist over the opening but are zero outside it. It has been shown, by comparison with measurements and other available data, that this approximate equivalent yields the best results.

B. Radiated Fields

Using a procedure similar to that of the previous section, the radiation characteristics of this aperture can be derived. A summary of them is shown in Table 12.1.

The field components of this aperture are identical in form to those of the aperture when it is mounted on an infinite ground plane if the $(1 + \cos\theta)$ term in each component is replaced by 2. Thus for small values of θ (in the main lobe and especially near its maximum), the patterns of the two apertures are almost identical. This procedure can be used, in general, to relate the fields of an aperture when it is and it is not mounted on an infinite ground plane. However, the coordinate system chosen must have the z-axis perpendicular to the aperture.

A three-dimensional pattern for an aperture with $a = 3\lambda$, $b = 2\lambda$ was computed, and it is shown in Figure 12.11. The dimensions of this aperture are the same as those of Figure 12.8. However the angular limits over which the radiated fields now exist have been extended to $0° \le \theta \le 180°$. Although the general structures of the two patterns are similar, they are not identical. Becuse of the enlarged space over which fields now exist, additional minor lobes are formed.

C. Beamwidths and Side Lobe Levels

To find the beamwidths and the angle at which the maximum of the side lobe occurs, it is usually assumed that the $(1 + \cos\theta)$ term is a much slower varying function than the $\sin(ka \sin\theta/2)/(ka \sin\theta/2)$ or the $\sin(kb \sin\theta/2)/(kb \sin\theta/2)$ terms. This is an approximation, and it is more valid for large apertures (large a and/or b) and for

Table 12.1 EQUIVALENTS, FIELDS, BEAMWIDTHS, SIDE LOBE LEVELS, AND DIRECTIVITIES OF RECTANGULAR APERTURES

	Uniform Distribution Aperture on Ground Plane	Uniform Distribution Aperture in Free-Space	TE_{10}-Mode Distribution Aperture on Ground Plane
Aperture distribution of tangential components (analytical)	$\mathbf{E}_a = \hat{\mathbf{a}}_y E_0 \Big\} \begin{matrix} -a/2 \le x' \le a/2 \\ -b/2 \le y' \le b/2 \end{matrix}$	$\mathbf{E}_a = \hat{\mathbf{a}}_y E_0$ $\mathbf{H}_a = -\hat{\mathbf{a}}_x \frac{E_0}{\eta} \Big\} \begin{matrix} -a/2 \le x' \le a/2 \\ -b/2 \le y' \le b/2 \end{matrix}$	$\mathbf{E}_a = \hat{\mathbf{a}}_y E_0 \cos\left(\frac{\pi}{a}x'\right) \begin{matrix} -a/2 \le x' \le a/2 \\ -b/2 \le y' \le b/2 \end{matrix}$
Aperture distribution of tangential components (graphical)	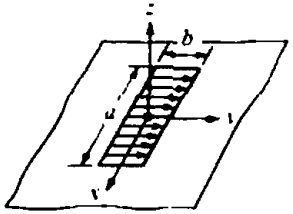	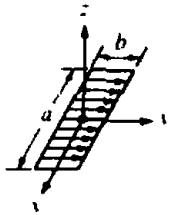	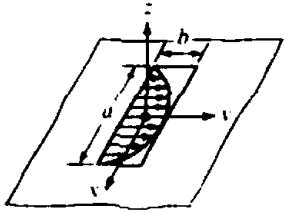
Equivalent	$\mathbf{M}_s = \begin{cases} -2\hat{\mathbf{n}} \times \mathbf{E}_a & \begin{matrix} -a/2 \le x' \le a/2 \\ -b/2 \le y' \le b/2 \end{matrix} \\ 0 & \text{elsewhere} \end{cases}$ $\mathbf{J}_s = 0$ everywhere	$\mathbf{M}_s = -\hat{\mathbf{n}} \times \mathbf{E}_a$ $\mathbf{J}_s = \hat{\mathbf{n}} \times \mathbf{H}_a \Big\} \begin{matrix} -a/2 \le x' \le a/2 \\ -b/2 \le y' \le b/2 \end{matrix}$ $\mathbf{M}_s \simeq \mathbf{J}_s \simeq 0$ elsewhere	$\mathbf{M}_s = \begin{cases} -2\hat{\mathbf{n}} \times \mathbf{E}_a & \begin{matrix} -a/2 \le x' \le a/2 \\ -b/2 \le y' \le b/2 \end{matrix} \\ 0 & \text{elsewhere} \end{cases}$ $\mathbf{J}_s = 0$ everywhere
Far-zone fields $X = \frac{ka}{2}\sin\theta\cos\phi$ $Y = \frac{kb}{2}\sin\theta\sin\phi$ $C = j\frac{abkE_0 e^{-jkr}}{2\pi r}$	$E_r = H_r = 0$ $E_\theta = C\sin\phi\frac{\sin X}{X}\frac{\sin Y}{Y}$ $E_\phi = C\cos\theta\cos\phi\frac{\sin X}{X}\frac{\sin Y}{Y}$ $H_\theta = -E_\phi/\eta$ $H_\phi = E_\theta/\eta$	$E_r = H_r = 0$ $E_\theta = \frac{C}{2}\sin\phi(1+\cos\theta)\frac{\sin X}{X}\frac{\sin Y}{Y}$ $E_\phi = \frac{C}{2}\cos\phi(1+\cos\theta)\frac{\sin X}{X}\frac{\sin Y}{Y}$ $H_\theta = -E_\phi/\eta$ $H_\phi = E_\theta/\eta$	$E_r = H_r = 0$ $E_\theta = -\frac{\pi}{2}C\sin\phi\frac{\cos X}{(X)^2 - \left(\frac{\pi}{2}\right)^2}\frac{\sin Y}{Y}$ $E_\phi = -\frac{\pi}{2}C\cos\theta\cos\phi\frac{\cos X}{(X)^2 - \left(\frac{\pi}{2}\right)^2}\frac{\sin Y}{Y}$ $H_\theta = -E_\phi/\eta$ $H_\phi = E_\theta/\eta$

Table 12.1 (Continued)

Half-power beamwidth (degrees)	*E*-plane $b \gg \lambda$	$\frac{50.6}{b/\lambda}$	$\frac{50.6}{b/\lambda}$	$\frac{50.6}{b/\lambda}$
	H-plane $a \gg \lambda$	$\frac{50.6}{a/\lambda}$	$\frac{50.6}{a/\lambda}$	$\frac{68.8}{a/\lambda}$
First null beamwidth (degrees)	*E*-plane $b \gg \lambda$	$\frac{114.6}{b/\lambda}$	$\frac{114.6}{b/\lambda}$	$\frac{114.6}{b/\lambda}$
	H-plane $a \gg \lambda$	$\frac{114.6}{a/\lambda}$	$\frac{114.6}{a/\lambda}$	$\frac{171.9}{a/\lambda}$
First side lobe max. (to main max.) (dB)	*E*-plane	-13.26	-13.26	-13.26
	H-plane	-13.26 $a \gg \lambda$	-13.26 $a \gg \lambda$	-23 $a \gg \lambda$
Directivity D_0 (dimensionless)		$\frac{4\pi}{\lambda^2}(\text{area}) = 4\pi\left(\frac{ab}{\lambda^2}\right)$	$\frac{4\pi}{\lambda^2}(\text{area}) = 4\pi\left(\frac{ab}{\lambda^2}\right)$	$\frac{8}{\pi^2}\left[4\pi\left(\frac{ab}{\lambda^2}\right)\right] = 0.81\left[4\pi\left(\frac{ab}{\lambda^2}\right)\right]$

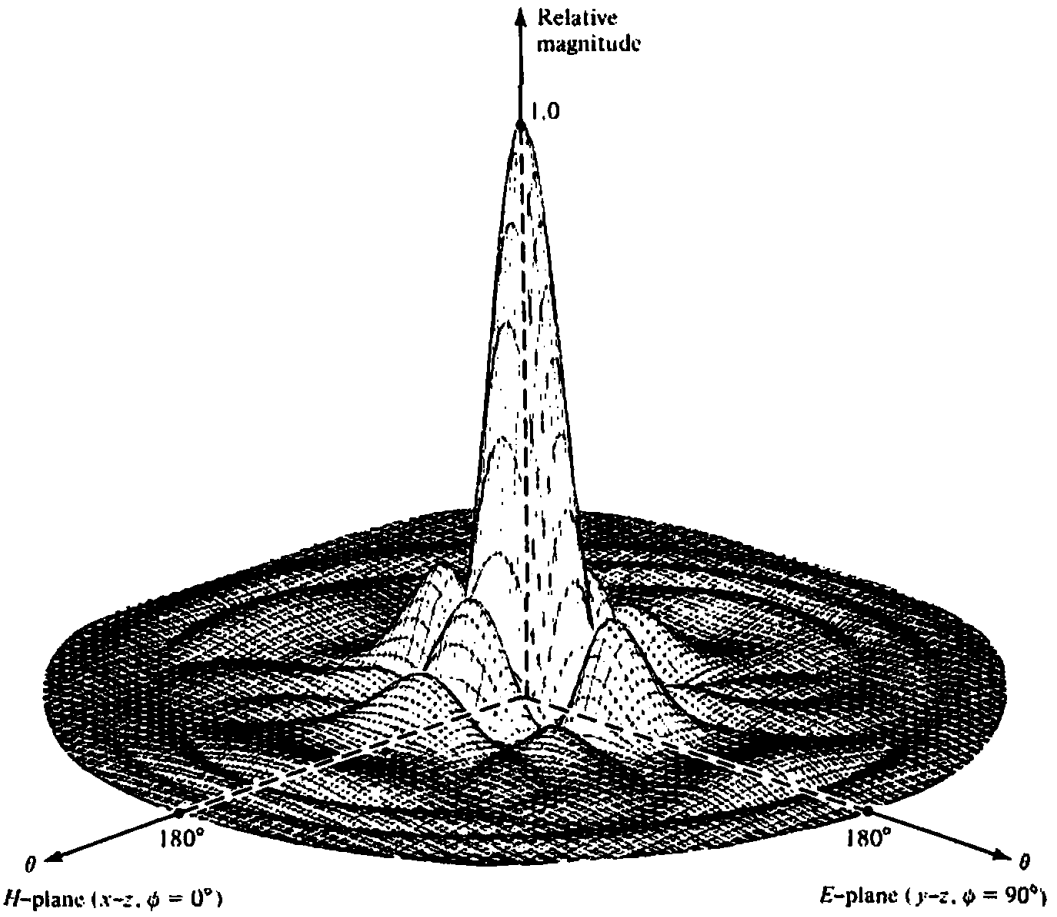

Figure 12.11 Three-dimensional field pattern of a constant field rectangular aperture ($a = 3\lambda$, $b = 2\lambda$).

angles near the main maximum. More accurate results can be obtained by considering the $(1 + \cos\theta)$ term. Thus (12-26)–(12-33) can be used, to a good approximation, to compute the beamwidths and side lobe level. A summary is included in Table 12.1.

D. Directivity

Although the physical geometry of the opening of this problem is identical to that of Section 12.5.1, their directivities are not identical. This is evident by examining their far-zone field expressions or by realizing that the fields outside the aperture along the x-y plane are not exactly the same.

To derive an exact expression for the directivity of this aperture would be a very difficult task. Since the patterns of the apertures are nearly the same, especially at the main lobe, their directivities are almost the same. To verify this, an example is taken.

Example 12.3

Repeat the problem of Example 12.2 for an aperture that is not mounted on an infinite ground plane.

SOLUTION

Since the E-plane patterns of the two apertures are identical, the FNBW, HPBW, FSLBW, and FSLMM are the same. The directivities as computed by (12-37), are

also the same. Since the fields radiated by the two apertures are not identical, their directivities computed using the far-zone fields will not be exactly the same. Therefore for this problem

$$D_0 \simeq 81.16 \text{ (dimensionless)} = 19.09 \text{ dB}$$

As with Example 12.2, the directivities computed using (12-37) and the computer program do not agree exactly. For this problem, however, neither one is exact. For (12-37), it has been assumed that the aperture tangential magnetic field is related to the aperture tangential electric field by the intrinsic impedance η. This relationship is good but not exact. For the computer program, the formulation is based on the equivalent of this section where the fields outside the aperture were assumed to be negligible. Again this is a good assumption for some problems, but it is not exact.

A summary of the radiation characteristics of this aperture is included in Table 12.1 where it is compared with that of other apertures.

12.5.3 TE_{10}-Mode Distribution on an Infinite Ground Plane

In practice, a commonly used aperture antenna is that of a rectangular waveguide mounted on an infinite ground plane. At the opening, the field is usually approximated by the dominant TE_{10}-mode. Thus

$$\mathbf{E}_a = \hat{\mathbf{a}}_y E_0 \cos\left(\frac{\pi}{a}x'\right) \qquad \begin{cases} -a/2 \le x' \le +a/2 \\ -b/2 \le y' \le +b/2 \end{cases} \tag{12-39}$$

A. Equivalent, Radiated Fields, Beamwidths, and Side Lobe Levels

Because the physical geometry of this antenna is identical to that of Figure 12.7, their equivalents and the procedure to analyze each one are identical. They differ only in the field distribution over the aperture.

The details of the analytical formulation are not included. However, a summary of its radiation characteristics is included in Table 12.1. The E-plane pattern of this aperture is identical in form (with the exception of a normalization factor) to the E-plane of the aperture of Section 12.5.1. This is expected, since the TE_{10}-mode field distribution along the E-plane (y-z plane) is also a constant. That is not the case for the H-plane or at all other points removed from the principal planes. To demonstrate that, a three-dimensional pattern for the TE_{10}-mode aperture with $a = 3\lambda$, $b = 2\lambda$ was computed and it is shown in Figure 12.12. This pattern should be compared with that of Figure 12.8.

The expressions for the beamwidths and side lobe level in the E-plane are identical to those given by (12-26)–(12-33). However those for the H-plane are more complex, and a simple procedure is not available. Computations for the HPBW, FNBW, FSLBW, FSLMM in the E- and H-planes were made, and they are shown graphically in Figures 12.13 and 12.14.

B. Directivity and Aperture Efficiency

The directivity of this aperture is found in the same manner as that of the uniform distribution aperture of Section 12.5.1. Using the aperture electric field of (12-39),

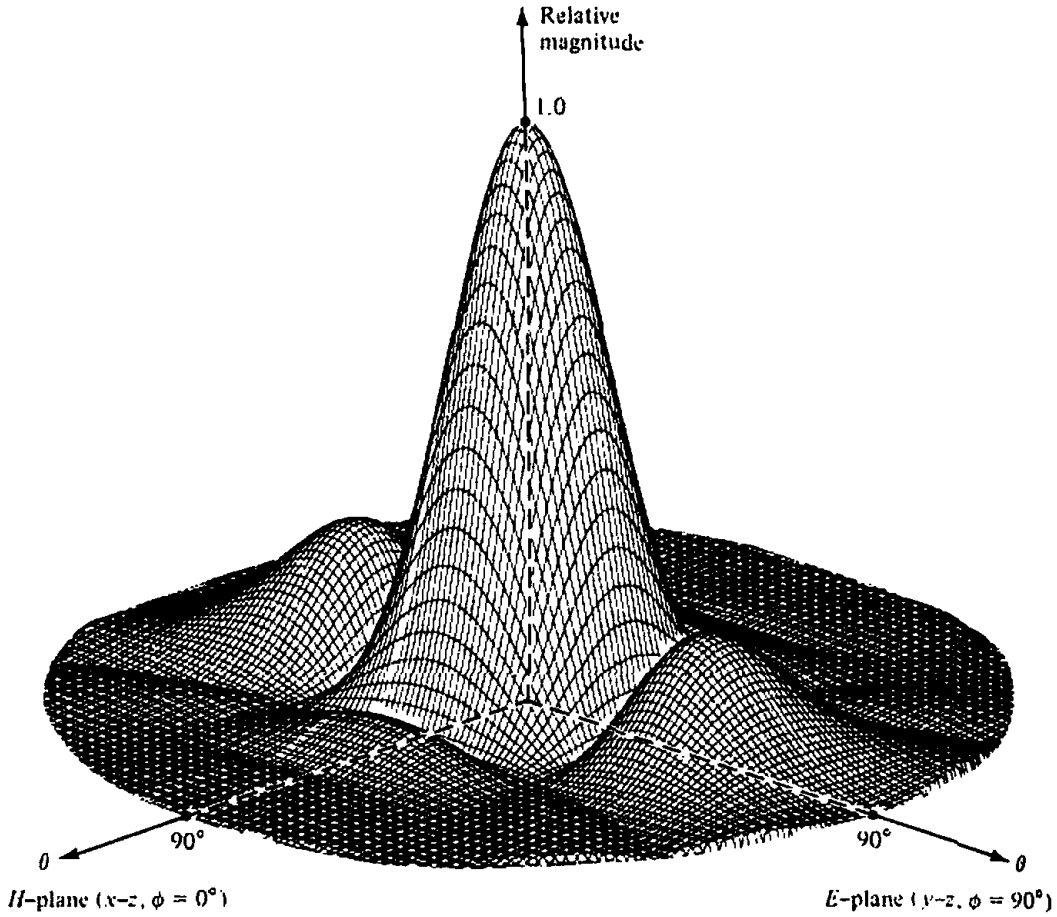

Figure 12.12 Three-dimensional field pattern of a TE_{10}-mode rectangular waveguide mounted on an infinite ground plane ($a = 3\lambda$, $b = 2\lambda$).

and assuming that the aperture magnetic field is related to the electric field by the intrinsic impedance η, the radiated power can be written as

$$P_{\text{rad}} = \oiint_S \mathbf{W}_{\text{av}} \cdot d\mathbf{s} = ab\frac{|E_0|^2}{4\eta} \tag{12-39a}$$

The maximum radiation intensity occurs at $\theta = 0°$, and it is given by

$$U_{\max} = \frac{8}{\pi^2}\left(\frac{ab}{\lambda}\right)^2 \frac{|E_0|^2}{4\eta} \tag{12-39b}$$

Thus the directivity is equal to

$$D_0 = \frac{8}{\pi^2}\left[ab\left(\frac{4\pi}{\lambda^2}\right)\right] = 0.81\left[ab\left(\frac{4\pi}{\lambda^2}\right)\right] = 0.81A_p\left(\frac{4\pi}{\lambda^2}\right) = A_{\text{em}}\left(\frac{4\pi}{\lambda^2}\right) \tag{12-39c}$$

In general, the maximum effective area A_{em} is related to the physical area A_p by

$$A_{\text{em}} = \epsilon_{\text{ap}} A_p, \qquad 0 \le \epsilon_{\text{ap}} \le 1 \tag{12-40}$$

where ϵ_{ap} is the aperture efficiency. For this problem $\epsilon_{\text{ap}} = 8/\pi^2 \simeq 0.81$. The aperture efficiency is a figure-of-merit which indicates how efficiently the physical area of the antenna is utilized. Typically, aperture antennas have aperture efficiencies from about

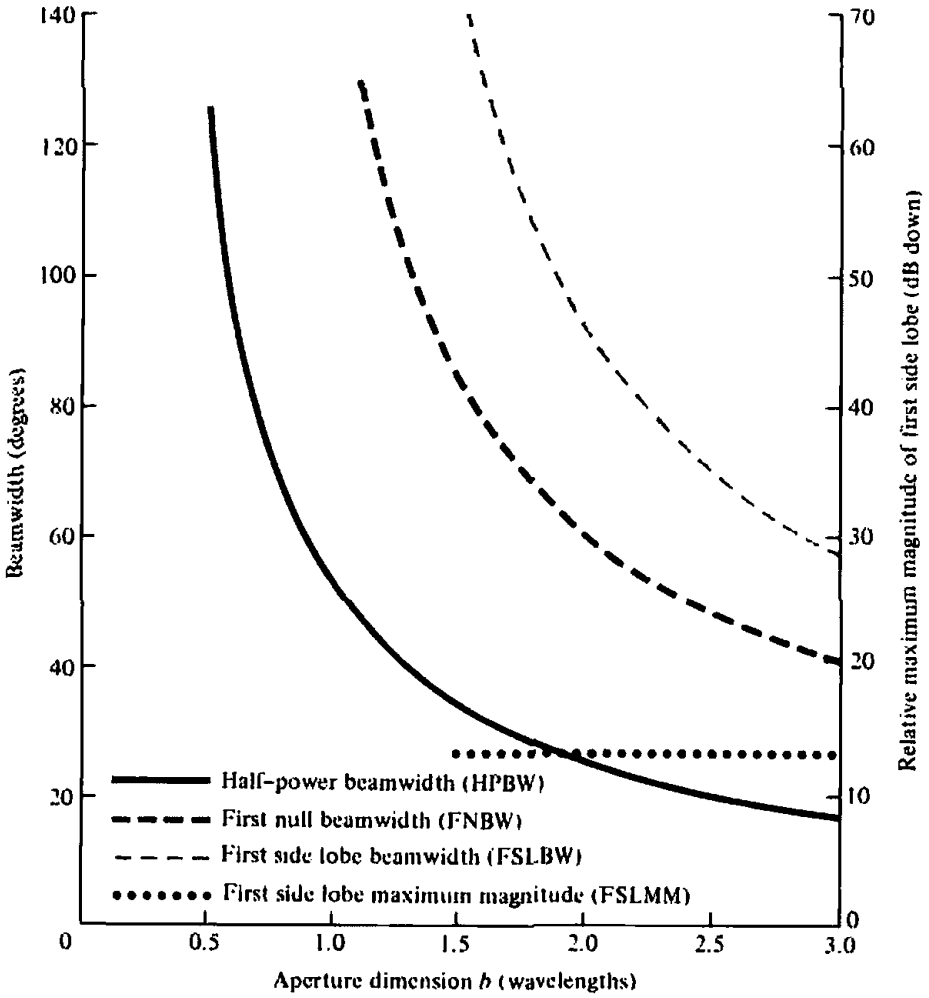

Figure 12.13 E-plane beamwidths and first side lobe relative maximum magnitude for TE_{10}-mode rectangular waveguide mounted on an infinite ground plane.

30% to 90%, horns from 35% to 80% (optimum gain horns have $\epsilon_{ap} \simeq 50\%$), and circular reflectors from 50% to 80%.

For reflectors, the aperture efficiency is a function of many factors. The most prominent are the spillover, amplitude taper, phase distribution, polarization uniformity, blockage, and surface random errors. These are discussed in detail in Section 15.4.1 of Chapter 15.

12.5.4 Beam Efficiency

The beam efficiency for an antenna was introduced in Section 2.10 and was defined by (2-53). When the aperture is mounted on the x-y plane, the beam efficiency can be calculated using (2-54). The beam efficiency can be used to judge the ability of the antenna to discriminate between signals received through its main lobe and those through the minor lobes. Beam efficiencies for rectangular apertures with different aperture field distributions are plotted, versus the half-cone angle θ_1, in Figure 12.15 [11]. The uniform field distribution aperture has the least ability to discriminate between main lobe and minor lobe signals. The aperture radiates in an unbounded medium, and it is not mounted on an infinite ground plane. The lower abscissa scale is in terms of θ_1 (in degrees), and it should be used only when $a = b = 20\lambda$. The upper abscissa scale is in terms of $u[u = (ka/2)\sin\theta_1 = (kb/2)\sin\theta_1]$, and it should be used for any square aperture.

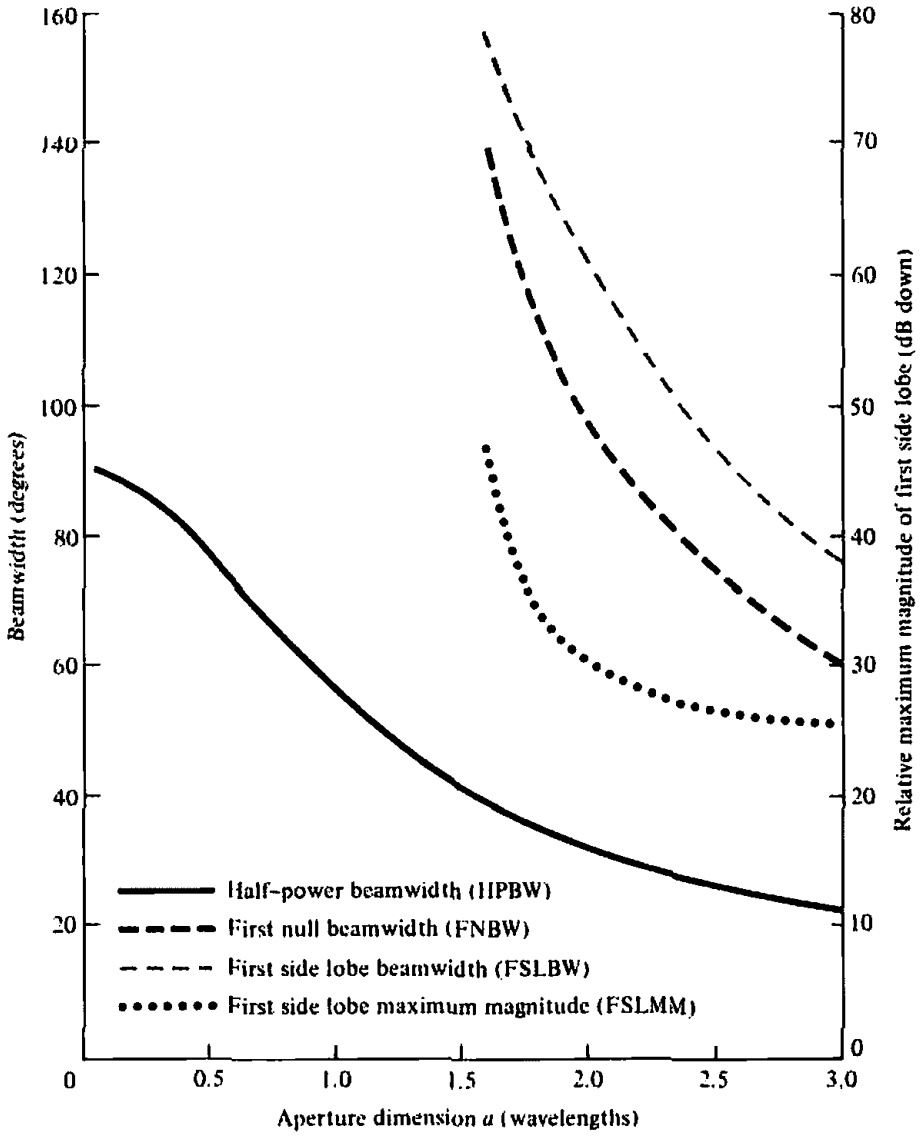

Figure 12.14 *H*-plane beamwidths and first side lobe relative maximum magnitude for TE_{10}-mode rectangular waveguide mounted on an infinite ground plane.

Example 12.4

Determine the beam efficiency, within a cone of half-angle $\theta_1 = 10°$, for a square aperture with uniform field distribution and with

(a) $a = b = 20\lambda$

(b) $a = b = 3\lambda$

SOLUTION

The solution is carried out using the curves of Figure 12.15.

(a) When $a = b = 20\lambda$, the lower abscissa scale can be used. For $\theta_1 = 10°$, the efficiency for the uniform aperture is about 94%.

(b) For $a = b = 3\lambda$ and $\theta_1 = 10°$

$$u = \frac{ka}{2}\sin\theta_1 = 3\pi\sin(10°) = 1.64$$

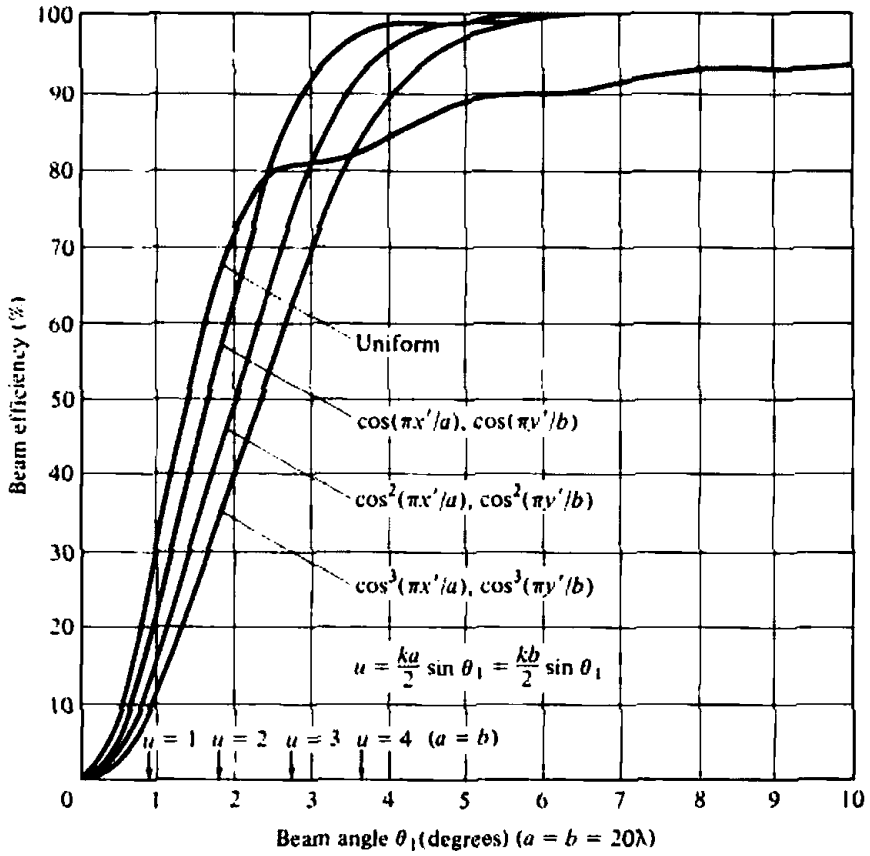

Figure 12.15 Beam efficiency versus half-cone angle θ_1, for a square aperture with different field distributions. The aperture is not mounted on an infinite ground plane. (SOURCE: D. G. Fink (ed.), *Electronics Engineers' Handbook*, Section 18 (by W. F. Croswell), McGraw-Hill, New York, 1975)

Using the upper abscissa scale, the efficiency for the uniform aperture at $u = 1.64$ is about 58%.

12.6 CIRCULAR APERTURES

A widely used microwave antenna is the circular aperture. One of the attractive features of this configuration is its simplicity in construction. In addition, closed form expressions for the fields of all the modes that can exist over the aperture can be obtained.

The procedure followed to determine the fields radiated by a circular aperture is identical to that of the rectangular, as summarized in Section 12.3. The primary differences lie in the formulation of the equivalent current densities (J_x, J_y, J_z, M_x, M_y, M_z), the differential paths from the source to the observation point ($r' \cos \psi$), and the differential area (ds'). Before an example is considered, these differences will be reformulated for the circular aperture.

Because of the circular profile of the aperture, it is often convenient and desirable to adopt cylindrical coordinates for the solution of the fields. In most cases, therefore, the electric and magnetic field components over the circular opening will be known in cylindrical form; that is, E_ρ, E_ϕ, E_z, H_ρ, H_ϕ, and H_z. Thus the components of the equivalent current densities $\mathbf{M}_s$ and $\mathbf{J}_s$ would also be conveniently expressed in cylindrical form (M_ρ, M_ϕ, M_z, J_ρ, J_ϕ, J_z). In addition, the required integration over the

aperture to find N_θ, N_ϕ, L_θ, and L_ϕ of (12-12a)–(12-12d) should also be done in cylindrical coordinates. It is then desirable to reformulate $r' \cos\psi$ and ds', as given by (12-15a)–(12-16c).

The most convenient position for placing the aperture is that shown in Figure 12.16 (aperture on x-y plane). The transformation between the rectangular and cylindrical components of $\mathbf{J}_s$ is given by (see Appendix VII)

$$\begin{bmatrix} J_x \\ J_y \\ J_z \end{bmatrix} = \begin{bmatrix} \cos\phi' & -\sin\phi' & 0 \\ \sin\phi' & \cos\phi' & 0 \\ 0 & 0 & 1 \end{bmatrix} \begin{bmatrix} J_\rho \\ J_\phi \\ J_z \end{bmatrix} \tag{12-41a}$$

A similar transformation exists for the components of $\mathbf{M}_s$. The rectangular and cylindrical coordinates are related by (see Appendix VII)

$$\begin{aligned} x' &= \rho' \cos\phi' \\ y' &= \rho' \sin\phi' \\ z' &= z' \end{aligned} \tag{12-41b}$$

Using (12-41a), (12-12a)–(12-12d) can be written as

$$N_\theta = \iint_S [J_\rho \cos\theta \cos(\phi - \phi') + J_\phi \cos\theta \sin(\phi - \phi') - J_z \sin\theta] \times e^{+jkr'\cos\psi}\, ds' \tag{12-42a}$$

$$N_\phi = \iint_S [-J_\rho \sin(\phi - \phi') + J_\phi \cos(\phi - \phi')]\, e^{+jkr'\cos\psi}\, ds' \tag{12-42b}$$

$$L_\theta = \iint_S [M_\rho \cos\theta \cos(\phi - \phi') + M_\phi \cos\theta \sin(\phi - \phi') - M_z \sin\theta] \times e^{+jkr'\cos\psi}\, ds' \tag{12-42c}$$

$$L_\phi = \iint_S [-M_\rho \sin(\phi - \phi') + M_\phi \cos(\phi - \phi')]\, e^{+jkr'\cos\psi}\, ds' \tag{12-42d}$$

where $r' \cos\psi$ and ds' can be written, using (12-15c) and (12-41b), as

$$r' \cos\psi = x' \sin\theta \cos\phi + y' \sin\theta \sin\phi = \rho' \sin\theta \cos(\phi - \phi') \tag{12-43a}$$

$$ds' = dx'\, dy' = \rho'\, d\rho'\, d\phi' \tag{12-43b}$$

In summary, for a circular aperture antenna the fields radiated can be obtained by *either* of the following:

1. If the fields over the aperture are known in *rectangular components*, use the same procedure as for the rectangular aperture with (12-43a) and (12-43b) substituted in (12-12a)–(12-12d).
2. If the fields over the aperture are known in *cylindrical components*, use the same procedure as for the rectangular aperture with (12-42a)–(12-42d), along with (12-43a) and (12-43b), taking the place of (12-12a)–(12-12d).

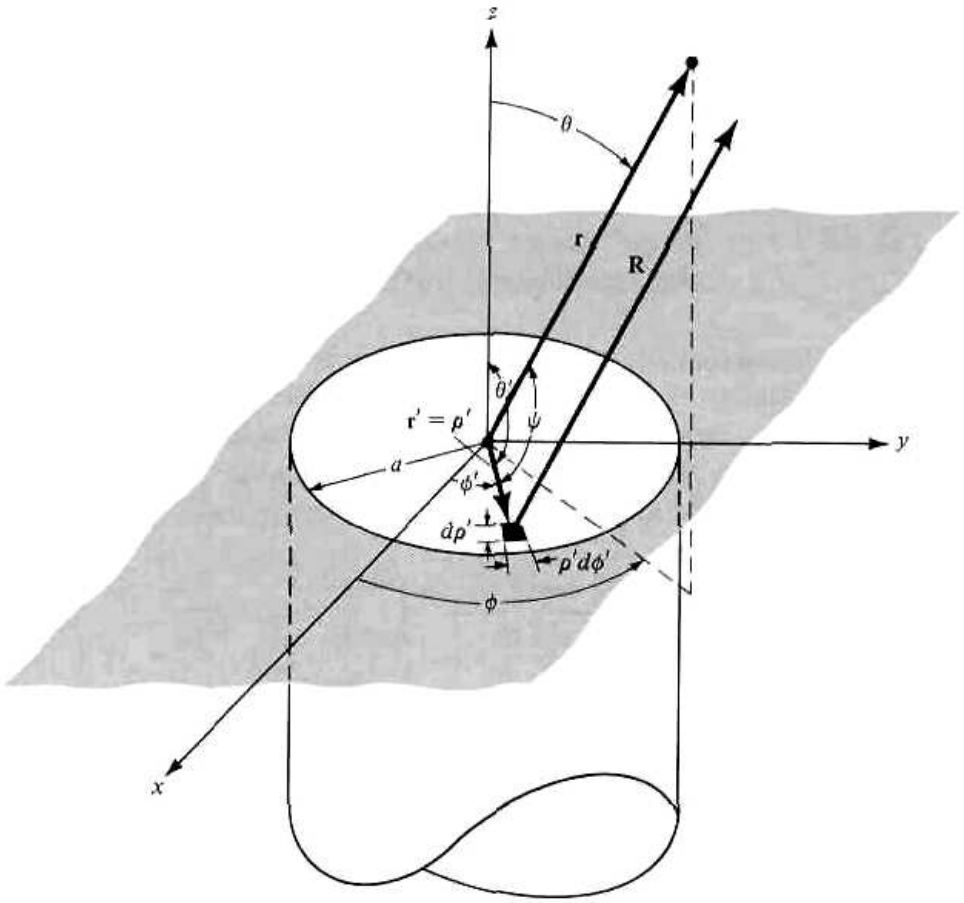

Figure 12.16 Circular aperture mounted on an infinite ground plane.

12.6.1 Uniform Distribution on an Infinite Ground Plane

To demonstrate the methods, the field radiated by a circular aperture mounted on an infinite ground plane will be formulated. To simplify the mathematical details, the field over the aperture is assumed to be constant and given by

$$\mathbf{E}_a = \hat{\mathbf{a}}_y E_0 \qquad \rho' \leq a \tag{12-44}$$

where E_0 is a constant.

A. Equivalent and Radiation Fields

The equivalent problem of this is identical to that of Figure 12.7. That is,

$$\left.\begin{aligned} \mathbf{M}_s &= \begin{cases} -2\hat{\mathbf{n}} \times \mathbf{E}_a = \hat{\mathbf{a}}_x 2E_0 & \rho' \leq a \\ 0 & \text{elsewhere} \end{cases} \\ \mathbf{J}_s &= 0 \qquad\qquad\qquad\quad \text{everywhere} \end{aligned}\right\} \tag{12-45}$$

Thus,

$$N_\theta = N_\phi = 0 \tag{12-46}$$

$$L_\theta = 2E_0 \cos\theta \cos\phi \int_0^a \rho' \left[\int_0^{2\pi} e^{+jk\rho' \sin\theta \cos(\phi - \phi')} d\phi' \right] d\rho' \tag{12-47}$$

Because

$$\int_0^{2\pi} e^{+jk\rho' \sin\theta\cos(\phi-\phi')} d\phi' = 2\pi J_0(k\rho' \sin\theta) \tag{12-48}$$

(12-47) can be written as

$$L_\theta = 4\pi E_0 \cos\theta \cos\phi \int_0^a J_0(k\rho' \sin\theta)\rho' \, d\rho' \tag{12-49}$$

where $J_0(t)$ is the Bessel function of the first kind of order zero. Making the substitution

$$\begin{aligned} t &= k\rho' \sin\theta \\ dt &= k \sin\theta \, d\rho' \end{aligned} \tag{12-49a}$$

reduces (12-49) to

$$L_\theta = \frac{4\pi E_0 \cos\theta \cos\phi}{(k \sin\theta)^2} \int_0^{ka\sin\theta} tJ_0(t) \, dt \tag{12-49b}$$

Since

$$\int_0^\beta zJ_0(z) \, dz = zJ_1(z)\Big|_0^\beta = \beta J_1(\beta) \tag{12-50}$$

where $J_1(\beta)$ is the Bessel function of order one, (12-49b) takes the form of

$$L_\theta = 4\pi a^2 E_0 \left\{ \cos\theta \cos\phi \left[\frac{J_1(ka \sin\theta)}{ka \sin\theta} \right] \right\} \tag{12-51}$$

Similarly

$$L_\phi = -4\pi a^2 E_0 \sin\phi \left[\frac{J_1(ka \sin\theta)}{ka \sin\theta} \right] \tag{12-52}$$

Using (12-46), (12-51), and (12-52), the electric field components of (12-10a)–(12-10c) can be written as

$$E_r = 0 \tag{12-53a}$$

$$E_\theta = j \frac{ka^2 E_0 e^{-jkr}}{r} \left\{ \sin\phi \left[\frac{J_1(ka \sin\theta)}{ka \sin\theta} \right] \right\} \tag{12-53b}$$

$$E_\phi = j \frac{ka^2 E_0 e^{-jkr}}{r} \left\{ \cos\theta \cos\phi \left[\frac{J_1(ka \sin\theta)}{ka \sin\theta} \right] \right\} \tag{12-53c}$$

In the principal E- and H-planes, the electric field components simplify to

E-Plane ($\phi = \pi/2$)

$$E_r = E_\phi = 0 \tag{12-54a}$$

$$E_\theta = j \frac{ka^2 E_0 e^{-jkr}}{r} \left[\frac{J_1(ka \sin\theta)}{ka \sin\theta} \right] \tag{12-54b}$$

H-Plane ($\phi = 0$)

$$E_r = E_\theta = 0 \tag{12-55a}$$

$$E_\phi = j\frac{ka^2E_0e^{-jkr}}{r}\left\{\cos\theta\left[\frac{J_1(ka\sin\theta)}{ka\sin\theta}\right]\right\} \tag{12-55b}$$

A three-dimensional pattern has been computed for the constant field circular aperture of $a = 1.5\lambda$, and it is shown in Figure 12.17. The pattern of Figure 12.17 seems to be symmetrical. However closer observation, especially through the two-dimensional E- and H-plane patterns, will reveal that not to be the case. It does, however, possess characteristics that are almost symmetrical.

B. Beamwidth, Side Lobe Level, and Directivity

Exact expressions for the beamwidths and side lobe levels cannot be obtained easily. However approximate expressions are available, and they are shown tabulated in Table 12.2. More exact data can be obtained by numerical methods.

Since the field distribution over the aperture is constant, the directivity is given by

$$\boxed{D_0 = \frac{4\pi}{\lambda^2}A_{em} = \frac{4\pi}{\lambda^2}A_p = \frac{4\pi}{\lambda^2}(\pi a^2) = \left(\frac{2\pi a}{\lambda}\right)^2 = \left(\frac{C}{\lambda}\right)^2} \tag{12-56}$$

since the maximum effective area A_{em} is equal to the physical area A_p of the aperture [as shown for the rectangular aperture in (12-37)].

A summary of the radiation parameters of this aperture is included in Table 12.2.

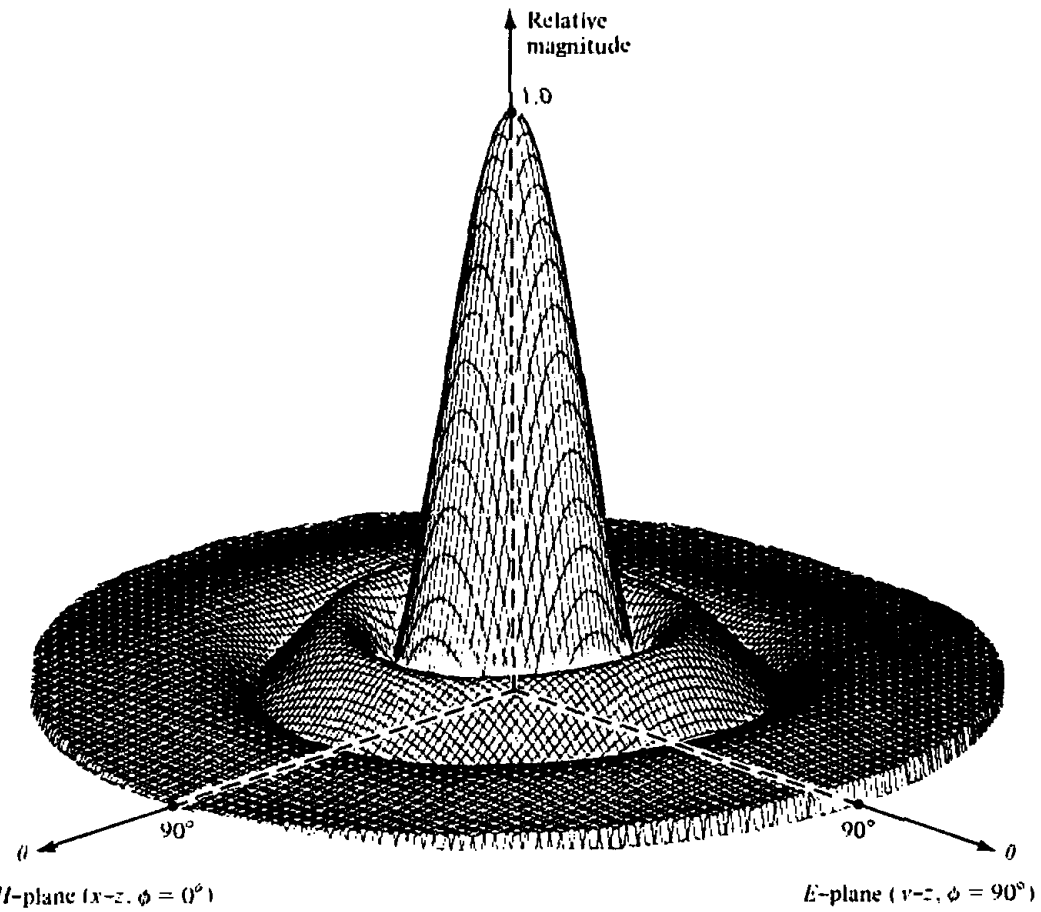

Figure 12.17 Three-dimensional field pattern of a constant field circular aperture mounted on an infinite ground plane ($a = 1.5\lambda$).

Table 12.2 EQUIVALENTS, FIELDS, BEAMWIDTHS, SIDE LOBE LEVELS, AND DIRECTIVITIES OF CIRCULAR APERTURES

	Uniform Distribution Aperture on Ground Plane	TE_{11}-Mode Distribution Aperture on Ground Plane
Aperture distribution of tangential components (analytical)	$\mathbf{E}_a = \hat{\mathbf{a}}_x E_0 \qquad \rho' \le a$	$\mathbf{E}_a = \hat{\mathbf{a}}_\rho E_\rho + \hat{\mathbf{a}}_\phi E_\phi$ $E_\rho = E_0 J_1(\chi'_{11}\rho'/a)\sin\phi'/\rho'$ $E_\phi = E_0 J_1'(\chi'_{11}\rho'/a)\cos\phi'$ $\rho' \le a$ $\chi'_{11} = 1.841$ $' = \dfrac{\partial}{\partial\rho'}$
Aperture distribution of tangential components (graphical)	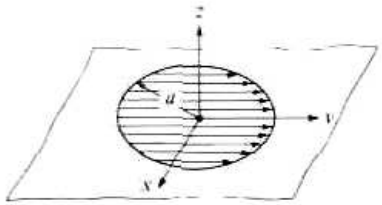	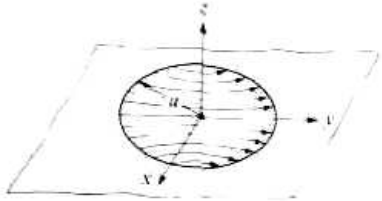
Equivalent	$\mathbf{M}_s = \begin{cases} -2\hat{\mathbf{n}} \times \mathbf{E}_a & \rho' \le a \\ 0 & \text{elsewhere} \end{cases}$ $\mathbf{J}_s = 0 \qquad \text{everywhere}$	$\mathbf{M}_s = \begin{cases} -2\hat{\mathbf{n}} \times \mathbf{E}_a & \rho' \le a \\ 0 & \text{elsewhere} \end{cases}$ $\mathbf{J}_s = 0 \qquad \text{everywhere}$
Far-zone fields $Z = ka\sin\theta$ $C_1 = j\dfrac{ka^2E_0e^{-jkr}}{r}$ $C_2 = j\dfrac{kaE_0J_1(\chi'_{11})e^{-jkr}}{r}$ $\chi'_{11} = 1.841$	$E_r = H_r = 0$ $E_\theta = jC_1\sin\phi\dfrac{J_1(Z)}{Z}$ $E_\phi = jC_1\cos\theta\cos\phi\dfrac{J_1(Z)}{Z}$ $H_\theta = -E_\phi/\eta$ $H_\phi = E_\theta/\eta$	$E_r = H_r = 0$ $E_\theta = C_2\sin\phi\dfrac{J_1(Z)}{Z}$ $E_\phi = C_2\cos\theta\cos\phi\dfrac{J_1'(Z)}{1-(Z/\chi'_{11})^2}$ $H_\theta = -E_\phi/\eta$ $H_\phi = E_\theta/\eta$ $J_1'(Z) = J_0(Z) - J_1(Z)/Z$

Table 12.2 (Continued)

Half-power beamwidth (degrees)	E-plane $a \gg \lambda$	$\frac{29.2}{a/\lambda}$	$\frac{29.2}{a/\lambda}$
	H-plane $a \gg \lambda$	$\frac{29.2}{a/\lambda}$	$\frac{37.0}{a/\lambda}$
First null beamwidth (degrees)	E-plane $a \gg \lambda$	$\frac{69.9}{a/\lambda}$	$\frac{69.9}{a/\lambda}$
	H-plane $a \gg \lambda$	$\frac{69.9}{a/\lambda}$	$\frac{98.0}{a/\lambda}$
First side lobe max. (to main max.) (dB)	E-plane	-17.6	-17.6
	H-plane	-17.6	-26.2
Directivity D_0 (dimensionless)		$\frac{4\pi}{\lambda^2}(\text{area}) = \frac{4\pi}{\lambda^2}(\pi a^2) = \left(\frac{2\pi a}{\lambda}\right)^2$	$0.836\left(\frac{2\pi a}{\lambda}\right)^2 = 10.5\pi\left(\frac{a}{\lambda}\right)^2$

12.6.2 TE_{11}-Mode Distribution on an Infinite Ground Plane

A very practical antenna is a circular waveguide of radius a mounted on an infinite ground plane, as shown in Figure 12.16. However, the field distribution over the aperture is usually that of the dominant TE_{11}-mode for a circular waveguide given by

$$\left.\begin{aligned} E_{\rho'} &= \frac{E_0}{\rho'} J_1\left(\frac{\chi'_{11}}{a}\rho'\right)\sin\phi' \\ E_{\phi'} &= E_0 \frac{\partial}{\partial\rho'}\left[J_1\left(\frac{\chi'_{11}}{a}\rho'\right)\right]\cos\phi' \\ E_{z'} &= 0 \\ \chi'_{11} &= 1.841 \end{aligned}\right\} \tag{12-57}$$

The analysis of this problem is assigned, at the end of this chapter, as an exercise to the reader (Problem 12.33). However, a three-dimensional pattern for $a = 1.5\lambda$ was calculated, and it is shown in Figure 12.18. This pattern should be compared with that of Figure 12.17 for the constant aperture field distribution.

The beamwidths and the side lobe levels in the E- and H-planes are different, and exact closed form expressions cannot be obtained. However, they can be calculated using iterative methods, and the data are shown in Figures 12.19 and 12.20 for the E- and H-planes, respectively.

A summary of all the radiation characteristics is included in Table 12.2.

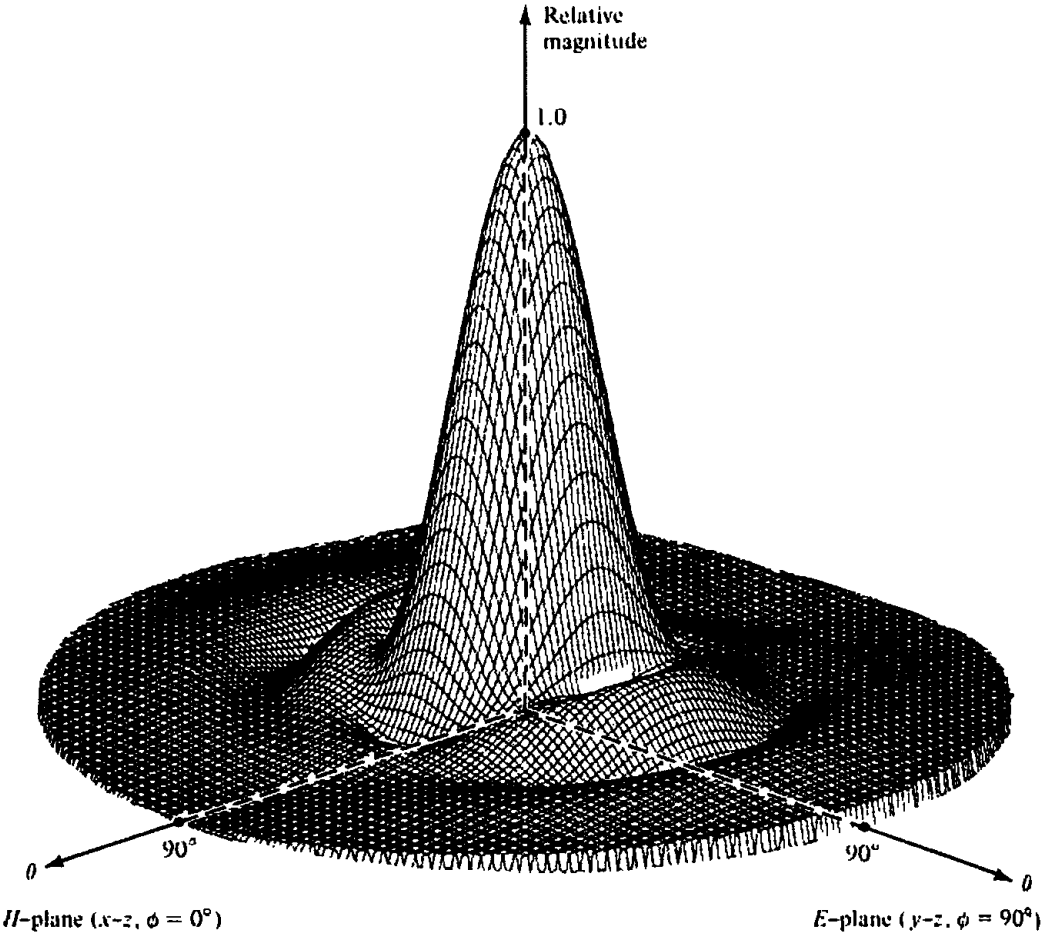

Figure 12.18 Three-dimensional field pattern of a TE_{11}-mode circular waveguide mounted on an infinite ground plane ($a = 1.5\lambda$).

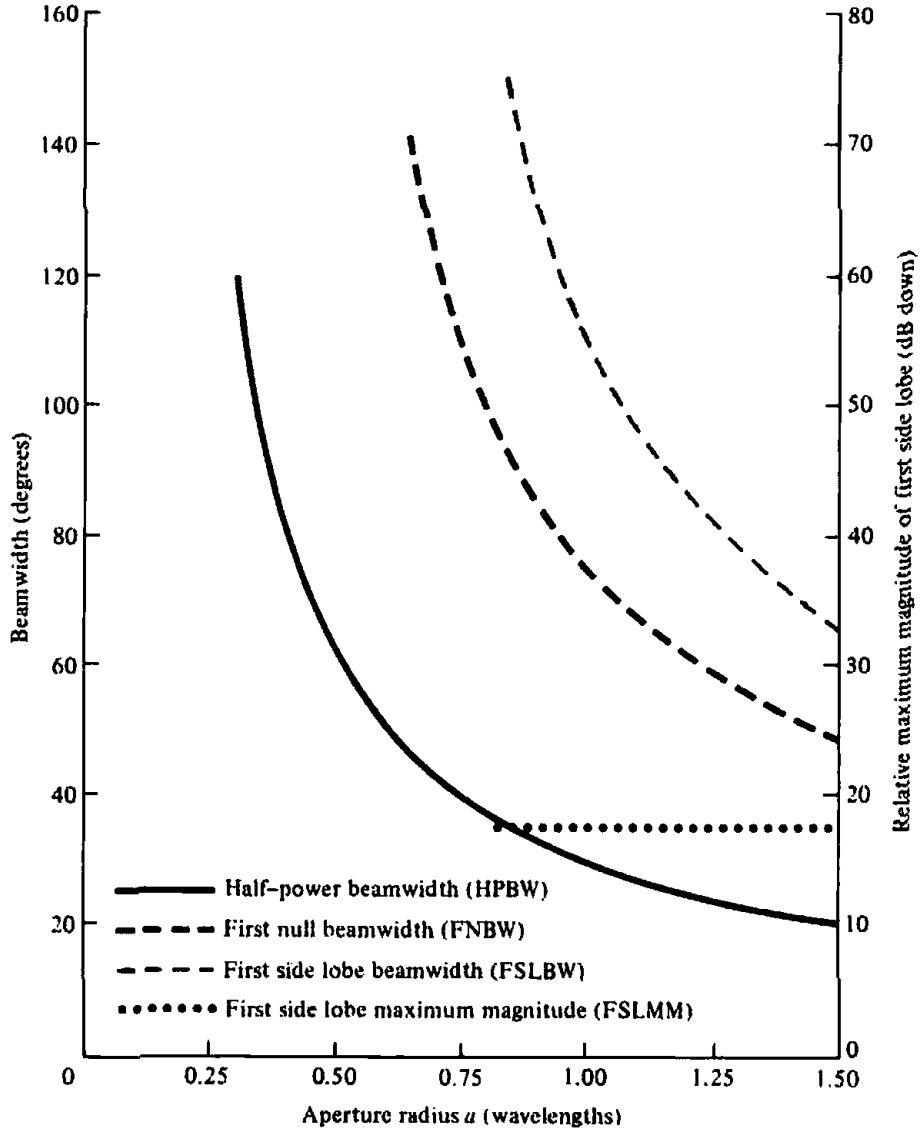

Figure 12.19 *E*-plane beamwidths and first side lobe relative maximum magnitude for TE_{11}-mode circular aperture mounted on an infinite ground plane.

12.6.3 Beam Efficiency

Beam efficiency, as defined by (2-53) and calculated by (2-54), for circular apertures not mounted on infinite ground planes is shown in Figure 12.21 [11]. The lower abscissa scale (in degrees) is in terms of the half-cone angle θ_1 (in degrees), and it should be used only when the radius of the aperture is 20λ ($a = 20\lambda$). The upper abscissa scale is in terms of u ($u = ka \sin \theta_1$), and it should be used for any radius circular aperture.

The procedure for finding the beam efficiency of a circular aperture is similar to that of a rectangular aperture as discussed in Section 12.5.4, illustrated in Figure 12.15, and demonstrated by Example 12.4.

12.7 DESIGN CONSIDERATIONS

As is the case for arrays, aperture antennas can be designed to control their radiation characteristics. Typically the level of the minor lobes can be controlled by tapering the distribution across the aperture: the smoother the taper from the center of the

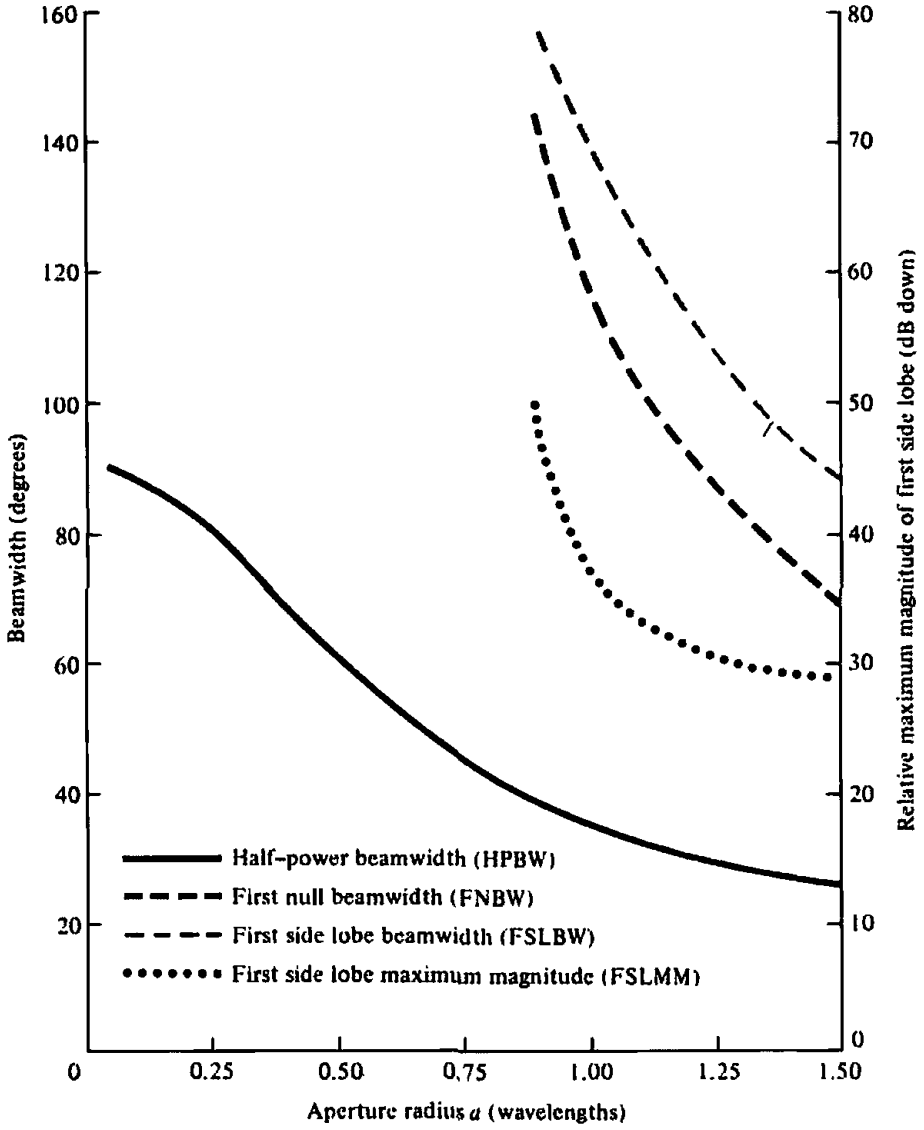

Figure 12.20 *H*-plane beamwidths and first side lobe relative maximum magnitude for TE_{11}-mode circular waveguide mounted on an infinite ground plane.

aperture toward the edge, the lower the side lobe level and the larger the half-power beamwidth, and conversely. Therefore a very smooth taper, such as that represented by a binomial distribution or others, would result in very low sidelobes but larger half-power beamwidths. In contrast, an abrupt distribution, such as that of uniform illumination, exhibits the smaller half-power beamwidth but the highest side lobe level (about -13.5 dB). Therefore if it is desired to achieve simultaneously both a very low sidelobe level, as well as a small half-power beamwidth, a compromise has to be made. Typically an intermediate taper, such as that of a Tschebyscheff distribution or any other similar one, will have to be selected. This has been discussed in detail both in Chapter 6 for arrays and in Chapter 7 for continuous sources. These can be used to design continuous distributions for apertures.

Aperture antennas, both rectangular and circular, can also be designed for satellite applications where the beamwidth can be used to determine the "footprint" area of the coverage. In such designs, it is important to relate the beamwidth to the size of the aperture. In addition, it is also important to maximize the directivity of the antennas within a desired angular sector defined by the beamwidth, especially at the edge-of-

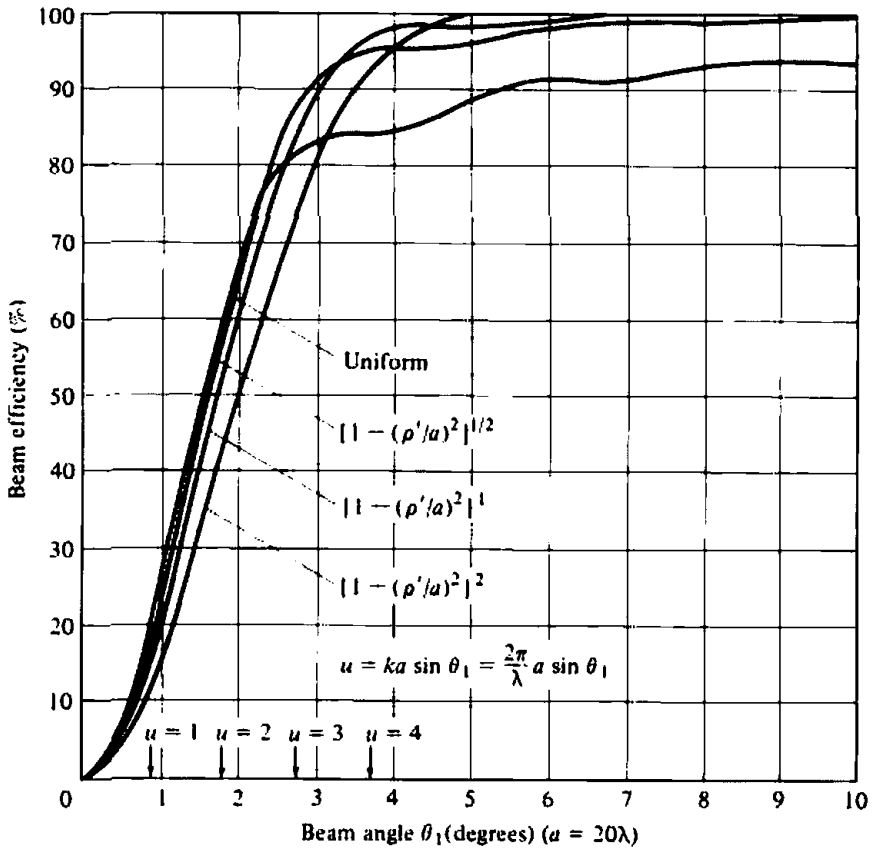

Figure 12.21 Beam efficiency versus half-cone angle θ_1, for a circular aperture with different field distributions. The aperture is not mounted on an infinite ground plane. (SOURCE: D. G. Fink (ed.), *Electronics Engineers' Handbook*, Section 18 (by W. F. Croswell), McGraw-Hill, New York, 1975)

coverage (EOC) [12]. This can be accomplished, using approximate closed-form expressions, as outlined in [12]. This procedure was used in Section 6.11 of Chapter 6 for arrays, and it is applicable for apertures, both rectangular and circular.

12.7.1 Rectangular Aperture

For a rectangular aperture, of dimensions a and b, with a uniform distribution the procedure to determine the optimum aperture dimensions a,b to maximize the directivity at an edge angle θ_e of a given angular sector ($0 \leq \theta \leq \theta_e$) is identical to that outlined in Section 6.11. Thus to determine the optimum dimension b of the aperture so that the directivity is maximum at an edge-of-coverage angle θ_{eo} of an angular sector $0 \leq \theta \leq \theta_{eo}$ in the E-plane is given by (6-105a), or

$$E\text{-Plane:} \qquad b = \frac{\lambda}{2 \sin \theta_{eo}} \tag{12-58a}$$

Similarly for the H-plane, the optimum dimension b is determined by

$$H\text{-Plane:} \qquad a = \frac{\lambda}{2 \sin \theta_{eh}} \tag{12-58b}$$

where θ_{eh} is the angle, in the H-plane, at the edge-of-coverage (EOC) angular sector where the directivity needs to be maximized.

Since the aperture antenna is uniformly illuminated, the directivity of (6-103) based on the optimum dimensions of (12-58a) and (12-58b) is

$$D_0 = \frac{4\pi}{\lambda^2} A_{em} = \frac{4\pi}{\lambda^2} A_p = \frac{4\pi}{\lambda^2} \left(\frac{\lambda}{2 \sin \theta_{ce}}\right)\left(\frac{\lambda}{2 \sin \theta_{ch}}\right) \tag{12-59}$$

12.7.2 Circular Aperture

A procedure similar to that for the rectangular aperture can be used for the circular aperture. In fact, it can be used for circular apertures with uniform distributions as well as tapered (parabolic or parabolic with a pedestal) [12].

For a circular aperture with uniform distribution, the normalized power pattern multiplied by the maximum directivity can be written as

$$P(\theta) = (2\pi a)^2 \left\{\frac{2J_1(ka \sin \theta)}{ka \sin \theta}\right\}^2 \tag{12-60}$$

The maximum value of (12-60) occurs when $\theta = 0$. However, for any other angle $\theta = \theta_c$, the maximum of the pattern occurs when

$$ka \sin \theta_c = 1.841 \tag{12-61}$$

or

$$a = \frac{1.841\lambda}{2\pi \sin \theta_c} = \frac{\lambda}{3.413 \sin \theta_c} \tag{12-61a}$$

Therefore to maximize the directivity at the edge $\theta = \theta_c$ of a given angular sector $0 \le \theta \le \theta_c$, the optimum radius of the uniformly illuminated circular aperture must be chosen according to (12-61a).

The maximum value of (12-60), which occurs at $\theta = 0$, is equal to

$$P(\theta = 0)|_{\max} = (2\pi a)^2 \tag{12-62}$$

while at the edge of the angular sector ($\theta = \theta_c$) is equal to

$$P(\theta = \theta_c) = (2\pi a)^2 \left\{\frac{2(0.5818)}{1.841}\right\}^2 = (2\pi a)^2(0.3995) \tag{12-63}$$

Therefore the value of the directivity at the edge of the desired coverage ($\theta = \theta_c$), relative to its maximum value at $\theta = 0$, is

$$\frac{P(\theta = \theta_c)}{P(\theta = 0)} = 0.3995 = -3.985 \text{ dB} \tag{12-64}$$

Since the aperture is uniformly illuminated, the directivity based on the optimum radius of (12-61a) is

$$D_0 = \frac{4\pi}{\lambda^2} A_p = \frac{4\pi}{\lambda^2} \pi \left(\frac{1.841}{2\pi \sin \theta_c}\right)^2 = \frac{3.4129}{\sin^2 \theta_c} = \frac{1.086\pi}{\sin^2 \theta_c} \tag{12-65}$$

A similar procedure can be followed for circular apertures with radial taper (parabolic) and radial taper squared of Table 7.2, as well as radial taper (parabolic) with pedestal. The characteristics of these, along with those of the uniform, are listed in Table 12.3.

Table 12.3 EDGE-OF-COVERAGE (EOC) DESIGNS FOR SQUARE AND CIRCULAR APERTURES

Aperture	Distribution	Size Square: Side Circular: Radius	Directivity	EOC Directivity (relative to peak)
Square	Uniform	$\frac{\lambda}{2\sin(\theta_c)}$	$\frac{\pi}{\sin^2(\theta_c)}$	−3.920 dB
Circular	Uniform	$\frac{\lambda}{3.413\sin(\theta_c)}$	$\frac{1.086\pi}{\sin^2(\theta_c)}$	−3.985 dB
Circular	Parabolic taper	$\frac{\lambda}{2.732\sin(\theta_c)}$	$\frac{1.263\pi}{\sin^2(\theta_c)}$	−4.069 dB
Circular	Parabolic taper with −10 dB pedestal	$\frac{\lambda}{3.064\sin(\theta_c)}$	$\frac{1.227\pi}{\sin^2(\theta_c)}$	−4.034 dB

(SOURCE: K. Praba, "Optimal Aperture for Maximum Edge-of-Coverage (EOC) Directivity," *IEEE Antennas & Propagation Magazine*, Vol. 36, No. 3, pp. 72–74, June 1994. © (1994) IEEE)

Example 12.5:

It is desired to design an aperture antenna, with uniform illumination, so that the directivity is maximized at an angle 30° from the normal to the aperture. Determine the optimum dimension and its associated directivity when the aperture is

(a) Square
(b) Circular

SOLUTION

For a square aperture $\theta_{cc} = \theta_{ch}$. Therefore the optimum dimension, according to (12-58a) or (12-58b), is

$$a = b = \frac{\lambda}{2\sin(30°)} = \lambda$$

while the directivity, according to (12-59), is

$$D_0 = \frac{\pi}{\sin^2\theta_c} = \frac{\pi}{\sin^2(30°)} = 12.5664 = 10.992 \text{ dB}$$

The directivity at $\theta = 30°$ is −3.920 dB from the maximum at $\theta = 0°$, or 7.072 dB.

For a circular aperture the optimum radius, according to (12-61a), is

$$a = \frac{\lambda}{3.413\sin(30°)} = \frac{\lambda}{3.413(0.5)} = 0.586\lambda$$

while the directivity, according to (12-65), is

$$D_0 = \frac{1.086\pi}{\sin^2 \theta_c} = \frac{1.086\pi}{\sin^2(30°)} = 13.647 = 11.35 \text{ dB}$$

The directivity at $\theta = 30°$ is -3.985 dB from the maximum at $\theta = 0°$, or 7.365 dB.

12.8 BABINET'S PRINCIPLE

Now that wire and aperture antennas have been analyzed, one may inquire as to whether there is any relationship between them. This can be answered better by first introducing *Babinet's principle* which in optics states that *when the field behind a screen with an opening is added to the field of a complementary structure, the sum is equal to the field when there is no screen.* Babinet's principle in optics does not consider polarization, which is so vital in antenna theory; it deals primarily with absorbing screens. An extension of Babinet's principle, which includes polarization and the more practical conducting screens, was introduced by Booker [13], [14]. Referring to Figure 12.22(a), let us assume that an electric source $\mathbf{J}$ radiates into an unbounded medium of intrinsic impedance $\eta = (\mu/\epsilon)^{1/2}$ and produces at point P the fields $\mathbf{E}_0$, $\mathbf{H}_0$. The same fields can be obtained by combining the fields when the electric source radiates in a medium with intrinsic impedance $\eta = (\mu/\epsilon)^{1/2}$ in the presence of

1. an infinite, planar, very thin, perfect electric conductor with an opening S_a, which produces at P the fields $\mathbf{E}_c$, $\mathbf{H}_c$ [Figure 12.22(b)]
2. a flat, very thin, perfect magnetic conductor S_a, which produces at P the fields $\mathbf{E}_m$, $\mathbf{H}_m$ [Figure 12.22(c)].

That is,

$$\begin{aligned} \mathbf{E}_0 &= \mathbf{E}_c + \mathbf{E}_m \\ \mathbf{H}_0 &= \mathbf{H}_c + \mathbf{H}_m \end{aligned} \tag{12-66a}$$

The field produced by the source in Figure 12.22(a) can also be obtained by combining the fields of

1. an electric source $\mathbf{J}$ radiating in a medium with intrinsic impedance $\eta = (\mu/\epsilon)^{1/2}$ in the presence of an infinite, planar, very thin, perfect electric conductor S_a, which produces at P the fields $\mathbf{E}_c$, $\mathbf{H}_c$ [Figure 12.22(b)]
2. a magnetic source $\mathbf{M}$ radiating in a medium with intrinsic impedance $\eta_d = (\epsilon/\mu)^{1/2}$ in the presence of a flat, very thin, perfect electric conductor S_a, which produces at P the fields $\mathbf{E}_d$, $\mathbf{H}_d$ [Figure 12.22(d)]

That is,

$$\begin{aligned} \mathbf{E}_0 &= \mathbf{E}_c + \mathbf{H}_d \\ \mathbf{H}_0 &= \mathbf{H}_c - \mathbf{E}_d \end{aligned} \tag{12-66b}$$

The dual of Figure 12.22(d) is more easily realized in practice than that of Figure 12.22(c).

To obtain Figure 12.22(d) from Figure 12.22(c), $\mathbf{J}$ is replaced by $\mathbf{M}$, $\mathbf{E}_m$ by $\mathbf{H}_d$, $\mathbf{H}_m$ by $-\mathbf{E}_d$, ϵ by μ, and μ by ϵ. This is a form of duality so often used in electromagnetics (see Section 3.7, Table 3.2). The electric screen with the opening in Figure

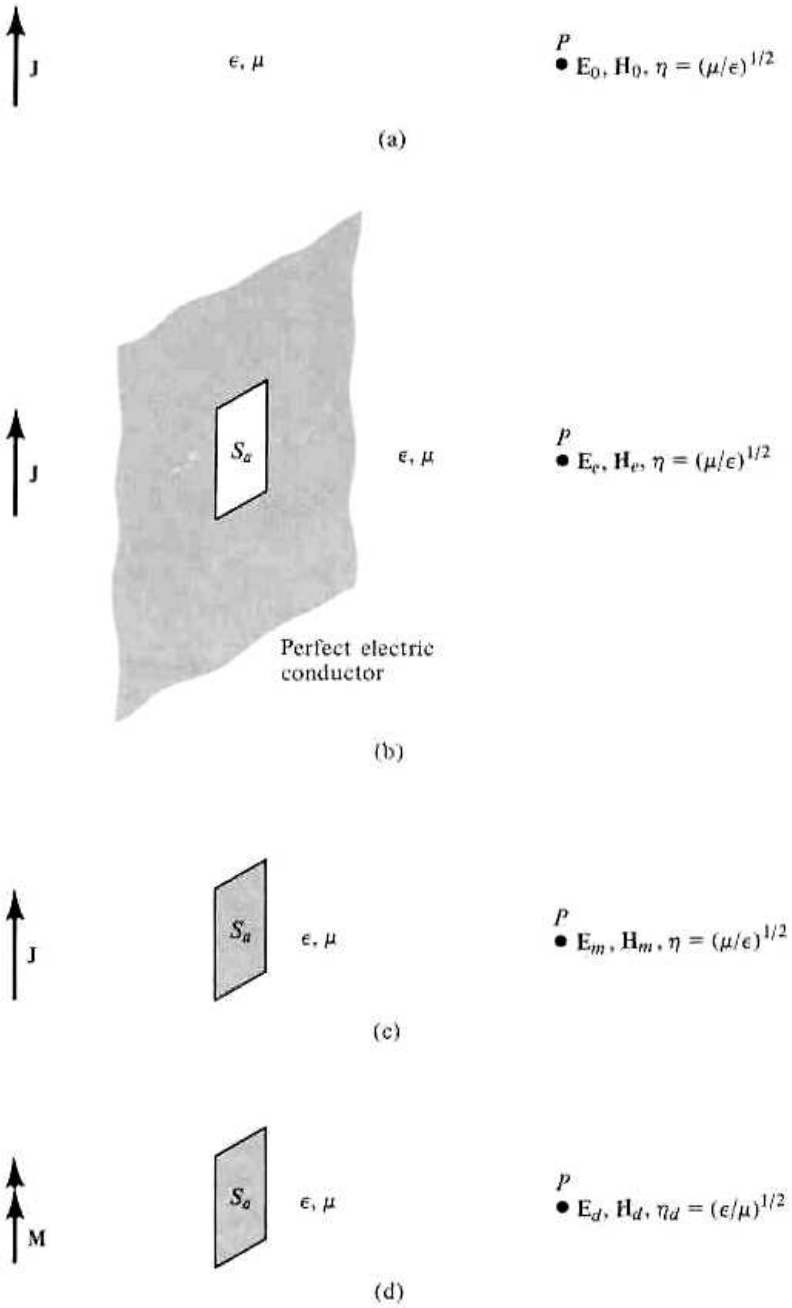

Figure 12.22 Electric source in an unbounded medium and Babinet's principle equivalents.

12.22(b) and the electric conductor of Figure 12.22(d) are also dual. They are usually referred to as *complementary structures*, because when combined they form a single solid screen with no overlaps. A proof of Babinet's principle and its extension can be found in the literature [5].

Using Booker's extension it can be shown [13], [14] by referring to Figure 12.23, that if a screen and its complement are immersed in a medium with an intrinsic impedance η and have terminal impedances of Z_s and Z_c, respectively, the impedances are related by

$$\boxed{Z_s Z_c = \frac{\eta^2}{4}} \tag{12-67}$$

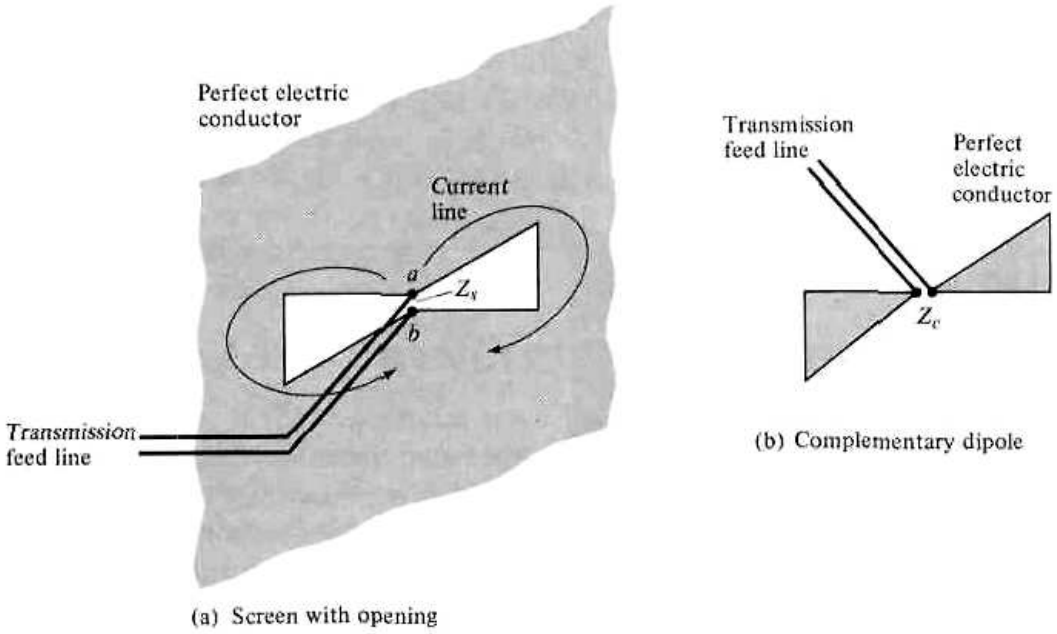

Figure 12.23 Opening on a screen and its complementary dipole.

To obtain the impedance Z_c of the complement (dipole) in a practical arrangement, a gap must be introduced to represent the feed points. In addition, the far-zone fields radiated by the opening on the screen ($E_{\theta s}$, $E_{\phi s}$, $H_{\theta s}$, $H_{\phi s}$) are related to the far-zone fields of the complement ($E_{\theta c}$, $E_{\phi c}$, $H_{\theta c}$, $H_{\phi c}$) by

$$E_{\theta s} = H_{\theta c}, \quad E_{\phi s} = H_{\phi c}, \quad H_{\theta s} = -\frac{E_{\theta c}}{\eta_0^2}, \quad H_{\phi s} = -\frac{E_{\phi c}}{\eta_0^2} \tag{12-68}$$

Infinite, flat, very thin conductors are not realizable in practice but can be closely approximated. If a slot is cut into a plane conductor that is large compared to the wavelength and the dimensions of the slot, the behavior predicted by Babinet's principle can be realized to a high degree. The impedance properties of the slot may not be affected as much by the finite dimensions of the plane as would be its pattern. The slot of Figure 12.23(a) will also radiate on both sides of the screen. Unidirectional radiation can be obtained by placing a backing (box or cavity) behind the slot, forming a so-called *cavity-backed slot* whose radiation properties (impedance and pattern) are determined by the dimensions of the cavity.

To demonstrate the application of Babinet's principle, an example is considered.

Example 12.6

A very thin half-wavelength slot is cut on an infinite, planar, very thin, perfectly conducting electric screen as shown in Figure 12.24(a). Find its input impedance. Assume it is radiating into free-space.

SOLUTION

From Babinet's principle and its extension we know that a very thin half-wavelength dipole, shown in Figure 12.24(b), is the complementary structure to the slot. From

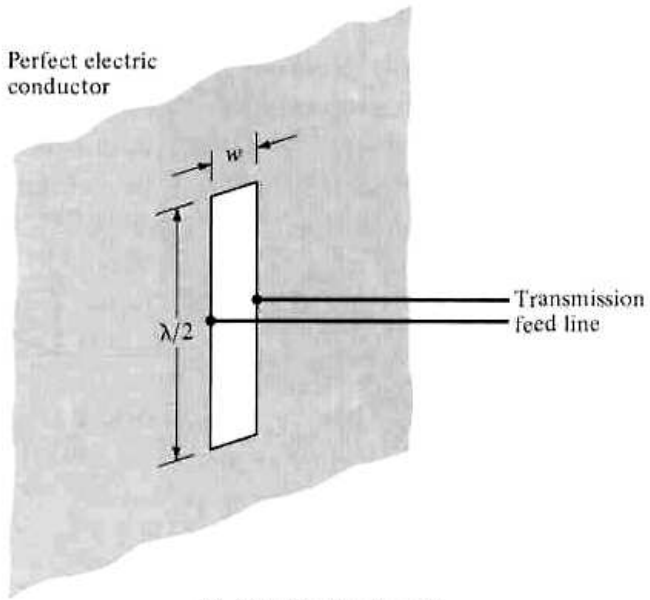

(a) $\lambda/2$ thin slot ($w \to 0$)

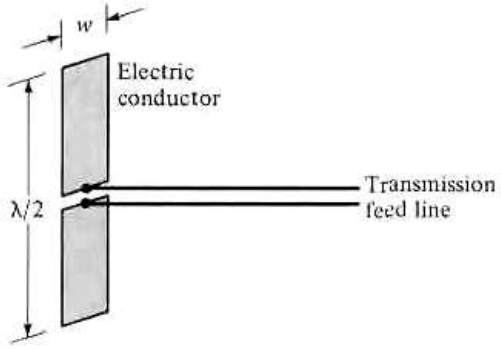

(b) $\lambda/2$ flat thin dipole ($w \to 0$)

Figure 12.24 Half-wavelength thin slot on an electric screen and its complement.

Chapter 4, the terminal (input) impedance of the dipole is $Z_c = 73 + j42.5$. Thus the terminal (input) impedance of the slot, using (12-67), is given by

$$Z_s = \frac{\eta_0^2}{4Z_c} \simeq \frac{(376.7)^2}{4(73 + j42.5)} \simeq \frac{35{,}475.72}{73 + j42.5}$$

$$Z_s \simeq 362.95 - j211.31$$

The slot of Figure 12.24(a) can be made to resonate by choosing the dimensions of its complement (dipole) so that it is also resonant. The pattern of the slot is identical in shape to that of the dipole except that the **E**- and **H**-fields are interchanged. When a vertical slot is mounted on a vertical screen, as shown in Figure 12.25(a), its electric field is horizontally polarized while that of the dipole is vertically polarized [Fig. 12.25(b)]. Changing the angular orientation of the slot or screen will change the polarization.

The slot antenna, as a cavity-backed design, has been utilized in a variety of law enforcement applications. Its main advantage is that it can be fabricated and concealed within metallic objects, and with a small transmitter it can provide covert communications. There are various methods of feeding a slot antenna [15]. For proper operation,

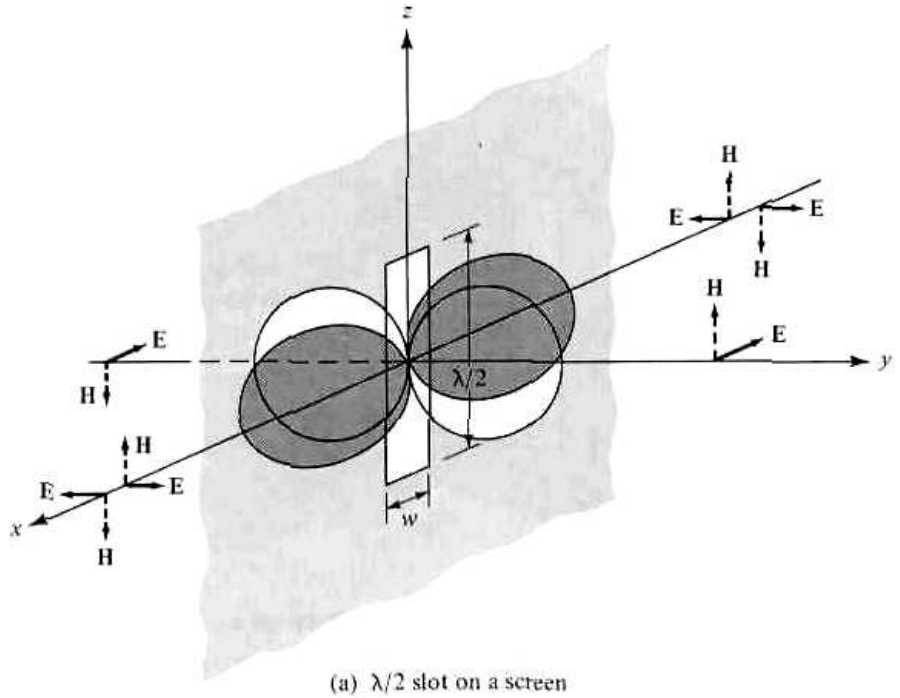

(a) λ/2 slot on a screen

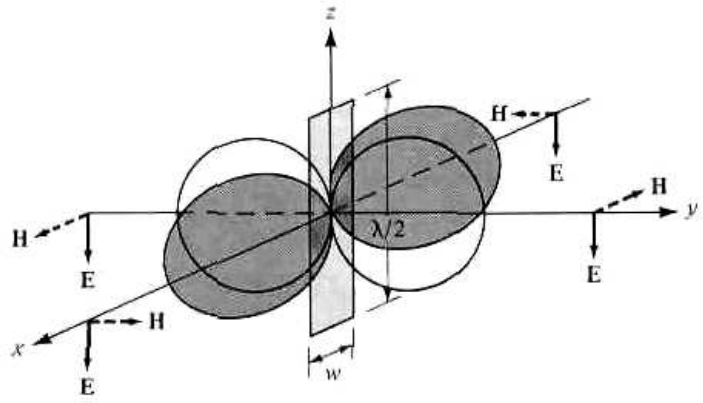

(b) λ/2 flat dipole

Figure 12.25 Radiation fields of a λ/2 slot on a screen and of a λ/2 flat dipole. (SOURCE: J. D. Kraus, *Antennas*, McGraw-Hill, New York, 1988, Chapter 13)

the cavity depth must be equal to odd multiples of $\lambda_g/4$, where λ_g is the guide wavelength.

12.9 FOURIER TRANSFORMS IN APERTURE ANTENNA THEORY

Previously the spatial domain analysis of aperture antennas was introduced, and it was applied to rectangular and circular apertures radiating in an infinite, homogeneous, lossless medium. The analysis of aperture antennas mounted on infinite ground planes, covered with lossless and/or lossy dielectric media, becomes too complex when it is attempted in the spatial domain. Considerable simplification can result with the utility of the frequency (*spectral*) domain.

12.9.1 Fourier Transforms-Spectral Domain

From Fourier series analysis, any periodic function $f(x)$ with a period T can be represented by a Fourier series of cosine and sine terms. If the function $f(x)$ is aperiodic and exists only in the interval of $0 < x < T$, a Fourier series can be formed by constructing, in a number of ways, a periodic function. The Fourier series for the constructed periodic function represents the actual aperiodic function $f(x)$ only in the interval $0 < x < T$. Outside this space, the aperiodic function $f(x)$ is zero and the series representation is not needed. A Fourier series for $f(x)$ converges to the values of $f(x)$ at each point of continuity and to the midpoint of its values at each discontinuity.

In addition, $f(x)$ can also be represented as a superposition of discrete complex exponentials of the form

$$f(x) = \sum_{n=-\infty}^{+\infty} c_n e^{-j(2n\pi/T)x} \tag{12-69}$$

$$c_n = \frac{1}{T}\int_0^T f(x)e^{+j(2n\pi/T)x}dx \tag{12-69a}$$

or of continuous complex exponentials of the form

$$f(x) = \frac{1}{2\pi}\int_{-\infty}^{+\infty} \mathcal{F}(\omega)e^{-jx\omega}\,d\omega \qquad -\infty < \omega < +\infty \tag{12-70a}$$

whose inverse is given by

$$\mathcal{F}(\omega) = \int_{-\infty}^{+\infty} f(x)e^{+j\omega x}\,dx \qquad -\infty < x < +\infty \tag{12-70b}$$

The integral operation in (12-70a) is referred to as the *direct transformation* and that of (12-70b) as the *inverse transformation* and both form a *transform pair.*

Another useful identity is *Parseval's theorem,* which for the transform pair, can be written as

$$\int_{-\infty}^{+\infty} f(x)g^*(x)\,dx = \frac{1}{2\pi}\int_{-\infty}^{+\infty} \mathcal{F}(\omega)\,\mathcal{G}^*(\omega)\,d\omega \tag{12-71}$$

where * indicates complex conjugate.

From the definitions of (12-70a), (12-70b) and (12-71), the Fourier transforms can be expanded to two dimensions and can be written as

$$f(x,y) = \frac{1}{4\pi^2}\int_{-\infty}^{+\infty}\int_{-\infty}^{+\infty} \mathcal{F}(\omega_1, \omega_2)e^{-j(\omega_1 x + \omega_2 y)}\,d\omega_1\,d\omega_2 \tag{12-72a}$$

$$\mathcal{F}(\omega_1,\omega_2) = \int_{-\infty}^{+\infty}\int_{-\infty}^{+\infty} f(x, y)e^{+j(\omega_1 x + \omega_2 y)}\,dx\,dy \tag{12-72b}$$

$$\int_{-\infty}^{+\infty}\int_{-\infty}^{+\infty} f(x, y)\,g^*(x, y)\,dx\,dy = \frac{1}{4\pi^2}\int_{-\infty}^{+\infty}\int_{-\infty}^{+\infty} \mathcal{F}(\omega_1, \omega_2)\,\mathcal{G}^*(\omega_1, \omega_2)\,d\omega_1\,d\omega_2 \tag{12-72c}$$

The process can be continued to n dimensions.

The definitions, theorems, and principles introduced will be utilized in the sections that follow to analyze the radiation characteristics of aperture antennas mounted on infinite ground planes.

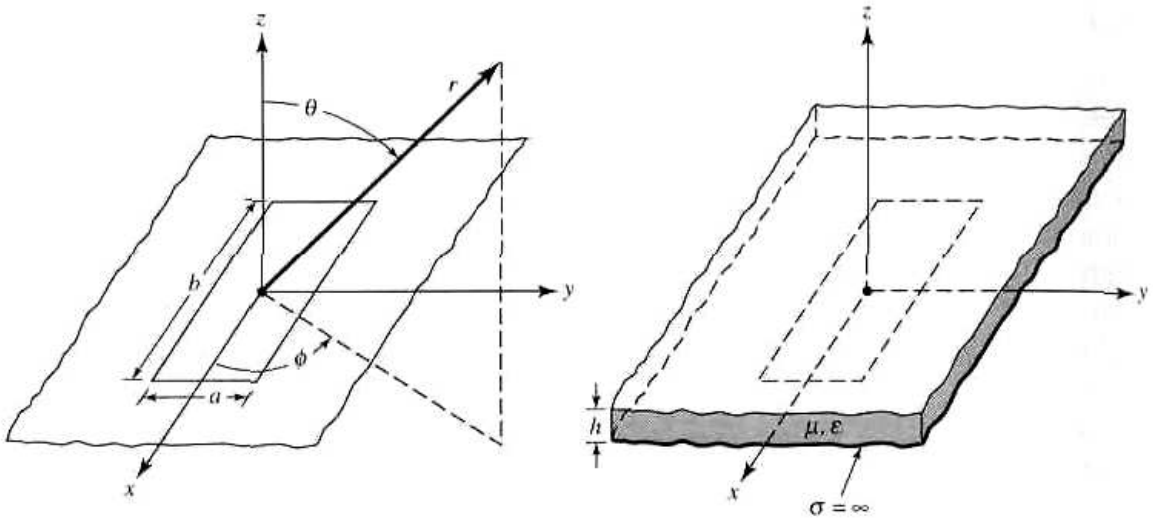

(a) Uncovered aperture (b) Dielectric-covered aperture

Figure 12.26 Rectangular apertures mounted on infinite ground planes.

12.9.2 Radiated Fields

To apply Fourier transforms (*spectral techniques*) to the analysis of aperture antennas, let us consider a rectangular aperture of dimensions a and b mounted on an infinite ground plane, as shown in Figure 12.26. In the source-free region ($z > 0$), the field $\mathbf{E}(x, y, z)$ of a monochromatic wave radiated by the aperture can be written as a superposition of plane waves (all of the same frequency, different amplitudes, and traveling in different directions) of the form $\mathbf{f}(k_x, k_y)e^{-j\mathbf{k}\cdot\mathbf{r}}$ [16], [17]. The function $\mathbf{f}(k_x, k_y)$ is the vector amplitude of the wave, and k_x and k_y are the spectral frequencies which extend over the entire frequency spectrum ($-\infty \leq k_x, k_y \leq \infty$). Thus the field $\mathbf{E}(x, y, z)$ can be written as

$$\mathbf{E}(x, y, z) = \frac{1}{4\pi^2}\int_{-\infty}^{+\infty}\int_{-\infty}^{+\infty}\mathbf{f}(k_x, k_y)e^{-j\mathbf{k}\cdot\mathbf{r}}\,dk_x\,dk_y \tag{12-73}$$

according to the definition of (12-72a). The object of a plane wave expansion is to determine the unknown amplitudes $\mathbf{f}(k_x, k_y)$ and the direction of propagation of the plane waves. Since

$$\mathbf{r} = \hat{\mathbf{a}}_x x + \hat{\mathbf{a}}_y y + \hat{\mathbf{a}}_z z \tag{12-74}$$

and the propagation factor $\mathbf{k}$ (often referred to as the *vector wavenumber*) can be defined as

$$\mathbf{k} = \hat{\mathbf{a}}_x k_x + \hat{\mathbf{a}}_y k_y + \hat{\mathbf{a}}_z k_z \tag{12-75}$$

(12-73) can be written as

$$\mathbf{E}(x, y, z) = \frac{1}{4\pi^2}\int_{-\infty}^{+\infty}\int_{-\infty}^{+\infty}[\mathbf{f}(k_x, k_y)e^{-jk_z z}]e^{-j(k_x x + k_y y)}\,dk_x\,dk_y. \tag{12-76}$$

The part of the integrand within the brackets can be regarded as the transform of $\mathbf{E}(x, y, z)$. This allows us to write the transform pair as

$$\boxed{\mathbf{E}(x, y, z) = \frac{1}{4\pi^2}\int_{-\infty}^{+\infty}\int_{-\infty}^{+\infty}\mathscr{E}(k_x, k_y, z)e^{-j(k_x x + k_y y)}\,dk_x\,dk_y} \tag{12-77a}$$

$$\boxed{\mathscr{E}(k_x, k_y, z) = \int_{-\infty}^{+\infty}\int_{-\infty}^{+\infty} \mathbf{E}(x, y, z)e^{+j(k_x x + k_y y)}\,dx\,dy} \tag{12-77b}$$

where

$$\boxed{\mathscr{E}(k_x, k_y, z) = \mathbf{f}(k_x, k_y)e^{-jk_z z}} \tag{12-77c}$$

In principle then, according to (12-77a) and (12-77b) the fields radiated by an aperture $\mathbf{E}(x, y, z)$ can be found provided its transform $\mathscr{E}(k_x, k_y, z)$ is known. To this point the transform field $\mathscr{E}(k_x, k_y, z)$ can only be found provided the actual field $\mathbf{E}(x, y, z)$ is known *a priori*. In other words, the answer must be known beforehand! However, as it will be seen from what follows, if the transform field at $z = 0$

$$\mathscr{E}(k_x, k_y, z = 0) = \mathbf{f}(k_x, k_y) \tag{12-78}$$

is formed, it will be sufficient to determine $\mathbf{E}(x, y, z)$. To form the transform $\mathscr{E}(k_x, k_y, z = 0) = \mathbf{f}(k_x, k_y)$, it will be necessary and sufficient to know only the tangential components of the **E**-field at $z = 0$. For the problem of Figure 12.26(a), the tangential components of the **E**-field at $z = 0$ exist only over the bounds of the aperture (they vanish outside it because of the presence of the infinite ground plane).

In general

$$\mathbf{f}(k_x, k_y) = \hat{\mathbf{a}}_x f_x(k_x, k_y) + \hat{\mathbf{a}}_y f_y(k_x, k_y) + \hat{\mathbf{a}}_z f_z(k_x, k_y) \tag{12-79}$$

which can also be written as

$$\mathbf{f}(k_x, k_y) = \mathbf{f}_t(k_x, k_y) + \hat{\mathbf{a}}_z f_z(k_x, k_y) \tag{12-79a}$$

$$\mathbf{f}_t(k_x, k_y) = \hat{\mathbf{a}}_x f_x(k_x, k_y) + \hat{\mathbf{a}}_y f_y(k_x, k_y) \tag{12-79b}$$

For aperture antennas positioned along the xy-plane, the only components of $\mathbf{f}(k_x, k_y)$ that need to be found are f_x and f_y. As will be shown in what follows, f_z can be found once f_x and f_y are known. This is a further simplification of the problem. The functions f_x and f_y are found, using (12-77a) and (12-77b), provided the tangential components of the **E**-field over the aperture (E_{xa} and E_{ya}) are specified. The solution of (12-77c) is valid provided the z variations of $\mathbf{E}(k_x, k_y, z)$ are separable. In addition, in the source-free region the field $\mathbf{E}(x, y, z)$ of (12-77a) must satisfy the homogeneous vector wave equation. These allow us to relate the propagation constant k_z to k_x, k_y and $k = (\omega\sqrt{\mu\epsilon})$, by

$$k_z^2 = k^2 - (k_x^2 + k_y^2) \tag{12-80}$$

or

$$k_z = \begin{cases} +[k^2 - (k_x^2 + k_y^2)]^{1/2} & \text{when } k^2 \geq k_x^2 + k_y^2 \quad (12\text{-}80a) \\ -j[(k_x^2 + k_y^2) - k^2]^{1/2} & \text{when } k^2 < k_x^2 + k_y^2 \quad (12\text{-}80b) \end{cases}$$

This is left as an exercise to the reader. The form of k_z as given by (12-80a) contributes to the propagating waves (radiation field) of (12-76) and (12-77a) whereas that of (12-80b) contributes to the evanescent waves. Since the field in the far-zone of the antenna is of the radiation type, its contribution comes from the part of the k_x, k_y spectrum which satisfies (12-80a). The values of k_x and k_y in (12-80)-(12-80b) are analogous to the eigenvalues for the fields inside a rectangular waveguide [12]. In

addition, k_z is analogous to the propagation constant for waveguides which is used to define cutoff.

To find the relation between f_z and f_x, f_y, we proceed as follows. In the source-free region ($z > 0$) the field $\mathbf{E}(x, y, z)$, in addition to satisfying the vector wave equation, must also be solenoidal so that

$$\nabla \cdot \mathbf{E}(x, y, z) = \nabla \cdot \left\{ \frac{1}{4\pi^2} \int_{-\infty}^{+\infty} \int_{-\infty}^{+\infty} \mathbf{f}(k_x, k_y) e^{-j\mathbf{k}\cdot\mathbf{r}} \, dk_x \, dk_y \right\} = 0 \quad (12\text{-}81)$$

Interchanging differentiation with integration and using the vector identity

$$\nabla \cdot (\alpha \mathbf{A}) = \alpha \nabla \cdot \mathbf{A} + \mathbf{A} \cdot \nabla \alpha \quad (12\text{-}82)$$

reduces (12-81) to

$$\frac{1}{4\pi^2} \int_{-\infty}^{+\infty} \int_{-\infty}^{+\infty} [\mathbf{f} \cdot \nabla (e^{-j\mathbf{k}\cdot\mathbf{r}})] \, dk_x \, dk_y = 0 \quad (12\text{-}83)$$

since $\nabla \cdot \mathbf{f}(k_x, k_y) = 0$. Equation (12-83) is satisfied provided that

$$\mathbf{f} \cdot \nabla e^{-j\mathbf{k}\cdot\mathbf{r}} = -j\mathbf{f} \cdot \mathbf{k} e^{-j\mathbf{k}\cdot\mathbf{r}} = 0 \quad (12\text{-}84)$$

or

$$\mathbf{f} \cdot \mathbf{k} = (\mathbf{f}_t + \hat{\mathbf{a}}_z f_z) \cdot \mathbf{k} = 0 \quad (12\text{-}84a)$$

or

$$f_z = -\frac{\mathbf{f}_t \cdot \mathbf{k}}{k_z} = -\frac{(f_x k_x + f_y k_y)}{k_z} \quad (12\text{-}84b)$$

From (12-84b) it is evident that f_z can be formed once f_x and f_y are known.

All three components of $\mathbf{f}$ (f_x, f_y and f_z) can be found, using (12-77b) and (12-78), provided the two components of $\mathbf{E}$ (E_x, E_y) at $z = 0$, which is the plane of the aperture and ground plane of Figure 12.26(a), are known. Because E_x and E_y along the $z = 0$ plane are zero outside the bounds of the aperture ($|x| > a/2$, $|y| > b/2$), (12-77b) and (12-78) reduce for f_x and f_y to

$$\boxed{f_x(k_x, k_y) = \int_{-b/2}^{+b/2} \int_{-a/2}^{+a/2} E_{xa}(x', y', z' = 0) e^{+j(k_x x' + k_y y')} \, dx' \, dy'} \quad (12\text{-}85a)$$

$$\boxed{f_y(k_x, k_y) = \int_{-b/2}^{+b/2} \int_{-a/2}^{+a/2} E_{ya}(x', y', z' = 0) e^{+j(k_x x' + k_y y')} \, dx' \, dy'} \quad (12\text{-}85b)$$

where primes indicate source points. $E_{xa}(x', y', z' = 0)$ and $E_{ya}(x', y', z' = 0)$, which represent the tangential components of the electric field over the aperture, are the only fields that need to be known. Once f_x and f_y are found by using (12-85a) and (12-85b), f_z and $\mathscr{E}(k_x, k_y, z)$ can be formed using (12-84a) and (12-77c), respectively. Thus, the solution for $\mathbf{E}(x, y, z)$ for the aperture in Figure 12.26(a) is given by

$$\mathbf{E}(x, y, z) = \frac{1}{4\pi^2} \left\{ \iint_{k_z = [k^2 - (k_x^2 + k_y^2)]^{1/2}}^{k_x^2 + k_y^2 \le k^2} \mathscr{E}(k_x, k_y, z) e^{-j(k_x x + k_y y)} \, dk_x \, dk_y \right.$$

(Equation continues on top of page 625.)

$$+ \iint_{\substack{k_x^2+k_y^2 > k^2 \\ k_z=-j\sqrt{(k_x^2+k_y^2)-k^2}}} \mathscr{C}(k_x, k_y, z)e^{-j(k_x x + k_y y)}\, dk_x\, dk_y \Bigg\} \tag{12-86}$$

$$\boxed{\mathscr{C}(k_x, k_y, z) = \left[\hat{\mathbf{a}}_x f_x + \hat{\mathbf{a}}_y f_y - \hat{\mathbf{a}}_z\left(\frac{f_x k_x + f_y k_y}{k_z}\right)\right] e^{-jk_z z}} \tag{12-86a}$$

where f_x and f_y are given by (12-85a) and (12-85b).

In summary, the field radiated by the aperture of Figure 12.26(a) can be found by the following procedure:

1. Specify the tangential components of the **E**-field (E_{xa} and E_{ya}) over the bounds of the aperture.
2. Find f_x and f_y using (12-85a) and (12-85b), respectively.
3. Find f_z using (12-85b).
4. Find $\mathscr{C}(k_x, k_y, z)$ using (12-86a).
5. Formulate $\mathbf{E}(x, y, z)$ using (12-86).

This completes the solution for $\mathbf{E}(x, y, z)$. However, as is evident from (12-86), the integration is quite difficult even for the simplest of problems. However, if the observations are restricted in the far-field region, many simplifications in performing the integrations can result. This was apparent in Chapters 4, 5 and in others. In many practical problems, the far-zone is usually the region of greatest importance. Since it is also known that for all antennas the fields in the far-zone are primarily of the radiated type (*propagating waves*), then only the first integral in (12-86) contributes in that region.

In the next section, our attention is directed toward the evaluation of (12-86a) or (12-73) in the far-zone region (large values of kr). This is accomplished by evaluating (12-73) asymptotically for large values of kr by the method of *Stationary Phase* [18], [19].

To complete the formulation of the radiated fields in all regions, let us outline the procedure to find $\mathbf{H}(x, y, z)$. From Maxwell's equations

$$\begin{aligned}\mathbf{H}(x, y, z) &= -\frac{1}{j\omega\mu}\nabla \times \mathbf{E}(x, y, z) \\ &= -\frac{1}{j\omega\mu}\nabla \times \left[\frac{1}{4\pi^2}\int_{-\infty}^{+\infty}\int_{-\infty}^{+\infty} \mathbf{f}(k_x, k_y)e^{-j\mathbf{k}\cdot\mathbf{r}}\, dk_x\, dk_y\right]\end{aligned} \tag{12-87}$$

Interchanging integration with differentiation and using the vector identity

$$\nabla \times (\alpha\mathbf{A}) = \alpha\nabla \times \mathbf{A} + (\nabla\alpha) \times \mathbf{A} \tag{12-88}$$

reduces (12-87) to

$$\mathbf{H}(x, y, z) = -\frac{1}{4\pi^2 k\eta}\int_{-\infty}^{+\infty}\int_{-\infty}^{+\infty} (\mathbf{f} \times \mathbf{k})e^{-j\mathbf{k}\cdot\mathbf{r}} dk_x\, dk_y \tag{12-89}$$

since $\nabla \times \mathbf{f}(k_x, k_y) = 0$ and $\nabla(e^{-j\mathbf{k}\cdot\mathbf{r}}) = -j\mathbf{k}e^{-j\mathbf{k}\cdot\mathbf{r}}$ from (12-84).

12.9.3 Asymptotic Evaluation of Radiated Field

The main objective in this section is the evaluation of (12-73) or (12-86a) for observations made in the far-field. For most practical antennas, the field distribution on the

aperture is such that an exact evaluation of (12-73) in closed form is not possible. However, if the observations are restricted to the far-field region (large kr), the integral evaluation becomes less complex. This was apparent in Chapters 4, 5, and others. The integral of (12-73) will be evaluated asymptotically for large values of kr using the method of *Stationary Phase* (Appendix VIII) [18], [19].

The stationary phase method assumes that the main contribution to the integral of (12-73) comes from values of k_x and k_y where $\mathbf{k} \cdot \mathbf{r}$ does not change for first order changes in k_x and k_y. That is to say $\mathbf{k} \cdot \mathbf{r}$ remains stationary at those points. For the other values of k_x and k_y, $\mathbf{k} \cdot \mathbf{r}$ changes very rapidly and the function $e^{-j\mathbf{k}\cdot\mathbf{r}}$ oscillates very rapidly between the values of $+1$ and -1. Assuming that $\mathbf{f}(k_x, k_y)$ is a slowly varying function of k_x and k_y, the integrand of (12-73) oscillates very rapidly outside the stationary points so that the contribution to the integral from that region is negligible. As the observation point approaches infinity, the contributions to the integral from the region outside the stationary points is zero. For practical applications, the observation point cannot be at infinity. However, it will be assumed to be far enough *such that the major contributions come from the stationary points.*

The first task in the asymptotic evaluation of (12-73) is to find the stationary points of $\mathbf{k} \cdot \mathbf{r}$. For that $\mathbf{k} \cdot \mathbf{r}$ is written as

$$\mathbf{k} \cdot \mathbf{r} = (\hat{\mathbf{a}}_x k_x + \hat{\mathbf{a}}_y k_y + \hat{\mathbf{a}}_z k_z) \cdot \hat{\mathbf{a}}_r r \tag{12-90}$$

Using the inverse transformation of (4-5), (12-90) can be written as

$$\mathbf{k} \cdot \mathbf{r} = r(k_x \sin\theta\cos\phi + k_y \sin\theta\sin\phi + k_z \cos\theta) \tag{12-91}$$

which reduces, using (12-80a) to

$$\mathbf{k} \cdot \mathbf{r} = r[k_x \sin\theta\cos\phi + k_y \sin\theta\sin\phi + \sqrt{k^2 - k_x^2 - k_y^2}\cos\theta] \tag{12-92}$$

The stationary points can be found by

$$\frac{\partial(\mathbf{k} \cdot \mathbf{r})}{\partial k_x} = 0 \tag{12-93a}$$

$$\frac{\partial(\mathbf{k} \cdot \mathbf{r})}{\partial k_y} = 0 \tag{12-93b}$$

Using (12-92) and (12-80), (12-93a) and (12-93b) reduce to

$$\frac{\partial(\mathbf{k} \cdot \mathbf{r})}{\partial k_x} = r\left(\sin\theta\cos\phi - \frac{k_x}{k_z}\cos\theta\right) = 0 \tag{12-94a}$$

$$\frac{\partial(\mathbf{k} \cdot \mathbf{r})}{\partial k_y} = r\left(\sin\theta\sin\phi - \frac{k_y}{k_z}\cos\theta\right) = 0 \tag{12-94b}$$

whose solutions are given, respectively, by

$$k_x = k_z \frac{\sin\theta\cos\phi}{\cos\theta} \tag{12-95a}$$

$$k_y = k_z \frac{\sin\theta\sin\phi}{\cos\theta} \tag{12-95b}$$

Using (12-95a) and (12-95b), (12-80) can be written as

$$k^2 = k_z^2 + k_x^2 + k_y^2 = k_z^2\left(1 + \frac{\sin^2\theta}{\cos^2\theta}\right) \tag{12-96}$$

which reduces for k_z to

$$k_z = k \cos \theta \tag{12-97}$$

With the aid of (12-97), the stationary point of (12-95a) and (12-95b) simplify to

$$k_x = k \sin \theta \cos \phi = k_1 \tag{12-98a}$$

$$k_y = k \sin \theta \sin \phi = k_2 \tag{12-98b}$$

The function $\mathbf{k} \cdot \mathbf{r}$ can be expanded into a Taylor series, about the stationary point k_1, k_2, and it can be approximated by the zero, first, and second order terms. That is,

$$\begin{aligned}\mathbf{k} \cdot \mathbf{r} \simeq \mathbf{k} \cdot \mathbf{r}\Big|_{k_1,k_2} &+ \frac{\partial(\mathbf{k} \cdot \mathbf{r})}{\partial k_x}\Big|_{k_1,k_2} (k_x - k_1) + \frac{\partial(\mathbf{k} \cdot \mathbf{r})}{\partial k_y}\Big|_{k_1,k_2} (k_y - k_2) \\ &+ \frac{1}{2}\frac{\partial^2(\mathbf{k} \cdot \mathbf{r})}{\partial k_x^2}\Big|_{k_1,k_2} (k_x - k_1)^2 + \frac{1}{2}\frac{\partial^2(\mathbf{k} \cdot \mathbf{r})}{\partial k_y^2}\Big|_{k_1,k_2} (k_y - k_2)^2 \\ &+ \frac{\partial^2(\mathbf{k} \cdot \mathbf{r})}{\partial k_x \partial k_y}\Big|_{k_1,k_2} (k_x - k_1)(k_y - k_2)\end{aligned} \tag{12-99}$$

Since the second and third terms vanish at the stationary point $k_x = k_1$ and $k_y = k_2$, (12-99) can be expressed as

$$\mathbf{k} \cdot \mathbf{r} = \mathbf{k} \cdot \mathbf{r}\Big|_{k_1,k_2} - A\xi^2 - B\eta^2 - C\xi\eta \tag{12-100}$$

where

$$A = -\frac{1}{2}\frac{\partial^2(\mathbf{k} \cdot \mathbf{r})}{\partial k_x^2}\Big|_{k_1,k_2} \tag{12-100a}$$

$$B = -\frac{1}{2}\frac{\partial^2(\mathbf{k} \cdot \mathbf{r})}{\partial k_y^2}\Big|_{k_1,k_2} \tag{12-100b}$$

$$C = -\frac{\partial^2(\mathbf{k} \cdot \mathbf{r})}{\partial k_x \partial k_y}\Big|_{k_1,k_2} \tag{12-100c}$$

$$\xi = (k_x - k_1) \tag{12-100d}$$

$$\eta = (k_y - k_2) \tag{12-100e}$$

Using (12-97)-(12-98b), (12-90) reduces to

$$\mathbf{k} \cdot \mathbf{r}\Big|_{k_1,k_2} = kr \tag{12-101}$$

Similarly, with the aid of (12-92), A, B, and C can be written, after a few manipulations, as

$$A = -\frac{1}{2}\frac{\partial^2(\mathbf{k} \cdot \mathbf{r})}{\partial k_x^2}\Big|_{k_1,k_2} = \frac{r}{2k}\left(1 + \frac{\sin^2 \theta \cos^2 \phi}{\cos^2 \theta}\right) \tag{12-102a}$$

$$B = -\frac{1}{2}\frac{\partial^2(\mathbf{k} \cdot \mathbf{r})}{\partial k_y^2}\Big|_{k_1,k_2} = \frac{r}{2k}\left(1 + \frac{\sin^2 \theta \sin^2 \phi}{\cos^2 \theta}\right) \tag{12-102b}$$

$$C = -\frac{\partial^2(\mathbf{k} \cdot \mathbf{r})}{\partial k_x \partial k_y}\Big|_{k_1,k_2} = \frac{r}{k}\frac{\sin^2 \theta}{\cos^2 \theta} \cos \phi \sin \phi \tag{12-102c}$$

Thus (12-73) can be approximated around the stationary point $k_x = k_1$ and $k_y = k_2$, which contributes mostly to the integral, by

$$\mathbf{E}(x, y, z) \simeq \frac{1}{4\pi^2}\iint_{S_{1,2}} \mathbf{f}(k_x = k_1, k_y = k_2)e^{-j(kr - A\xi^2 - B\eta^2 - C\xi\eta)}\,d\xi\,d\eta \quad (12\text{-}103)$$

or

$$\mathbf{E}(x, y, z) \simeq \frac{1}{4\pi^2}\mathbf{f}(k_1, k_2)e^{-jkr}\iint_{S_{1,2}} e^{+j(A\xi^2 + B\eta^2 + C\xi\eta)}\,d\xi\,d\eta \quad (12\text{-}103a)$$

where $S_{1,2}$ is the surface near the stationary point.

The integral of (12-103a) can be evaluated with the method of *Stationary Phase*. That is, (see Appendix VIII)

$$\boxed{\iint_{S_{1,2}} e^{j(A\xi^2 + B\eta^2 + C\xi\eta)}\,d\xi\,d\eta = j\frac{2\pi\delta}{\sqrt{|4AB - C^2|}}} \quad (12\text{-}104)$$

$$\boxed{\delta = \begin{cases} +1 & \text{if } 4AB > C^2 \text{ and } A > 0 \\ -1 & \text{if } 4AB > C^2 \text{ and } A < 0 \\ -j & \text{if } 4AB < C^2 \end{cases}} \quad (12\text{-}104a)$$

With the aid of (12-102a)-(12-102c), the factor $4AB - C^2$ is

$$4AB - C^2 = \left(\frac{r}{k\cos\theta}\right)^2 \quad (12\text{-}105)$$

Since $4AB > C^2$ and $A > 0$, (12-103) reduces to

$$\iint_{S_{1,2}} e^{j(A\xi^2 + B\eta^2 + C\xi\eta)}\,d\xi\,d\eta = j\frac{2\pi k}{r}\cos\theta \quad (12\text{-}106)$$

and (12-103a) to

$$\mathbf{E}(r, \theta, \phi) \simeq j\frac{ke^{-jkr}}{2\pi r}\left[\cos\theta\,\mathbf{f}(k_1 = k\sin\theta\cos\phi, k_2 = k\sin\theta\sin\phi)\right] \quad (12\text{-}107)$$

In the far-field region, only the θ and ϕ components of the electric and magnetic fields are dominant. Therefore, the E_θ and E_ϕ components of (12-107) can be written in terms of f_x and f_y. With the aid of (12-84b), $\mathbf{f}$ can be expressed as

$$\mathbf{f} = \hat{\mathbf{a}}_x f_x + \hat{\mathbf{a}}_y f_y + \hat{\mathbf{a}}_z f_z = \left[\hat{\mathbf{a}}_x f_x + \hat{\mathbf{a}}_y f_y - \hat{\mathbf{a}}_z\frac{(f_x k_x + f_y k_y)}{k_z}\right] \quad (12\text{-}108)$$

At the stationary point ($k_x = k_1 = k\sin\theta\cos\phi$, $k_y = k_2 = k\sin\theta\sin\phi$, $k_z = k\cos\theta$), (12-108) reduces to

$$\mathbf{f}(k_1, k_2) = \left[\hat{\mathbf{a}}_x f_x + \hat{\mathbf{a}}_y f_y - \hat{\mathbf{a}}_z\frac{\sin\theta}{\cos\theta}(f_x\cos\phi + f_y\sin\phi)\right] \quad (12\text{-}109)$$

Using the inverse transformation of (4-5), the θ and ϕ components of $\mathbf{f}$ can be written as

$$\boxed{f_\theta = \frac{f_x\cos\phi + f_y\sin\phi}{\cos\theta}} \quad (12\text{-}110a)$$

$$\boxed{f_\phi = -f_x \sin\phi + f_y \cos\phi} \tag{12-110b}$$

The **E**-field of (12-107) reduces, for the θ and ϕ components, to

$$\boxed{\mathbf{E}(r, \theta, \phi) \simeq j\frac{ke^{-jkr}}{2\pi r}[\hat{\mathbf{a}}_\theta(f_x \cos\phi + f_y \sin\phi) + \hat{\mathbf{a}}_\phi \cos\theta(-f_x \sin\phi + f_y \cos\phi)]} \tag{12-111}$$

and the **H**-field to

$$\mathbf{H}(r, \theta, \phi) = \sqrt{\frac{\epsilon}{\mu}}[\hat{\mathbf{a}}_r \times \mathbf{E}(r, \theta, \phi)] \tag{12-112}$$

where from (12-85a) and (12-85b)

$$\boxed{\begin{aligned} &f_x(k_x = k_1, k_y = k_2) \\ &= \int_{-b/2}^{+b/2}\int_{-a/2}^{+a/2} E_{xa}(x', y', z' = 0)\, e^{jk(x' \sin\theta\cos\phi + y' \sin\theta\sin\phi)}\, dx'\, dy' \end{aligned}} \tag{12-113a}$$

$$\boxed{\begin{aligned} &f_y(k_x = k_1, k_y = k_2) \\ &= \int_{-b/2}^{+b/2}\int_{-a/2}^{+a/2} E_{ya}(x', y', z' = 0)\, e^{jk(x' \sin\theta\cos\phi + y' \sin\theta\sin\phi)}\, dx'\, dy' \end{aligned}} \tag{12-113b}$$

To illustrate the frequency domain (*spectral*) techniques, the problem of a uniform illuminated aperture, which was previously analyzed in Section 12.5.1 using spatial methods, will be solved again using transform methods.

Example 12.7

A rectangular aperture of dimensions a and b is mounted on an infinite ground plane, as shown in Figure 12.26(a). Find the field radiated by it assuming that over the opening the electric field is given by

$$\mathbf{E}_a = \hat{\mathbf{a}}_y E_0, \qquad \begin{aligned} -a/2 \le x' \le a/2 \\ -b/2 \le y' \le b/2 \end{aligned}$$

where E_0 is a constant.

SOLUTION

From (12-113a) and (12-113b)

$$f_x = 0$$
$$f_y = E_0 \int_{-b/2}^{+b/2} e^{jky' \sin\theta\sin\phi}\, dy' \int_{-a/2}^{+a/2} e^{jkx' \sin\theta\cos\phi}\, dx'$$

which, when integrated, reduces to

$$f_y = abE_0\left(\frac{\sin X}{X}\right)\left(\frac{\sin Y}{Y}\right)$$

$$X = \frac{ka}{2} \sin\theta \cos\phi$$

$$Y = \frac{kb}{2} \sin\theta \sin\phi$$

The θ and ϕ components of (12-111) can be written as

$$E_\theta = j\frac{abkE_0 e^{-jkr}}{2\pi r}\left\{ \sin\phi \left[\frac{\sin X}{X}\right]\left[\frac{\sin Y}{Y}\right]\right\}$$

$$E_\phi = j\frac{abkE_0 e^{-jkr}}{2\pi r}\left\{ \cos\theta\cos\phi \left[\frac{\sin X}{X}\right]\left[\frac{\sin Y}{Y}\right]\right\}$$

which are identical to those of (12-23b) and (12-23c), respectively.

12.9.4 Dielectric Covered Apertures

The transform (*spectral*) technique can easily be extended to determine the field radiated by dielectric-covered apertures [20], [21]. For the sake of brevity, the details will not be included here. However, it can be shown that for a single lossless dielectric sheet cover of thickness h, dielectric constant ϵ_r, unity relative permeability, and free-space phase constant k_0, the far-zone radiated field E_θ, E_ϕ of the covered aperture of Figure 12.26(b) are related to E_θ^0, E_ϕ^0 of the uncovered aperture of Figure 12.26(a) by

$$\boxed{E_\theta(r, \theta, \phi) = f(\theta)\, E_\theta^0(r, \theta, \phi)} \tag{12-114a}$$

$$\boxed{E_\phi(r, \theta, \phi) = g(\theta)\, E_\phi^0(r, \theta, \phi)} \tag{12-114b}$$

where

E_θ, E_ϕ = field components of dielectric covered aperture [Fig. 12.26(b)]

E_θ^0, E_ϕ^0 = field components of uncovered aperture [Fig. 12.26(a)]

$$\boxed{f(\theta) = \frac{e^{jk_0 h\cos\theta}}{\cos\psi + jZ_h \sin\psi}} \tag{12-114c}$$

$$\boxed{g(\theta) = \frac{e^{jk_0 h\cos\theta}}{\cos\psi + jZ_e \sin\psi}} \tag{12-114d}$$

$$\boxed{\psi = k_0 h\sqrt{\epsilon_r - \sin^2\theta}} \tag{12-114e}$$

$$\boxed{Z_e = \frac{\cos\theta}{\sqrt{\epsilon_r - \sin^2\theta}}} \tag{12-114f}$$

$$\boxed{Z_h = \frac{\sqrt{\epsilon_r - \sin^2\theta}}{\epsilon_r \cos\theta}} \tag{12-114g}$$

The above relations do not include surface wave contributions which can be taken into account but are beyond the scope of this section [20].

To investigate the effect of the dielectric sheet, far-zone principal E- and H-plane patterns were computed for a rectangular waveguide shown in Figure 12.26(b). The waveguide was covered with a single dielectric sheet, was operating in the dominant TE_{10} mode, and was mounted on an infinite ground plane. The E- and H-plane patterns are shown in Figure 12.27(a) and 12.27(b), respectively. In the E-plane patterns, it is evident that the surface impedance of the modified ground plane forces the normal electric field component to vanish along the surface ($\theta = \pi/2$). This is similar to the effects experienced by the patterns of the vertical dipole above ground shown in Figure 4.28. Since the H-plane patterns have vanishing characteristics when the aperture is radiating in free-space, the presence of the dielectric sheet has a very small overall effect. This is similar to the effects experienced by the patterns of a horizontal dipole above ground shown in Figure 4.30. However, both the E- and H-plane patterns become more broad near the surface, and more narrow elsewhere, as the thickness increases.

12.9.5 Aperture Admittance

Another parameter of interest, especially when the antenna is used as a diagnostic tool, is its terminating impedance or admittance. In this section, using Fourier transform (*spectral*) techniques, the admittance of an aperture antenna mounted on an infinite ground plane and radiating into free-space will be formulated. Computations will be presented for a parallel-plate waveguide. The techniques can best be presented by considering a specific antenna configuration and field distribution. Similar steps can be used for any other geometry and field distribution.

The geometrical arrangement of the aperture antenna under consideration is shown in Figure 12.26(a). It consists of a rectangular waveguide mounted on an infinite ground plane. It is assumed that the field distribution, *above cutoff*, is that given by the TE_{10} mode, or

$$\mathbf{E}_a = \hat{\mathbf{a}}_y E_0 \cos\left(\frac{\pi}{a}x'\right) \qquad \begin{matrix} -a/2 \le x' \le a/2 \\ -b/2 \le y' \le b/2 \end{matrix} \tag{12-115}$$

where E_0 is a constant. The aperture admittance is defined as

$$Y_a = \frac{2P^*}{|V|^2} \tag{12-116}$$

where

P^* = conjugate of complex power transmitted by the aperture

V = aperture reference voltage.

The complex power transmitted by the aperture can be written as

$$P = \frac{1}{2}\int_{S_a}\int [\mathbf{E}(x', y', z' = 0) \times \mathbf{H}^*(x', y', z' = 0)] \cdot \hat{\mathbf{a}}_z \, dx' \, dy' \tag{12-117}$$

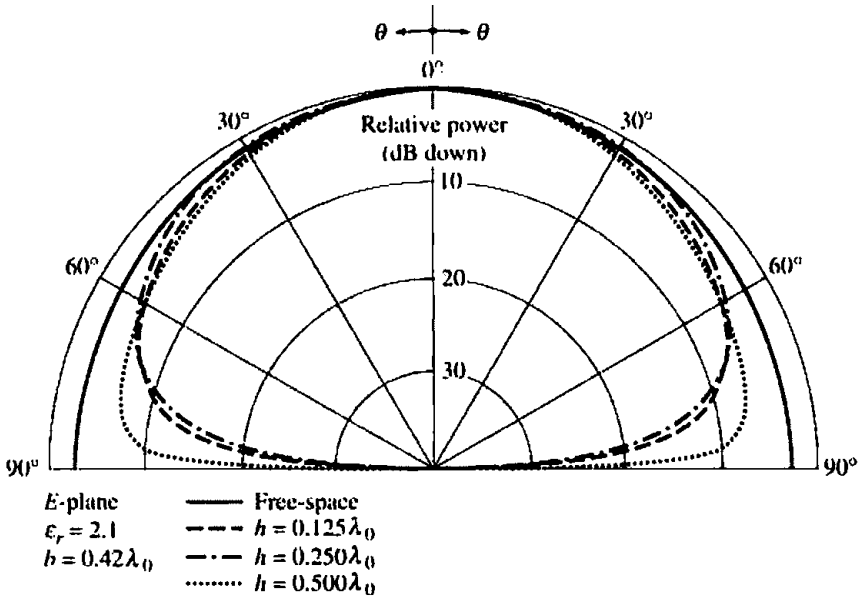

(a) E-plane

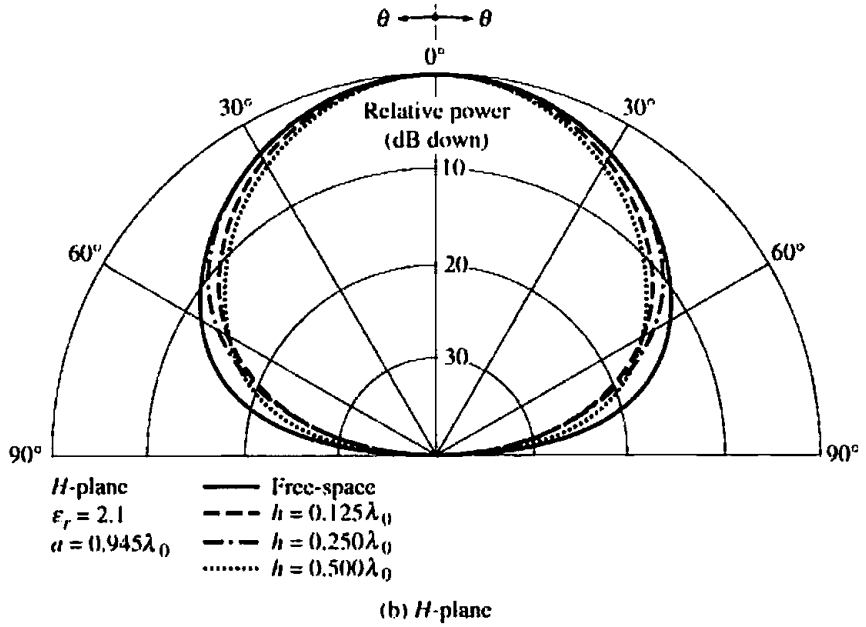

(b) H-plane

Figure 12.27 Amplitude radiation patterns of a dielectric covered waveguide mounted on an infinite ground plane and with a TE_{10} mode aperture field distribution.

where S_a is the aperture of the antenna. $\mathbf{E}(x', y', z' = 0)$ and $\mathbf{H}(x', y', z' = 0)$ represent the total electric and magnetic fields at the aperture including those of the modes which operate below cutoff and contribute to the imaginary power. For the field distribution given by (12-115), (12-117) reduces to

$$P = -\frac{1}{2}\int_{S_a}\int [E_y(x', y', z' = 0)H_x^*(x', y', z' = 0)]\, dx'\, dy' \quad (12\text{-}117a)$$

The amplitude coefficients of all modes that can exist within the waveguide, propagating and nonpropagating, can be evaluated provided the total tangential **E**- and/or **H**-field at any point within the waveguide is known. Assuming that (12-115)

represents the total tangential E-field, it allows the determination of all mode coefficients. Even though this can be accomplished, the formulation of (12-117a) in the spatial domain becomes rather complex [22].

An alternate and simpler method in the formulation of the aperture admittance is to use Fourier transforms. By Parseval's theorem of (12-72c), (12-117a) can be written as

$$P = -\frac{1}{2}\int_{-\infty}^{+\infty}\int_{-\infty}^{+\infty} E_y(x', y', z' = 0)\, H_x^*(x', y', z' = 0)\, dx'\, dy'$$

$$= -\frac{1}{8\pi^2}\int_{-\infty}^{+\infty}\int_{-\infty}^{+\infty} \mathscr{E}_y(k_x, k_y)\, \mathscr{H}_x^*(k_x, k_y)\, dk_x\, dk_y \tag{12-118}$$

where the limits of the first integral have been extended to infinity since $E_y(x', y', z' = 0)$ vanishes outside the physical bounds of the aperture. $\mathscr{E}_y(k_x, k_y)$ and $\mathscr{H}_x(k_x, k_y)$ are the Fourier transforms of the aperture E- and H-fields, respectively.

The transform $\mathscr{E}(k_x, k_y, z = 0)$ is obtained from (12-78) while $\mathscr{H}(k_x, k_y, z = 0)$ can be written, by referring to (12-89), as

$$\mathscr{H}(k_x, k_y, z = 0) = -\frac{1}{k\eta}(\mathbf{f} \times \mathbf{k}) \tag{12-119}$$

For the problem at hand, the transforms $\mathscr{E}_y$ and $\mathscr{H}_x$ are given by

$$\mathscr{E}_y(k_x, k_y) = f_y(k_x, k_y) \tag{12-120}$$

$$\mathscr{H}_x(k_x, k_y) = -\frac{1}{k\eta}\left(k_z + \frac{k_y^2}{k_z}\right) f_y = -\frac{1}{k\eta}\left(\frac{k^2 - k_x^2}{k_z}\right) f_y \tag{12-121}$$

Using (12-77b) and (12-115), (12-120) reduces to

$$f_y(k_x, k_y) = E_0 \int_{-b/2}^{+b/2}\int_{-a/2}^{+a/2} \cos\left(\frac{\pi}{a}x'\right) e^{j(k_x x' + k_y y')}\, dx'\, dy'$$

$$f_y(k_x, k_y) = \left(\frac{\pi ab}{2}\right) E_0 \left[\frac{\cos X}{(\pi/2)^2 - (X)^2}\right]\left[\frac{\sin Y}{Y}\right] \tag{12-122}$$

where

$$X = \frac{k_x a}{2} \tag{12-122a}$$

$$Y = \frac{k_y b}{2} \tag{12-122b}$$

Substituting (12-120)–(12-122b) into (12-118) leads to

$$P = \frac{(\pi ab E_0)^2}{32\pi^2 k\eta}\int_{-\infty}^{+\infty}\int_{-\infty}^{+\infty}\left\{\frac{(k^2 - k_x^2)}{k_z^*}\left[\frac{\cos X}{(\pi/2)^2 - (X)^2}\right]^2\left[\frac{\sin Y}{Y}\right]^2\right\} dk_x\, dk_y \tag{12-123}$$

If the reference aperture voltage is given by

$$V = \frac{ab}{\sqrt{2}} E_0 \tag{12-124}$$

the aperture admittance can be written as

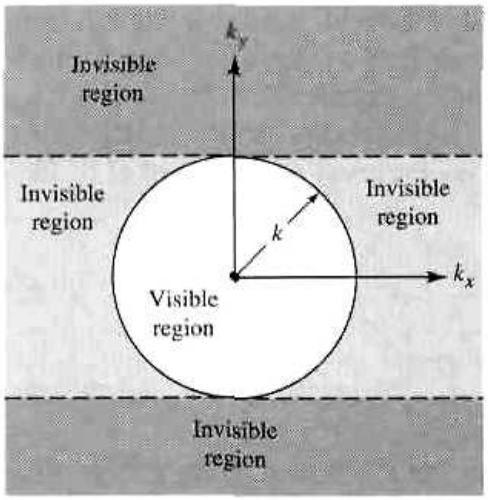

Figure 12.28 Visible and invisible regions in k-space.

$$Y_a = \frac{2P^*}{|V|^2} = \frac{1}{8k\eta}\int_{-\infty}^{+\infty}\left\{\left[\frac{\sin\left(\frac{k_y b}{2}\right)}{\frac{k_y b}{2}}\right]^2 \int_{-\infty}^{+\infty}\frac{(k^2 - k_x^2)}{k_z} \times \left[\frac{\cos\left(\frac{k_x a}{2}\right)}{\left(\frac{\pi}{2}\right)^2 - \left(\frac{k_x a}{2}\right)^2}\right]^2 dk_x\right\} dk_y \tag{12-125}$$

where k_z is given by (12-80a) and (12-80b). As stated before, the values of k_z as given by (12-80a) contribute to the radiated (real) power and those of (12-80b) contribute to the reactive (imaginary) power. Referring to Figure 12.28, values of k_x and k_y within the circle contribute to the aperture conductance, and the space is referred to as the *visible region.* Values of k_x and k_y outside the circle contribute to the aperture susceptance and constitute the *invisible region.* Thus (12-125) can be separated into its real and imaginary parts, and it can be written as

$$Y_a = G_a + jB_a \tag{12-126}$$

$$G_a = \frac{1}{4k\eta}\int_0^k \left[\frac{\sin\left(\frac{k_y b}{2}\right)}{\frac{k_y b}{2}}\right]^2 \left\{\int_0^{\sqrt{k^2 - k_y^2}} \frac{(k^2 - k_x^2)}{[k^2 - (k_x^2 + k_y^2)]^{1/2}} \times \left[\frac{\cos\left(\frac{k_x a}{2}\right)}{\left(\frac{\pi}{2}\right)^2 - \left(\frac{k_x a}{2}\right)^2}\right]^2 dk_x\right\} dk_y \tag{12-126a}$$

$$B_a = -\frac{1}{4k\eta}\left\{\int_0^k \left[\frac{\sin\left(\frac{k_y b}{2}\right)}{\frac{k_y b}{2}}\right]^2 \left\{\int_{\sqrt{k^2-k_y^2}}^{\infty} \frac{(k_x^2 - k^2)}{[(k_x^2 + k_y^2) - k^2]^{1/2}} \times \left[\frac{\cos\left(\frac{k_x a}{2}\right)}{\left(\frac{\pi}{2}\right)^2 - \left(\frac{k_x a}{2}\right)^2}\right]^2 dk_x\right\} dk_y + \int_k^{\infty} \left[\frac{\sin\left(\frac{k_y b}{2}\right)}{\frac{k_y b}{2}}\right]^2 \left\{\int_0^{\infty} \frac{(k_x^2 - k^2)}{[(k_x^2 + k_y^2) - k^2]^{1/2}} \times \left[\frac{\cos\left(\frac{k_x a}{2}\right)}{\left(\frac{\pi}{2}\right)^2 - \left(\frac{k_x a}{2}\right)^2}\right]^2 dk_x\right\} dk_y\right\} \tag{12-126b}$$

The first term in (12-126b) takes into account the contributions from the strip outside the circle for which $k_y < k$, and the second term includes the remaining space outside the circle.

The numerical evaluation of (12-126a) and (12-126b) is complex and will not be attempted here. Computations for the admittance of rectangular apertures radiating into lossless and lossy half-spaces have been carried out and appear in the literature [23]–[27]. Various ingenious techniques have been used to evaluate these integrals.

Because of the complicated nature of (12-126a) and (12-126b) to obtain numerical data, a simpler configuration will be considered as an example.

Example 12.8

A parallel plate waveguide is mounted on an infinite ground plane, as shown in Figure 12.29. Assuming the total electric field at the aperture is given by

$$\mathbf{E}_a = \hat{\mathbf{a}}_y E_0 \qquad -b/2 \le y' \le b/2$$

where E_0 is a constant, find the aperture admittance assuming the aperture voltage is given by $V = bE_0$.

SOLUTION

This problem bears a very close similarity to that of Figure 12.26(a), and most of the results of this example can be obtained almost directly from the previous formulation. Since the problem is two-dimensional, (12-120)–(12-122) reduce to

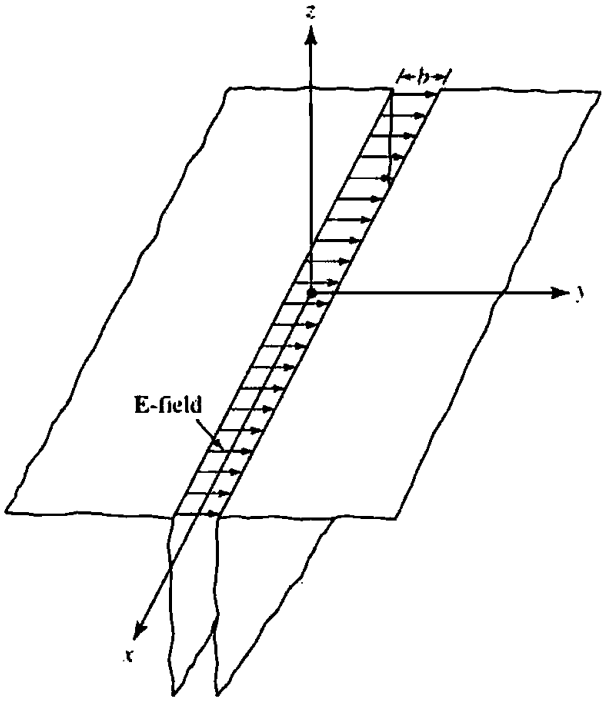

Figure 12.29 Parallel plate waveguide geometry and aperture field distribution.

$$\mathscr{E}_y(k_y) = f_y(k_y) = bE_0 \frac{\sin\left(\frac{k_y b}{2}\right)}{\frac{k_y b}{2}}$$

$$\mathscr{H}_x(k_y) = \frac{k}{\eta}\frac{f_y}{k_z} = \frac{kbE_0}{\eta k_z}\frac{\sin\left(\frac{k_y b}{2}\right)}{\frac{k_y b}{2}}$$

and (12-123) to

$$P = \frac{(bE_0)^2 k}{4\pi\eta}\int_{-\infty}^{+\infty}\frac{1}{k_z^*}\left[\frac{\sin\left(\frac{k_y b}{2}\right)}{\frac{k_y b}{2}}\right]^2 dk_y$$

Since the aperture voltage is given by $V = bE_0$, the aperture slot admittance (*per unit length along the x direction*) of (12-125) can be written as

$$Y_a = \frac{k}{2\pi\eta}\int_{-\infty}^{+\infty}\frac{1}{k_z}\left[\frac{\sin\left(\frac{k_y b}{2}\right)}{\frac{k_y b}{2}}\right]^2 dk_y$$

and the aperture slot conductance and susceptance of (12-126a) and (12-126b) as

$$G_a = \frac{k}{2\pi\eta}\int_{-k}^{k}\frac{1}{\sqrt{k^2 - k_y^2}}\left[\frac{\sin\left(\frac{k_y b}{2}\right)}{\frac{k_y b}{2}}\right]^2 dk_y$$

$$= \frac{k}{\pi\eta}\int_{0}^{k}\frac{1}{\sqrt{k^2 - k_y^2}}\left[\frac{\sin\left(\frac{k_y b}{2}\right)}{\frac{k_y b}{2}}\right]^2 dk_y$$

$$B_a = \frac{k}{2\pi\eta}\left\{\int_{-\infty}^{k}\frac{1}{\sqrt{k_y^2 - k^2}}\left[\frac{\sin\left(\frac{k_y b}{2}\right)}{\frac{k_y b}{2}}\right]^2 dk_y + \int_{k}^{\infty}\frac{1}{\sqrt{k_y^2 - k^2}}\left[\frac{\sin\left(\frac{k_y b}{2}\right)}{\frac{k_y b}{2}}\right]^2 dk_y\right\}$$

$$B_a = \frac{k}{\pi\eta}\int_{k}^{\infty}\frac{1}{\sqrt{k_y^2 - k^2}}\left[\frac{\sin\left(\frac{k_y b}{2}\right)}{\frac{k_y b}{2}}\right]^2 dk_y$$

If

$$w = \frac{b}{2}k_y$$

the expressions for the slot conductance and susceptance reduce to

$$G_a = \frac{2}{\eta\lambda}\int_{0}^{kb/2}\frac{1}{\sqrt{(kb/2)^2 - w^2}}\left(\frac{\sin w}{w}\right)^2 dw$$

$$B_a = \frac{2}{\eta\lambda}\int_{kb/2}^{\infty}\frac{1}{\sqrt{w^2 - (kb/2)^2}}\left(\frac{\sin w}{w}\right)^2 dw$$

The admittance will always be capacitive since B_a is positive.

The expressions for the slot conductance and susceptance (*per unit length along the x direction*) reduce for small values of kb to [5]

$$\left.\begin{aligned} G_a &\simeq \frac{\pi}{\eta\lambda}\left[1 - \frac{(kb)^2}{24}\right] \\ B_a &\simeq \frac{\pi}{\eta\lambda}\left[1 - 0.636\ln(kb)\right] \end{aligned}\right\} \quad \frac{b}{\lambda} < \frac{1}{10}$$

and for large values of kb to

$$\left.\begin{aligned} G_a &\simeq \frac{1}{\eta b} \\ B_a &\simeq \frac{\lambda}{\eta}\left(\frac{1}{\pi b}\right)^2\left[1 - \frac{1}{2}\sqrt{\frac{\lambda}{b}}\cos\left(\frac{2b}{\lambda} + \frac{1}{4}\right)\pi\right] \end{aligned}\right\} \quad \frac{b}{\lambda} > 1$$

Normalized values of λG_a and λB_a as a function of b/λ for an aperture radiating into free space are shown plotted in Figure 12.30.

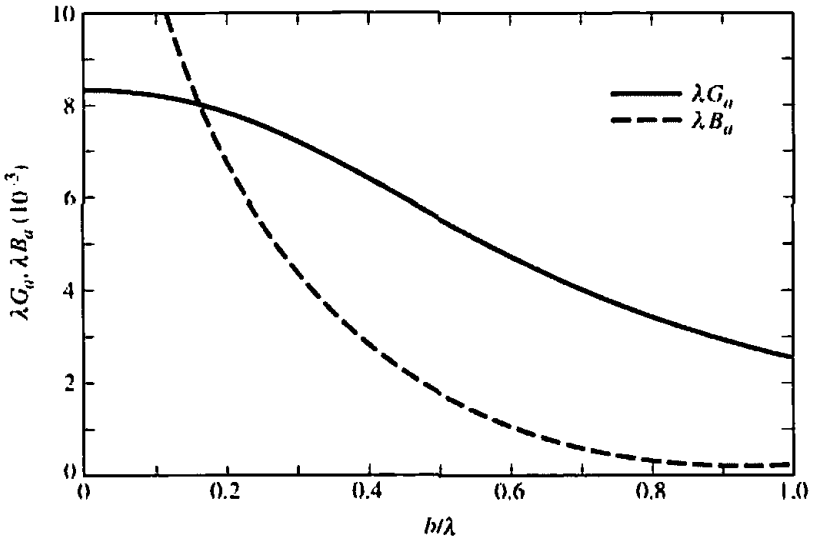

Figure 12.30 Normalized values of conductance and susceptance of narrow slot.

12.10 GROUND PLANE EDGE EFFECTS: THE GEOMETRICAL THEORY OF DIFFRACTION

Infinite size (physically and/or electrically) ground planes are not realizable in practice, but they can be approximated closely by very large structures. The radiation characteristics of antennas (current distribution, pattern, impedance, etc.) mounted on finite size ground planes can be modified considerably, especially in regions of very low intensity, by the effects of the edges. The ground plane edge diffractions for an aperture antenna are illustrated graphically in Figure 12.31. For these problems, rigorous solutions do not exist unless the object's surface can be described by curvilinear coordinates. Presently there are two methods that can be used conveniently to account for the edge effects. One technique is the *Moment Method* (MM) [28] discussed in Chapter 8 and the other is the *Geometrical Theory of Diffraction* (GTD) [29].

The Moment Method describes the solution in the form of an integral, and it can be used to handle arbitrary shapes. It mostly requires the use of a digital computer for numerical computations and, because of capacity limitations of computers, it is most computationally efficient for objects that are small electrically. Therefore, it is usually referred to as a *low-frequency asymptotic method.*

When the dimensions of the radiating object are large compared to the wavelength, *high-frequency asymptotic techniques* can be used to analyze many otherwise not mathematically tractable problems. One such technique, which has received consid-

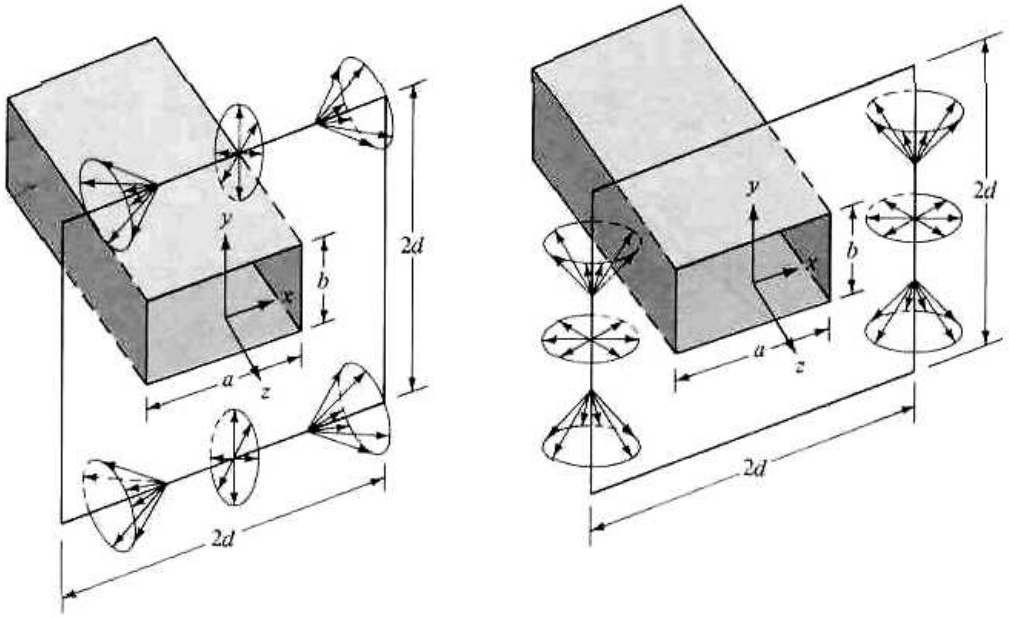

(a) Upper-lower (b) Left-right

Figure 12.31 Diffraction mechanisms for an aperture mounted on a finite size ground plane (diffractions at upper-lower and left-right edges of the ground plane).

erable attention in the past few years, is the *G*eometrical *T*heory of *D*iffraction (GTD) which was originally developed by Keller [29]. The GTD is an extension of the classical *G*eometrical *O*ptics (GO; direct, reflected, and refracted rays), and it overcomes some of the limitations of GO by introducing a diffraction mechanism [2].

The diffracted field, which is determined by a generalization of Fermat's principle [2], [30], is initiated at points on the surface of the object where there is a discontinuity in the incident GO field (incident and reflected shadow boundaries). The phase of the field on a diffracted ray is assumed to be equal to the product of the optical length of the ray (from some reference point) and the phase constant of the medium. Appropriate phase jumps must be added as a ray passes through caustics.* The amplitude is assumed to vary in accordance with the principle of conservation of energy in a narrow tube of rays. The initial value of the field on a diffracted ray is determined from the incident field with the aid of an appropriate diffraction coefficient (which, in general, is a dyadic for electromagnetic fields). The diffraction coefficient is usually determined from the asymptotic solutions of the simplest boundary-value problems which have the same local geometry at the points of diffraction as the object(s) of investigation. Geometries of this type are referred to as *canonical* problems. One of the simplest geometries is a conducting wedge [31], [32]. Another is that of a conducting, smooth and convex, surface [33]–[35].

The primary objective in using the GTD to solve complicated geometries is to resolve each such problem into smaller components [8]–[10], [35]. The partitioning is made so that each smaller component represents a canonical geometry of a known solution. These techniques have also been applied for the modeling and analysis of antennas on airplanes [36], and they have combined both wedge and smooth con-

*A caustic is a point or a line through which all the rays of a wave pass. Examples of it are the focal point of a paraboloid (parabola of revolution) and the focal line of a parabolic cylinder. The field at the caustic is infinite because, in principle, an infinite number of rays pass through it.

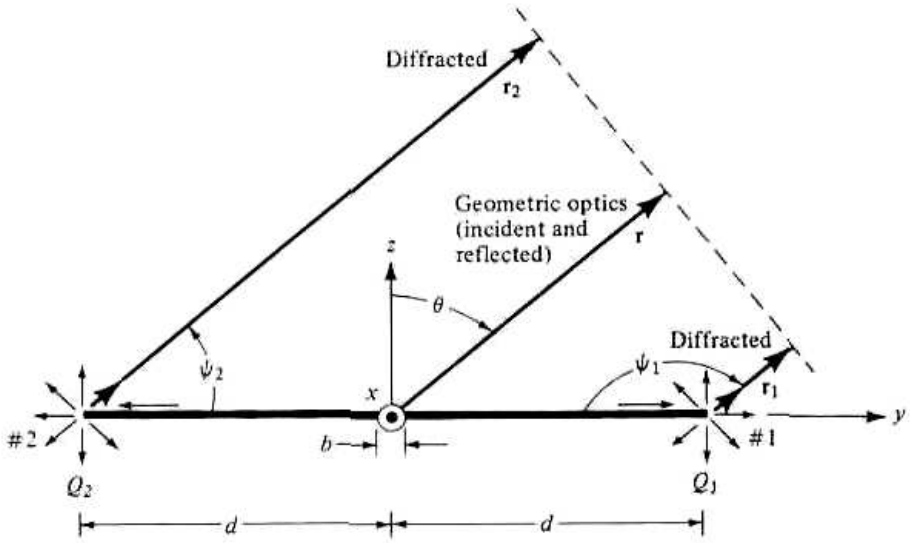

Figure 12.32 Aperture geometry in principal E-plane ($\phi \approx \pi/2$).

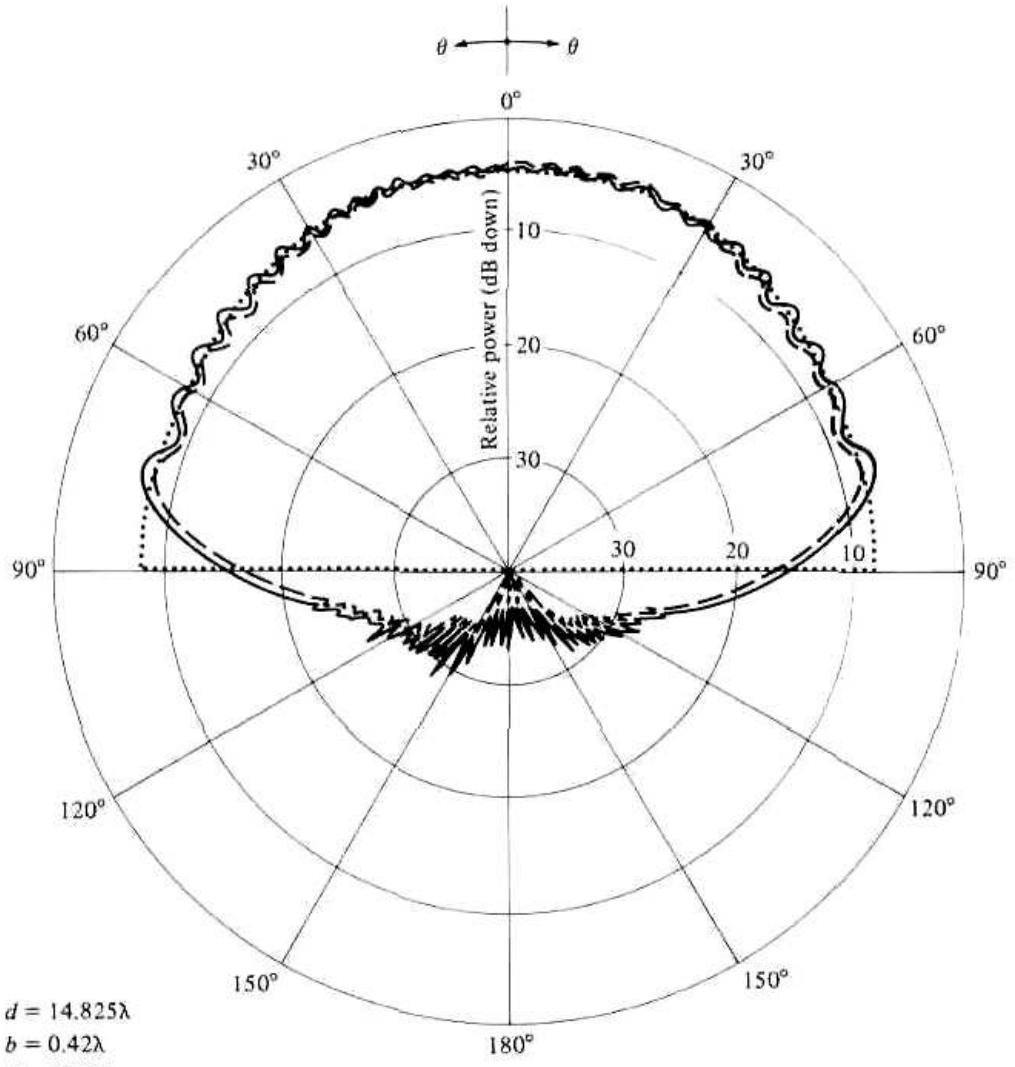

Figure 12.33 Principal E-plane amplitude patterns of an aperture antenna mounted on a finite size ground plane.

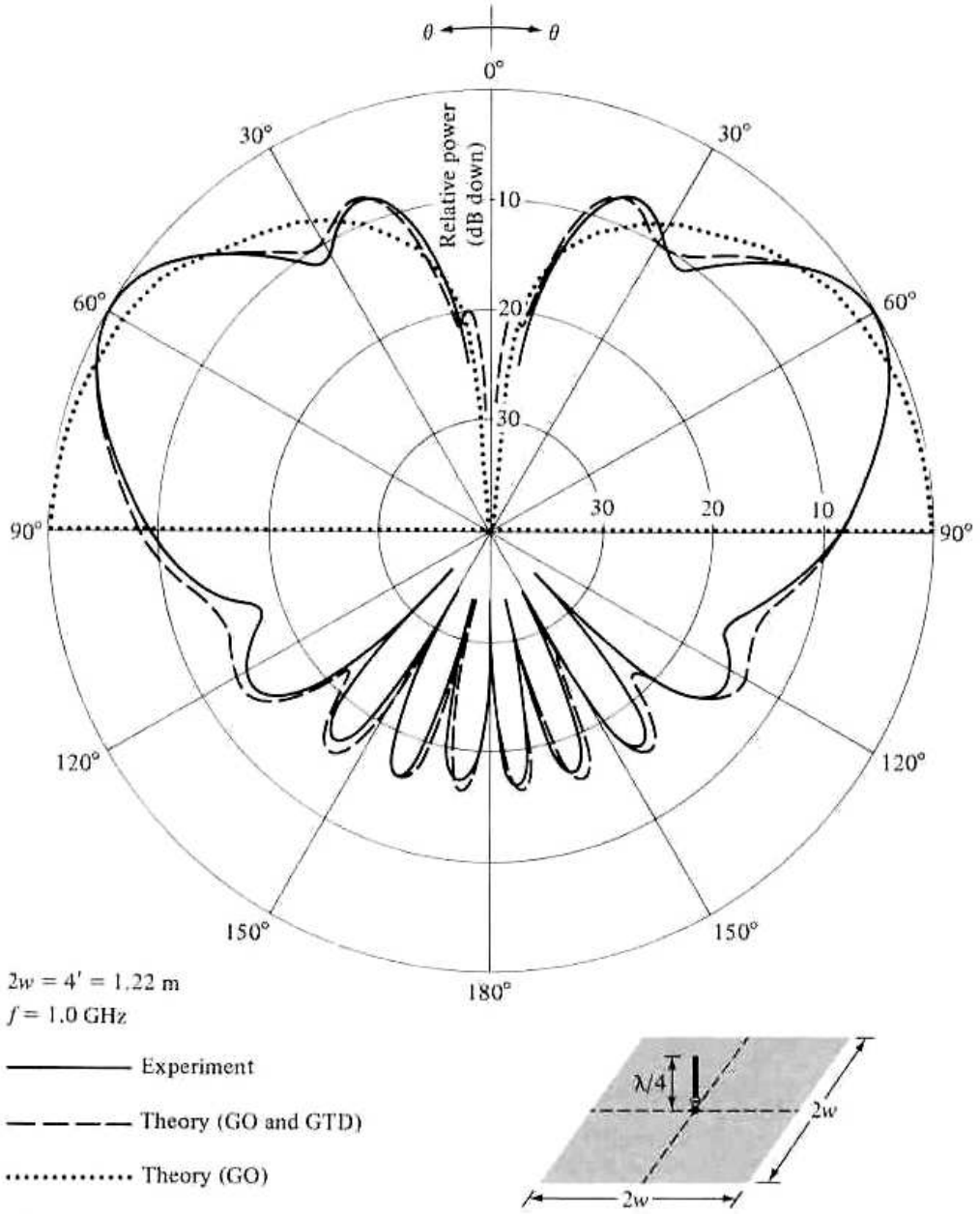

Figure 12.34 Measured and computed principal elevation plane amplitude patterns of a $\lambda/4$ monopole above infinite and finite square ground planes.

ducting surface diffractions [33], [35]. The ultimate solution is a superposition of the contributions from each canonical problem.

Some of the advantages of GTD are

1. It is simple to use.
2. It can be used to solve complicated problems that do not have exact solutions.
3. It provides physical insight into the radiation and scattering mechanisms from the various parts of the structure.
4. It yields accurate results which compare extremely well with experiments and other methods.
5. It can be combined with other techniques such as the Moment Method [37].

The derivation of the diffraction coefficients for a conducting wedge and their application are lengthy, and will not be repeated here. An extensive and detailed

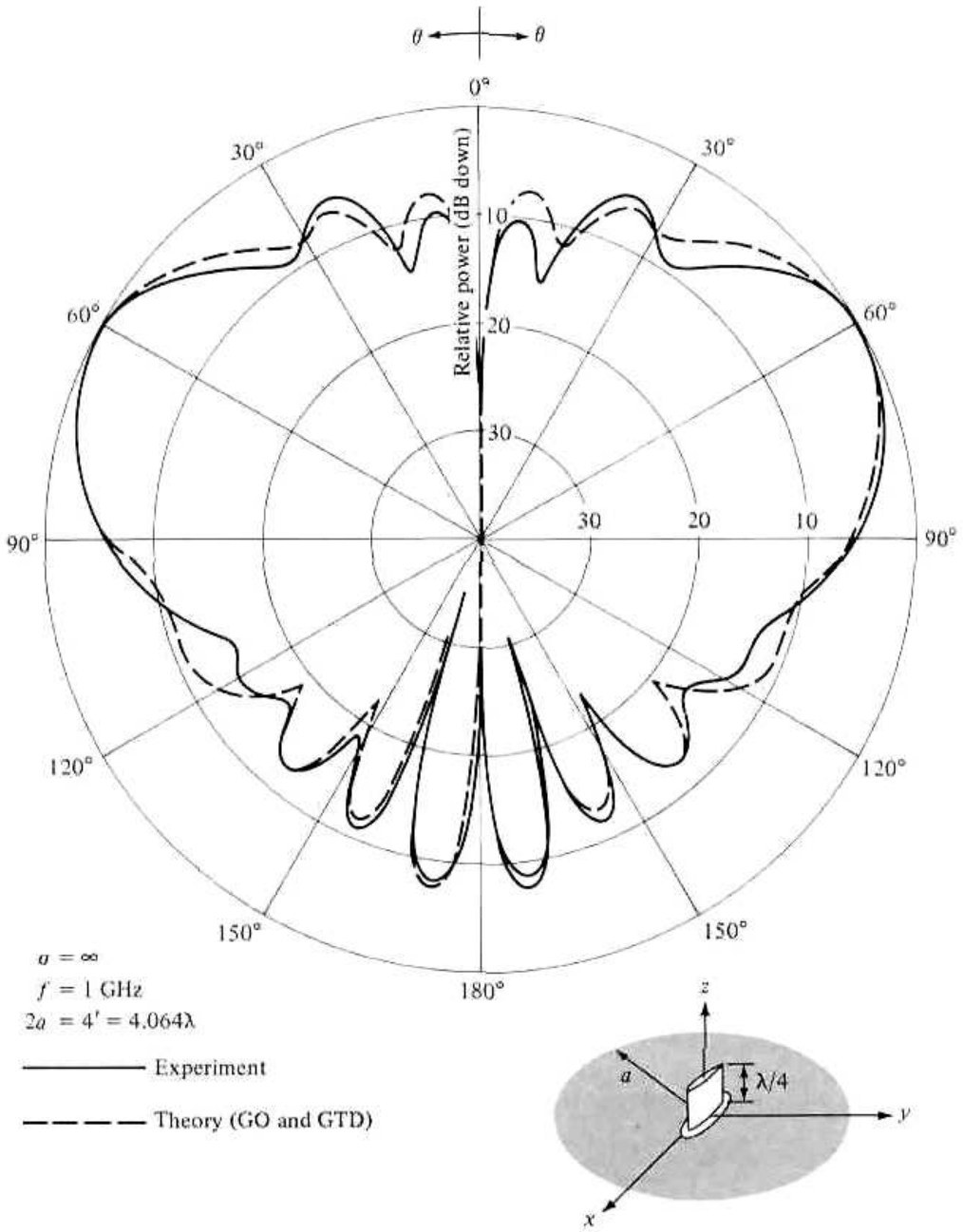

Figure 12.35 Measured and computed principal elevation plane amplitude patterns of a λ/4 monopole (blade) above a circular ground plane.

treatment of over 100 pages, for both antennas and scattering, can be found in [2]. However, to demonstrate the versatility and potential of the GTD, three examples are considered. The first is the *E*-plane pattern of a rectangular aperture of dimensions *a,b* mounted on a finite size ground plane, as shown in Figure 12.31. The GTD formulation along the *E*-plane includes the direct radiation and the fields diffracted by the two edges of the ground plane, as shown in Figure 12.32. The computed *E*-plane pattern along with the measured one are shown in Figure 12.33; an excellent agreement is indicated.

The two other examples considered here are the elevation pattern of a λ/4 monopole mounted on square and circular ground planes. The diffraction mechanism on the principal planes for these is the same as that of the aperture, which is shown in Figure 12.32. The corresponding principal elevation plane pattern of the monopole on the square ground plane is displayed in Figure 12.34 while that on the circular one is exhibited in Figure 12.35. For each case an excellent agreement is indicated with the measurements. It should be noted that the minor lobes near the symmetry axis

($\theta = 0°$ and $\theta = 180°$) for the circular ground plane of Figure 12.35 are more intense than the corresponding ones for the square ground plane of Figure 12.34. These effects are due to the ring-source radiation by the rim of the circular ground plane toward the symmetry axis [2], [10].

References

1. S. A. Schelkunoff. "Some Equivalence Theorems of Electromagnetics and Their Application to Radiation Problems," *Bell System Tech. J.* Vol. 15, pp. 92–112, 1936.
2. C. A. Balanis, *Advanced Engineering Electromagnetics*, John Wiley and Sons, New York, 1989.
3. C. Huygens, *Traite de la Lumiere*, Leyeden, 1690. Translated into English by S. P. Thompson, London, 1912, reprinted by The University of Chicago Press.
4. J. D. Kraus and K. R. Carver, *Electromagnetics* (second edition), McGraw-Hill, New York, 1973, pp. 464–467.
5. R. F. Harrington, *Time-Harmonic Electromagnetic Fields*, McGraw-Hill, New York, 1961, pp. 100–103, 143–263, 365–367.
6. A. E. H. Love, "The Integration of the Equations of Propagation of Electric Waves," *Phil. Trans. Roy. Soc. London, Ser. A*, Vol. 197, 1901, pp. 1–45.
7. R. Mittra (ed.), *Computer Techniques for Electromagnetics*, Pergamon Press, New York, 1973, pp. 9–13.
8. C. A. Balanis and L. Peters, Jr., "Equatorial Plane Pattern of an Axial-TEM Slot on a Finite Size Ground Plane," *IEEE Trans. Antennas Propagat.*, Vol. AP-17, No. 3, pp. 351–353, May 1969.
9. C. A. Balanis, "Pattern Distortion Due to Edge Diffractions," *IEEE Trans. Antennas Propagat.*, Vol. AP-18, No. 4, pp. 561–563, July 1970.
10. C. R. Cockrell and P. H. Pathak, "Diffraction Theory Techniques Applied to Aperture Antennas on Finite Circular and Square Ground Planes," *IEEE Trans. Antennas Propagat.*, Vol. AP-22, No. 3, pp. 443–448, May 1974.
11. D. G. Fink (ed.), *Electronics Engineers' Handbook*, Section 18 (Antennas by W. F. Croswell), McGraw-Hill, New York, 1975.
12. K. Praba, "Optimal Aperture for Maximum Edge-of-Coverage (EOC) Directivity," *IEEE Antennas and Propagatation Magazine*, Vol. 36, No. 3, pp. 72–74, June 1994.
13. H. G. Booker, "Slot Aerials and Their Relation to Complementary Wire Aerials," *J. Inst. Elec. Engrs.*, pt III A, 1946, pp. 620–626.
14. E. C. Jordan and K. G. Balmain, *Electromagnetic Waves and Radiating Systems*, Prentice-Hall, Inc., Englewood Cliffs, NJ, 1968.
15. J. D. Kraus, *Antennas*, McGraw-Hill, New York, 1988, Chapter 13.
16. H. G. Booker and P. C. Clemmow, "The Concept of an Angular Spectrum of Plane Waves, and its Relation to that of Polar Diagram and Aperture Distribution," *Proc. IEE* (London), Vol. 97, part III, January 1950, pp. 11–17.
17. G. Borgiotti, "Fourier Transforms Method of Aperture Antennas," *Alta Freq.*, Vol. 32, November 1963, pp. 196–204.
18. L. B. Felsen and N. Marcuvitz, *Radiation and Scattering of Waves*, Prentice-Hall, Englewood Cliffs, NJ, 1973.
19. R. E. Collin and F. J. Zucker, *Antenna Theory: Part 1*, Chapter 3, McGraw-Hill Book Co., New York, 1969.
20. C. M. Knop and G. I. Cohn, "Radiation from an Aperture in a Coated Plane," *Radio Science Journal of Research*, Vol. 68D, No. 4, April 1964, pp. 363–378.
21. F. L. Whetten, "Dielectric Coated Meandering Leaky-Wave Long Slot Antennas," Ph.D. Dissertation, Arizona State University, May 1993.
22. M. H. Cohen, T. H. Crowley, and C. A. Lewis, "The Aperture Admittance of a Rectangular Waveguide Radiating Into Half-Space," Antenna Lab., Ohio State University, Rept. 339-22, Contract W 33-038 ac21114, November 14, 1951.
23. R. T. Compton, "The Admittance of Aperture Antennas Radiating Into Lossy Media," Antenna Lab., Ohio State University Research Foundation, Rept. 1691-5, March 15, 1964.

24. A. T. Villeneuve, "Admittance of a Waveguide Radiating into a Plasma Environment," *IEEE Trans. Antennas Propagat.*, Vol. AP-13, No. 1, January 1965, pp. 115–121.
25. J. Galejs, "Admittance of a Waveguide Radiating Into a Stratified Plasma," *IEEE Trans. Antennas Propagat.*, Vol. AP-13, No. 1, January 1965, pp. 64–70.
26. M. C. Bailey and C. T. Swift, "Input Admittance of a Circular Waveguide Aperture Covered by a Dielectric Slab," *IEEE Trans. Antennas Propagat.*, Vol. AP-16, No. 4, July 1968, pp. 386–391.
27. W. F. Croswell, W. C. Taylor, C. T. Swift, and C. R. Cockrell, "The Input Admittance of a Rectangular Waveguide-Fed Aperture Under an Inhomogeneous Plasma: Theory and Experiment," *IEEE Trans. Antennas Propagat.*, Vol. AP-16, No. 4, July 1968, pp. 475–487.
28. R. F. Harrington, *Field Computation by Moment Methods*, Macmillan Co., New York, 1968.
29. J. B. Keller, "Geometrical Theory of Diffraction," *Journal Optical Society of America*, Vol. 52, No. 2, pp. 116–130, February 1962.
30. R. G. Kouyoumjian, "The Geometrical Theory of Diffraction and Its Applications," in *Numerical and Asymptotic Techniques in Electromagnetics* (R. Mittra, ed.), Springer-Verlag, New York, 1975.
31. R. G. Kouyoumjian and P. H. Pathak, "A Uniform Geometrical Theory of Diffraction for an Edge in a Perfectly Conducting Surface," *Proc. IEEE*, Vol. 62, No. 11, pp. 1448–1461, November 1974.
32. D. L. Hutchins, "Asymptotic Series Describing the Diffraction of a Plane Wave by a Two-Dimensional Wedge of Arbitrary Angle," Ph.D. Dissertation, The Ohio State University, Dept. of Electrical Engineering, 1967.
33. P. H. Pathak and R. G. Kouyoumjian, "An Analysis of the Radiation from Apertures on Curved Surfaces by the Geometrical Theory of Diffraction, *Proc. IEEE*, Vol. 62, No. 11, pp. 1438–1447, November 1974.
34. G. L. James, *Geometrical Theory of Diffraction for Electromagnetic Waves*, Peter Peregrinus, Ltd., Stevenage, Herts., England, 1976.
35. C. A. Balanis and L. Peters, Jr., "Analysis of Aperture Radiation from an Axially Slotted Circular Conducting Cylinder Using GTD," *IEEE Trans. Antennas Propagat.*, Vol. AP-17, No. 1, pp. 93–97, January 1969.
36. C. A. Balanis and Y.-B. Cheng, "Antenna Radiation and Modeling for Microwave Landing System," *IEEE Trans. Antennas Propagat.*, Vol. AP-24, No. 4, pp. 490–497, July 1976.
37. W. D. Burnside, C. L. Yu, and R. J. Marhefka, "A Technique to Combine the Geometrical Theory of Diffraction and the Moment Method," *IEEE Trans. Antennas Propagat.*, Vol. AP-23, No. 4, pp. 551–558, July 1975.

PROBLEMS

12.1. A uniform plane wave traveling in the $+z$ direction, whose magnetic field is expressed as

$$\mathbf{H}^i = \hat{\mathbf{a}}_y H_0 e^{-jkz} \qquad z \leq 0$$

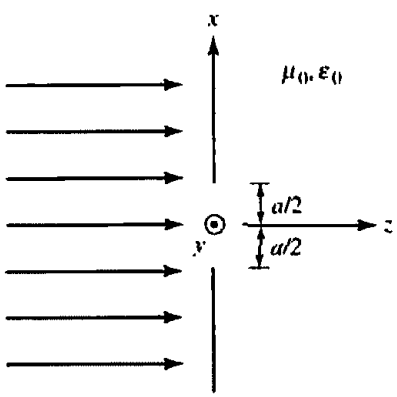

impinges upon an aperture on an infinite, flat, perfect electric conductor whose cross section is indicated in the figure.

(a) State the equivalent that must be used to determine the field radiated by the aperture to the right of the conductor ($z > 0$).

(b) Assuming the aperture dimension in the y direction is b, determine the far-zone fields for $z > 0$.

12.2. Repeat Problem 12.1 when the incident magnetic field is polarized in the x direction.

12.3. Repeat Problem 12.1 when the incident electric field is polarized in the y direction.

12.4. Repeat Problem 12.1 when the incident electric field is polarized in the x direction.

12.5. A perpendicularly polarized plane wave is obliquely incident upon an aperture, with dimension a and b, on a perfectly electric conducting ground plane of infinite extent, as shown in the figure. Assuming the field over the aperture is given by the incident field (ignore diffractions from the edges of the aperture), find the far-zone spherical components of the fields for $x > 0$.

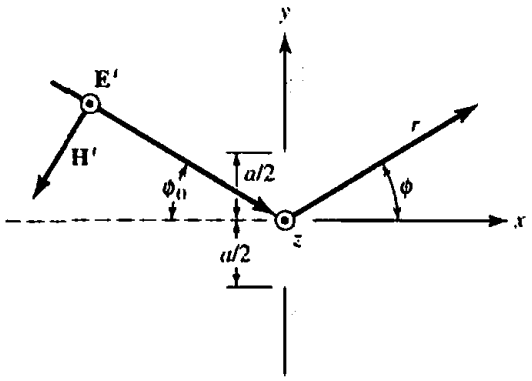

12.6. Repeat Problem 12.5 for a parallelly polarized plane wave (when the incident magnetic field is polarized in the z direction, i.e., the incident magnetic field is perpendicular to the x-y plane while the incident electric field is parallel to the x-y plane).

12.7. A narrow rectangular slot of size L by W is mounted on an infinite ground plane that covers the x-y plane. The tangential field over the aperture is given by

$$\mathbf{E}_a = \hat{\mathbf{a}}_y E_0 e^{-jk_0 r'\sqrt{2}/2}$$

Using the equivalence principle and image theory, we can replace the aperture and infinite ground plane with an equivalent magnetic current radiating in free space. Determine the

(a) appropriate equivalent

(b) far-zone spherical electric field components for $z > 0$

(c) direction (θ, ϕ) in which the radiation intensity is maximum

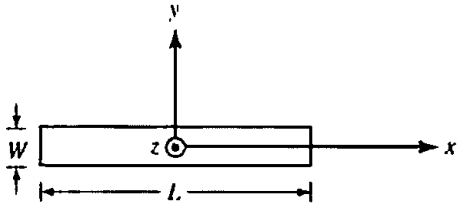

12.8. A rectangular aperture, of dimensions a and b, is mounted on an infinite ground plane, as shown in Figure 12.6(a). Assuming the tangential field over the aperture is given by

$$\mathbf{E}_a = \hat{\mathbf{a}}_z E_0 \qquad -a/2 \le y' \le a/2, \qquad -b/2 \le z' \le b/2$$

find the far-zone spherical electric and magnetic field components radiated by the aperture.

12.9. Repeat Problem 12.8 when the same aperture is analyzed using the coordinate system of Figure 12.6(b). The tangential aperture field distribution is given by

$$\mathbf{E}_a = \hat{\mathbf{a}}_x E_0 \qquad -b/2 \le x' \le b/2, \qquad -a/2 \le z' \le a/2$$

12.10. Repeat Problem 12.8 when the aperture field is given by

$$\mathbf{E}_a = \hat{\mathbf{a}}_x E_0 \cos\left(\frac{\pi}{a} y'\right) \qquad -a/2 \le y' \le a/2, \qquad -b/2 \le z' \le b/2$$

12.11. Repeat Problem 12.9 when the aperture field distribution is given by

$$\mathbf{E}_a = \hat{\mathbf{a}}_x E_0 \cos\left(\frac{\pi}{a} z'\right) \qquad -b/2 \le x' \le b/2 \qquad -a/2 \le z' \le a/2$$

12.12. Find the fields radiated by the apertures of Problems
(a) 12.8 (b) 12.9
(c) 12.10 (d) 12.11
when each of the apertures with their associated field distributions are *not* mounted on a ground plane. Assume the tangential **H**-field at the aperture is related to the **E**-field by the intrinsic impedance.

12.13. Find the fields radiated by the rectangular aperture of Section 12.5.3 when it is not mounted on an infinite ground plane.

12.14. For the rectangular aperture of Section 12.5.3 (with $a = 4\lambda$, $b = 3\lambda$), compute the
(a) E-plane beamwidth (*in degrees*) between the maxima of the *second* minor lobe
(b) E-plane amplitude (*in dB*) of the maximum of the second minor lobe (relative to the maximum of the major lobe)
(c) approximate directivity of the antenna using Kraus' formula. Compare it with the value obtained using the expression in Table 12.1.

12.15. For the rectangular aperture of Section 12.5.1 with $a = b = 3\lambda$, compute the directivity using (12-37) and the DIRECTIVITY computer program at the end of Chapter 2.

12.16. For the rectangular aperture of Section 12.5.2 with $a = b = 3\lambda$, compute the directivity using (12-37) and the DIRECTIVITY computer program at the end of Chapter 2.

12.17. Compute the directivity of the aperture of Section 12.5.3, using the DIRECTIVITY computer program at the end of Chapter 2, when
(a) $a = 3\lambda$, $b = 2\lambda$
(b) $a = b = 3\lambda$

12.18. Repeat Problem 12.17 when the aperture is not mounted on an infinite ground plane.

12.19. For the rectangular aperture of Section 12.5.3 with $a = 3\lambda$, $b = 2\lambda$, compute the
(a) E-plane half-power beamwidth
(b) H-plane half-power beamwidth
(c) E-plane first-null beamwidth
(d) H-plane first-null beamwidth
(e) E-plane first side lobe maximum (relative to main maximum)
(f) H-plane first side lobe maximum (relative to main maximum)
using the formulas of Table 12.1. Compare the results with the data from Figures 12.13 and 12.14.

12.20. A square waveguide aperture, of dimensions $a = b$ and lying on the x-y plane, is radiating into free-space. Assuming a $\cos(\pi x'/a)$ by $\cos(\pi y'/b)$ distribution over the aperture, find the dimensions of the aperture (in wavelengths) so that the beam efficiency within a 37° total included angle cone is 90%.

12.21. Verify (12-39a), (12-39b), (12-39c), and (12-40).

12.22. A rectangular aperture mounted on an infinite ground plane has aperture electric field distributions and corresponding efficiencies of

FIELD DISTRIBUTION	APERTURE EFFICIENCY
(a) Triangular	75%
(b) Cosine square	66.67%

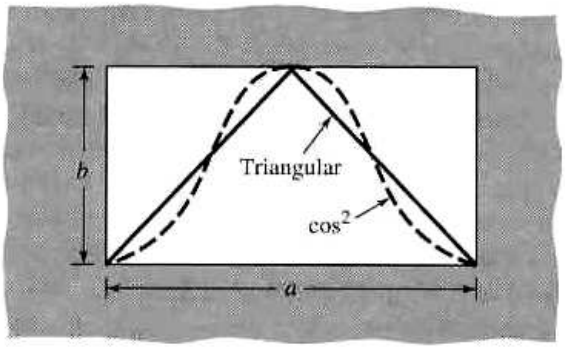

What are the corresponding directives (in dB) if the dimensions of the aperture are $a = \lambda/2$ and $b = \lambda/4$?

12.23. The physical area of an aperture antenna operating at 10 GHz is 200 cm^2 while its directivity is 23 dB. Assuming the antenna has an overall radiation efficiency of 90% and it is perfectly matched to the input transmission line, find the aperture efficiency of the antenna.

12.24. Two X-band (8.2–12.4 GHz) rectangular waveguides, each operating in the dominant TE_{10}-mode, are used, respectively, as transmitting and receiving antennas in a long distance communication system. The dimensions of each waveguide are $a = 2.286$ cm (0.9 in.) and $b = 1.016$ cm (0.4 in.) and the center frequency of operation is 10 GHz. Assuming the waveguides are separated by 10 kilometers and they are positioned for maximum radiation and reception toward each other, and the radiated power is 1 watt, find the:

(a) Incident power density at the receiving antenna

(b) Maximum power that can be delivered to a matched load

Assume the antennas are lossless, are polarization matched, and each is mounted on an infinite ground plane.

12.25. The normalized far-zone electric field radiated in the E-plane (x-z plane; $\phi = 0°$) by a waveguide aperture antenna of dimensions a and b, mounted on an infinite ground plane as shown in the figure, is given by

$$\mathbf{E} = -\hat{\mathbf{a}}_\theta j \frac{\omega\mu b I_0 e^{-jkr}}{4\pi r} \frac{\sin\left(\frac{kb}{2}\cos\theta\right)}{\frac{kb}{2}\cos\theta}$$

Determine in the E-plane the:

(a) Vector effective length of the antenna.

(b) Maximum value of the effective length.

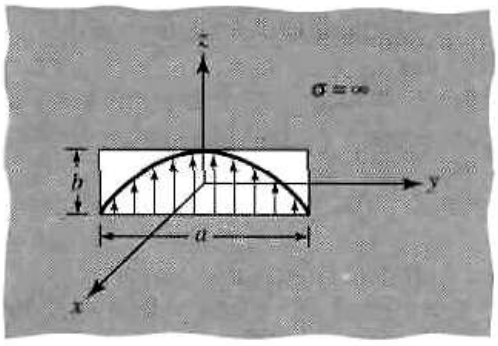

State the value of θ (in degrees) which maximizes the effective length.

12.26. A uniform plane wave is incident upon an X-band rectangular waveguide, with dimensions of 2.286 cm and 1.016 cm, mounted on an infinite ground plane. Assuming the waveguide is operating in the dominant TE_{10} mode, determine the maximum power that can be delivered to a matched load. The frequency is 10 GHz and the power density of the incident plane wave is 10^{-4} watts/m^2.

12.27. Compute the aperture efficiency of a rectangular aperture, mounted on an infinite ground plane as shown in Figure 12.7, with an E-field aperture distribution directed toward y but with variations
(a) triangular in the x and uniform in the y
(b) cosine-squared in the x and uniform in the y
(c) cosine in the x and cosine in the y
(d) cosine-squared in both the x and y directions.
How do they compare with those of a cosine distribution?

12.28. An X-band (8.2–12.4 GHz) WR 90 rectangular waveguide, with inner dimensions of 0.9 in. (2.286 cm) and 0.4 in. (1.016 cm), is mounted on an infinite ground plane. *Assuming the waveguide is operating in the dominant* TE_{10}*-mode, find its directivity* at $f = 10$ GHz using the
(a) computer program DIRECTIVITY at the end of Chapter 2
(b) formula in Table 12.1
Compare the answers.

12.29. Repeat Problem 12.28 at $f = 20$ GHz for a K-band (18–26.5 GHz) WR 42 rectangular waveguide with inner dimensions of 0.42 in. (1.067 cm) and 0.17 in. (0.432 cm).

12.30. Four rectangular X-band waveguides of dimensions $a = 0.9$ in. (2.286 cm) and $b = 0.4$ in. (1.016 cm) and each operating on the dominant TE_{10}-mode, are mounted on an infinite ground plane so that their apertures and the ground plane coincide with the x-y plane. The apertures form a linear array, are placed along the x-axis with a center-to-center separation of $d = 0.85\lambda$ apart, and they are fed so that they form a broadside Dolph-Tschebyscheff array of -30 dB minor lobes. Assuming a center frequency of 10 GHz, determine the overall directivity of the array in decibels.

12.31. Sixty-four (64) X-band rectangular waveguides are mounted so that the aperture of each is mounted on an infinite ground plane that coincides with the x-y plane, and all together form an $8 \times 8 = 64$ planar array. Each waveguide has dimensions of $a = 0.9$ in. (2.286 cm), $b = 0.4$ in. (1.086 cm) and the center-to-center spacing between the waveguides is $d_x = d_y = 0.85\lambda$. Assuming a TE_{10}-mode operation for each waveguide, a center frequency of 10 GHz, and the waveguides are fed to form a *uniform* broadside planar array, find the directivity of the total array.

12.32. Find the far-zone fields radiated when the circular aperture of Section 12.6.1 is not mounted on an infinite ground plane.

12.33. Derive the far-zone fields when the circular aperture of Section 12.6.2
(a) is
(b) is not
mounted on an infinite ground plane.

12.34. A circular waveguide (not mounted on a ground plane), operating in the dominant TE_{11} mode, is used as an antenna radiating in free space. Write in simplified form the normalized far-zone electric field components radiated by the waveguide antenna. You do not have to derive them.

12.35. For the circular aperture of Section 12.6.1, compute its directivity, using the DIRECTIVITY computer program at the end of Chapter 2, when its radius is
(a) $a = 0.5\lambda$
(b) $a = 1.5\lambda$
(c) $a = 3.0\lambda$
Compare the results with data from Table 12.2.

12.36. Repeat Problem 12.35 when the circular aperture of Section 12.6.1 is not mounted on an infinite ground plane. Compare the results with those of Problem 12.35.

12.37. For the circular aperture of Problem 12.33, compute the directivity, using the DIRECTIVITY computer program at the end of Chapter 2, when its radius is
(a) $a = 0.5\lambda$
(b) $a = 1.5\lambda$
(c) $a = 3.0\lambda$
Compare the results with data from Table 12.2.

12.38. For the circular aperture of Section 12.6.2 with $a = 1.5\lambda$, compute the
(a) E-plane half-power beamwidth
(b) H-plane half-power beamwidth
(c) E-plane first-null beamwidth
(d) H-plane first-null beamwidth
(e) E-plane first side lobe maximum (relative to main maximum)
(f) H-plane first side lobe maximum (relative to main maximum)
using the formulas of Table 12.2. Compare the results with the data from Figures 12.19 and 12.20.

12.39. A circular aperture of radius a is mounted on an infinite electric ground plane. Assuming the opening is on the x-y plane and its field distribution is given by

(a) $\mathbf{E}_a = \hat{\mathbf{a}}_y E_0 \left[1 - \left(\frac{\rho'}{a}\right)^2\right], \qquad \rho' \leq a$

(b) $\mathbf{E}_a = \hat{\mathbf{a}}_y E_0 \left[1 - \left(\frac{\rho'}{a}\right)^2\right]^2, \qquad \rho' \leq a$

find the far-zone electric and magnetic field components radiated by the antenna.

12.40. Repeat Problem 12.39 when the electric field is given by

$$\mathbf{E}_a = \hat{\mathbf{a}}_y E_0[1 - (\rho'/a)], \qquad \rho' \leq a$$

Find only the radiation vectors $\mathbf{L}$ and $\mathbf{N}$. Work as far as you can. If you find you cannot complete the solution in closed form, state clearly why you cannot. Simplify as much as possible.

12.41. A coaxial line of inner and outer radii a and b, respectively, is mounted on an infinite electric ground plane. Assuming that the electric field over the aperture of the coax is

$$\mathbf{E}_a = -\hat{\mathbf{a}}_\rho \frac{V}{\epsilon \ln(b/a)} \frac{1}{\rho'}, \qquad a \leq \rho' \leq b$$

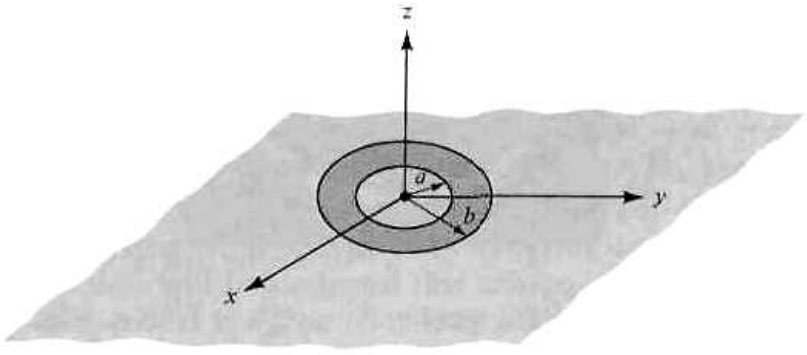

where V is the applied voltage and ϵ is the permittivity of the coax medium, find the far-zone spherical electric and magnetic field components radiated by the antenna.

12.42. It is desired to design a circular aperture antenna with a field distribution over its opening of

$$E = C[1 - (\rho'/a)^2]$$

where C is a constant, a its radius, and ρ' any point on the aperture, such that its beam efficiency within a 60° total included angle cone is 90%. Find its radius in wavelengths.

12.43. For the antenna of Problem 12.42, find its efficiency within a 40° total included angle cone when its radius is 2λ.

12.44. Design square apertures with uniform illumination so that the directivity at 60° from the normal is maximized relative to that at $\theta = 0°$. Determine the:
(a) Dimensions of the aperture (in λ)
(b) Maximum directivity (in dB)
(c) Directivity (in dB) at 60° from the maximum

12.45. Design a circular aperture with uniform illumination so that the directivity at 60° from the normal is maximized relative to that at $\theta = 0°$. Determine the
(a) Radius of the aperture (in λ)
(b) Maximum directivity (in dB)
(c) Directivity (in dB) at 60° from the maximum

12.46. Repeat Problem 12.45 for a circular aperture with a parabolic distribution.

12.47. Repeat Problem 12.45 for a circular aperture with a parabolic taper on -10 dB pedestal.

12.48. Derive the edge-of-coverage (EOC) design characteristics for a circular aperture with a parabolic taper.

12.49. A vertical dipole is radiating into a free-space medium and produces fields $\mathbf{E}_0$ and $\mathbf{H}_0$. Illustrate alternate methods for obtaining the same fields using Babinet's principle and extensions of it.

12.50. (a) (1) Sketch the six principal plane patterns, and (2) define the direction of $\mathbf{E}$ and $\mathbf{H}$ along the three principal axes and at 45° to the axes, for a thin slot one-half wavelength long, cut in a conducting sheet which has infinite conductivity and extending to infinity, and open on both sides. Inside dimensions of the slot are approximately 0.5λ by 0.1λ. Assume that the width (0.1λ) of the slot is small compared to a wavelength. Assume a coordinate system such that the conducting plane lies on the x-y plane with the larger dimension of the slot parallel to the y-axis.
(b) Sketch the six approximate principal plane patterns $E_\theta(\phi = 0°)$, $E_\phi(\phi \approx 0°)$, $E_\theta(\phi = 90°)$, $E_\phi(\phi = 90°)$, $E_\theta(\theta = 90°)$, $E_\phi(\theta = 90°)$.

12.51. A very thin circular annular slot with circumference of one wavelength is cut on a very thin, infinite, flat, perfectly electric conducting plate. The slot is radiating into free space. What is the impedance (real and imaginary parts) of the slot?

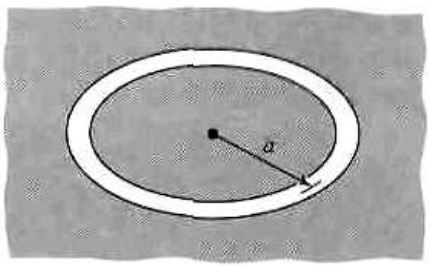

12.52. Repeat Example 12.7 for a rectangular aperture with an electric field distribution of

$$\mathbf{E}_a = \hat{\mathbf{a}}_y E_0 \cos\left(\frac{\pi}{a}x'\right), \qquad \begin{matrix} -a/2 \le x' \le a/2 \\ -b/2 \le y' \le b/2 \end{matrix}$$